

Fall 2011

# In-situ early detection of metal corrosion via "turn-on" fluorescence in "smart" epoxy coatings

Anita Augustyniak

*University of New Hampshire, Durham*

Follow this and additional works at: <https://scholars.unh.edu/dissertation>

---

## Recommended Citation

Augustyniak, Anita, "In-situ early detection of metal corrosion via "turn-on" fluorescence in "smart" epoxy coatings" (2011). *Doctoral Dissertations*. 622.

<https://scholars.unh.edu/dissertation/622>

This Dissertation is brought to you for free and open access by the Student Scholarship at University of New Hampshire Scholars' Repository. It has been accepted for inclusion in Doctoral Dissertations by an authorized administrator of University of New Hampshire Scholars' Repository. For more information, please contact [nicole.hentz@unh.edu](mailto:nicole.hentz@unh.edu).

**IN-SITU EARLY DETECTION OF METAL CORROSION VIA  
“TURN-ON” FLUORESCENCE IN “SMART” EPOXY COATINGS**

BY

ANITA AUGUSTYNIAK

M.S. Chemical Technology, West Pomeranian University of Technology  
(former Szczecin University of Technology), 2006

DISSERTATION

Submitted to the University of New Hampshire

in Partial Fulfillment of

the Requirements for the Degree of

Doctor of Philosophy

in

Materials Science

September 2011

UMI Number: 3488788

All rights reserved

INFORMATION TO ALL USERS

The quality of this reproduction is dependent upon the quality of the copy submitted.

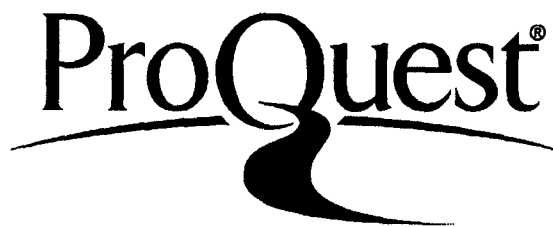
In the unlikely event that the author did not send a complete manuscript and there are missing pages, these will be noted. Also, if material had to be removed, a note will indicate the deletion.



UMI 3488788

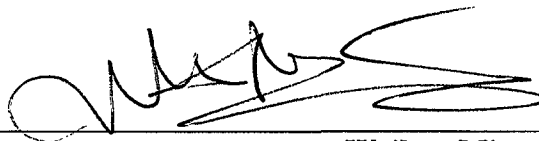
Copyright 2011 by ProQuest LLC.

All rights reserved. This edition of the work is protected against unauthorized copying under Title 17, United States Code.

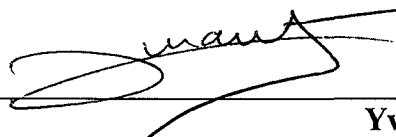


ProQuest LLC  
789 East Eisenhower Parkway  
P.O. Box 1346  
Ann Arbor, MI 48106-1346

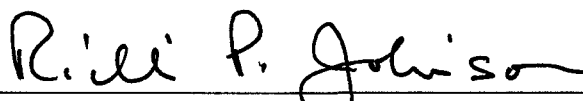
This dissertation has been examined and approved.



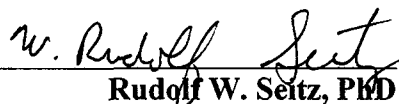
**Weihua Ming, PhD**  
Thesis Director, Research Associate Professor of Materials Science



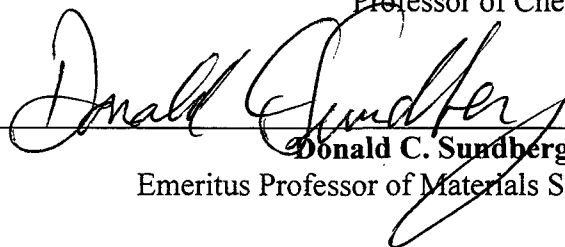
**Yvon Durant, PhD**  
Research Associate Professor of Materials Science



**Richard P. Johnson, PhD**  
Professor of Chemistry



**Rudolf W. Seitz, PhD**  
Professor of Chemistry



**Donald C. Sundberg, PhD**  
Emeritus Professor of Materials Science

7/25/11

Date

## DEDICATION

This thesis is dedicated to my husband and best friend, John. I couldn't have done this without you. You were my guardian angel through the good and through the not so good times. Your professional and life knowledge, love, support and patience were always with me. Thank you Pączek!

## ACKNOWLEDGMENTS

The financial support from the Office of Naval Research (Award Numbers N000140410693 and N000141110152) made this research possible and is greatly appreciated.

First I would like to thank my great advisor, Prof. Marshall Ming, for his guidance, love of science and willingness to share his great knowledge and experience. Thank you for trusting in my own decisions along this path and for providing guidance when I needed it.

There were so many people on the way to where I am now that I have reasons to thank:

Prof. Yvon Durant, Prof. Richard Johnson, Prof. Rudi Seitz and Prof. Roy Planalp  
for always being willing to answer my questions

Prof. Don Sundberg, for being probably the best teacher I've ever had, that could  
explain the most complicated concepts in a simple and exciting way

My parents and family (both Polish and American) for being always supportive  
and proud of me no matter what I do

My friend, Dr. Isabel Dregely, for having "the girl's talks" with me after tough  
days of "science talks"

All my lab colleagues, especially Haoran Chen and Mathieu Chirat for always being willing to help with the every day lab struggle

Chemistry PhD student, Rajesh Thamam, for helping me with the organic synthesis

## TABLE OF CONTENTS

DEDICATION .....	iii
ACKNOWLEDGMENTS .....	iv
TABLE OF CONTENTS.....	vi
LIST OF FIGURES.....	ix
ABSTRACT.....	xv
CHAPTER 1: INTRODUCTION .....	1
1.1 Background of Corrosion and its Consequences .....	2
1.1.1 Types of corrosion.....	5
1.1.2 Marine Corrosion .....	8
1.1.3 Corrosion of Construction Metals and Alloys .....	9
1.2 Corrosion Protection by Organic Coatings .....	12
1.2.1 Corrosion Protection by Epoxy Coatings .....	13
1.2.2 Protective Coating Failure Mechanisms and Corrosion of Coated Metals ...	16
1.2.3 “Smart Polymeric Coatings” for Corrosion Protection .....	21
1.3 Early Corrosion Detection Methods and its Significance .....	22
1.3.1 <i>In-situ</i> Early Corrosion Detection Methods.....	23
1.4 Objective and Outline of this Thesis.....	26
CHAPTER 2: CORROSION DETECTION BASED ON HIGH pH SENSING .....	28
2.1 Introduction and Literature Review .....	29
2.1.1 Phenolphthalein as a Chromophoric Acid-Base Indicator for Detection of Cathodic Corrosion Reaction .....	29
2.1.2 Fluorescent Acid-Base Indicators .....	31
2.1.3 <i>In-situ</i> Early Corrosion Detection at Cathodic Site of Corrosion via Indicators Embedded in Protective Organic Coating .....	33
2.2 Objectives of this Chapter .....	35
2.3 Experimental Section .....	36
2.3.1 Reagents and Materials.....	36
2.3.2 General Sample Preparation in this Chapter.....	36
2.4 Characterization Methods.....	37
2.5 Results and Discussion.....	38
2.5.1 Experiments with Phenolphthalein.....	38



2.5.2	Experiments with Alizarin Yellow R .....	48
2.6	Conclusions .....	50
CHAPTER 3: EARLY DETECTION OF STEEL CORROSION.....		52
3.1	Introduction and Literature Review .....	54
3.1.1	New Requirements for an Ideal <i>In-situ</i> Corrosion Indicator in Epoxy Based Coatings.....	54
3.1.2	<i>In-situ</i> Fluorescent Aluminum Corrosion Sensing via Complexation with Al <sup>3+</sup> .....	55
3.1.3	“Turn- on” Fluorescent Sensing via Complexation with Fe <sup>2+</sup> /Fe <sup>3+</sup> .....	57
3.1.4	Rational for choice of FD1 as a Steel corrosion Indicator .....	59
3.2	Objectives of this Chapter .....	62
3.3	Experimental Section .....	63
3.3.1	Reagents and Materials.....	63
3.3.2	Sample Preparation .....	64
3.3.3	FD1 Response to Fe <sup>3+</sup> in Solution.....	66
3.3.4	Preparation of FD1-Embedded Clear-Epoxy Fe <sup>3+</sup> -Sensing Films (AA1-62)	66
3.3.5	Preparation of FD1-Embedded Filled-Epoxy Fe <sup>3+</sup> -Sensing Films (AA1-84A).....	67
3.3.6	Preparation of Steel Coupons Coated with Fe <sup>3+</sup> -sensing Clear Model Epoxy Coating .....	68
3.3.7	Preparation of Steel Coupons Coated with Fe <sup>3+</sup> -sensing Filled Commercial Epoxy Coating .....	69
3.3.8	Preparation of Undercoating Corrosion-Sensing Panels .....	70
3.4	Characterization Methods.....	71
3.5	Results and Discussion.....	72
3.5.1	FD1 and Rhodamine B Hydrazide Synthesis .....	72
3.5.2	FD1 Response to Fe <sup>3+</sup> in Solution.....	73
3.5.3	FD1 Ability to Sense Fe <sup>3+</sup> when Embedded in Commercial Clear Epoxy Matrix.....	75
3.5.4	FD1 Ability to Sense Fe <sup>3+</sup> when Embedded in Commercial Filled Epoxy Matrix.....	77
3.5.5	Fluorescent Emission Response of FD1 in Fe <sup>3+</sup> -sensing Clear Model Epoxy Coating on Steel Coupons .....	78
3.5.6	Fluorescent emission response of FD1 in Fe <sup>3+</sup> -sensing filled commercial epoxy coating on steel coupons .....	83
3.5.7	Undercoating steel corrosion sensing in a filled commercial epoxy coating	86
3.6	Conclusions .....	91

CHAPTER 4: FD1 STABILITY IN AN EPOXY COATING .....	92
4.1 Introduction and Objectives of this Chapter .....	93
4.2 Experimental Section .....	94
4.2.1 Reagents and Materials.....	94
4.2.2 Sample Preparation and Characterization.....	94
4.3 Results and Discussion.....	99
4.3.1 FD1 Sensitivity to UV Light.....	99
4.3.2 FD1 Stability in the Epoxy Coating .....	105
4.4 Conclusions .....	115
CHAPTER 5: EXPLORATION OF FD1 SENSING MECHANISM .....	117
5.1 Introduction and Objectives of this Chapter.....	118
5.2 Experimental Section .....	120
5.2.1 Reagents and Materials.....	120
5.2.2 Sample Preparation .....	122
5.2.3 Characterization Methods.....	129
5.3 Results and Discussion.....	130
5.3.1 FD1 Corrosion Sensing Mechanism Based on Complexation with Fe <sup>3+</sup> ....	130
5.3.2 FD1 Corrosion Sensing Mechanism Based on Acid Catalyzed Hydrolysis	150
5.3.3 RBH as a Potential Early Corrosion Indicator .....	158
5.4 Conclusions .....	163
CHAPTER 6: FD1 AS AN INDICATOR FOR EARLY DETECTION OF ALUMINUM CORROSION.....	165
6.1 Introduction and the Objectives of this Chapter .....	166
6.2 Experimental Section .....	167
6.2.1 Reagents and Materials.....	167
6.2.2 Sample preparation.....	168
6.2.3 Characterization Methods.....	170
6.3 Results and Discussion.....	171
6.3.1 FD1 as a Corrosion Sensor in Clear Model Epoxy Coating on Al 1052 Alloy.....	171
6.3.2 FD1 as a Corrosion Sensor in Filled Epoxy Coating on Al 2024-T3 alloy.	173
6.4 Conclusions .....	175
CHAPTER 7: CONCLUSIONS AND OUTLOOK.....	176
REFERENCES.....	181

## LIST OF FIGURES

Figure 1. Scheme of iron corrosion. ....	3
Figure 2. Schematic illustration of the common forms of corrosion .....	6
Figure 3. Forms of localized corrosion .....	7
Figure 4. Pitting corrosion on aluminum alloys.....	12
Figure 5. Condensation polymerization of epichlorohydrin and bisphenol A.....	14
Figure 6. Curing of epoxy resin with tetrafunctional primary amine.....	15
Figure 7. Stages of coating degradation and undercoating corrosion (adapted from .....	17
Figure 8. Crevice corrosion of the metal substrate under the protective coating.....	20
Figure 9. Corrosion filament (left image) and filiform corrosion on aluminum panel coated with polyester paint (right image) . ....	21
Figure 10. Different forms of dissociation of phenolphthalein.....	30
Figure 11. Change in color of phenolphthalein in different pH solutions. ....	30
Figure 12. Corrosion of iron nails immersed in agar containing ferroxy indicator . ....	31
Figure 13. Different ionic forms of fluorescein occurring in aqueous solution at pH's exceeding 3.3. The dianion is highly fluorescent .....	32
Figure 14. Optical micrograph of Al 2024-T3 coated with acrylic-phenolphthalein (2.4 wt%) after immersion in 1 M NaCl for 9 hrs .....	34
Figure 15. Color change of commercial clear epoxy coating with 1 wt% phenolphthalein (AA1-06).....	38
Figure 16. Color change of component A of commercial clear epoxy coating after mixing with 1 wt% phenolphthalein. ....	40
Figure 17. Chemical structures of DGEBA and EBE. ....	41
Figure 18. Color change of clear model epoxy matrix with different rigidity mixed with 1 wt% of phenolphthalein. ....	42
Figure 19. Color change of: TEA and phenolphthalein (vial 1), DGEBA and phenolphthalein (vial 2) and DGEBA with phenolphthalein and a drop of TEA (vial 3) with time at 70°C.....	45

Figure 20. Response of clear model epoxy coatings with phenolphthalein to pH 9 solution.....	47
Figure 21. Chemical structure of Alizarin Yellow R sodium salt. ....	48
Figure 22. Change in color of Alizarin Yellow R in different pH solutions. ....	48
Figure 23. Color change of clear model epoxy matrix with different rigidity mixed with 0.06 wt% of Alizarin Yellow R.....	50
Figure 24. Structure of lumogallion . ....	55
Figure 25. Morin complexation with Al <sup>3+</sup> . ....	56
Figure 26. Chemical structure of 8-hydroxyquinoline-5-sulfonic acid hydrate .....	57
Figure 27. Spirolactam ring-opening reaction of a rhodamine derivative .....	59
Figure 28. Fluorescence response of FD1 (10 <sup>-6</sup> M) upon the addition of Fe <sup>3+</sup> at 25°C ....	60
Figure 29. Proposed coordination between FD1 and Fe <sup>3+</sup> ion resulting in the fluorescence enhancement .....	61
Figure 30. Synthesis of FD1 .....	62
Figure 31. Fluorescent response of FD1 (solution in CH <sub>3</sub> CN, 20 μM) to FeCl <sub>3</sub> solution in CH <sub>3</sub> CN (0 to 6 equiv.) (λ <sub>ex</sub> =510 nm). Right: color change of FD1 in CH <sub>3</sub> CN on FeCl <sub>3</sub> addition under UV and visible light. ....	74
Figure 32. Fluorescent response of FD1 embedded in the clear commercial epoxy coating (AA1-62) to aqueous FeCl <sub>3</sub> solution after 24 h of immersion (smaller piece of film in the left and the middle images). The large piece was not immersed in FeCl <sub>3</sub> , for comparison. Far right: fluorescent emission intensity of the small piece immersed in FeCl <sub>3</sub> solution for 24 h (data transformed from the lambda mode).....	76
Figure 33. Change in fluorescent emission intensity of filled FD1-epoxy sensing film in FeCl <sub>3</sub> aqueous solution (λ <sub>ex</sub> = 514 nm) at time 0 and after 24 h (data was transformed from lambda mode). ....	78
Figure 34. AREA2 in Fe <sup>3+</sup> -sensing clear model epoxy coating on steel substrate (AA1-71A) after exposure to 0.5M NaCl solution. Top row: digital camera images taken through the microscope eye-piece under UV light; bottom row: fluorescent images, of the same area, taken with the confocal microscope. ....	80
Figure 35. AREA3 in Fe <sup>3+</sup> -sensing clear model epoxy coating on steel substrate (AA1-71A) after exposure to 0.5M NaCl solution for 2 h. Left: fluorescent image taken with a	

confocal microscope; right: digital camera image, of the same area, taken through the microscope eye-piece under UV light. ....81

Figure 36. FD1 in model clear epoxy matrix after 11 months of exposure to air (AA1-71B, reference sample). Left: fluorescent image taken with the confocal microscope; middle: digital camera image, of the same area, taken through the microscope eye-piece under UV light; right digital image taken through the microscope eye-piece under visible light. ....82

Figure 37. FD1 in model clear epoxy matrix after exposure to 3.5% NaCl solution (AA2-48A2) Top row: digital camera images taken through the microscope eye-piece under UV light; bottom row: digital camera images, of the same area, taken through the microscope eye-piece under visible light. ....83

Figure 38. Scribed area on the coated steel coupon (AA1-71D) after various times of exposure to different corrosive environments: sample placed on a beaker with 0.5 M NaCl solution (a) at time 0 and (b) after 40 h, sample placed in the beaker with DI water after (c) 30 min and (d) 22 h, and (e) sample placed in 0.5 M NaCl solution after 30 min. Top row: fluorescent images taken on confocal microscope; bottom row: digital camera images of the same area, taken through the microscope eye-piece under UV light.....85

Figure 39. Optical images of the scribed area of the corrosion-sensing panel (AA1-71D) after (a) 30 min and (b) 2 h of immersion in 0.5 M NaCl. Images taken through the microscope eye-piece.....86

Figure 40. (a) Undercoating corrosion sensing panel (AA1-96A) after 1 day of exposure to 5% NaCl solution. Blue circle and red circle represent areas exposed to NaCl and a blister, respectively. “1” and “2” represent areas exposed to NaCl solution where silicone oil was applied and area not exposed to NaCl solution, respectively; (b) fluorescence image of the area in the red circle taken on the confocal microscope and (c) the lambda mode of the same area. ....88

Figure 41. Images of the blister in the undercoating corrosion sensing panel (AA1-96A) after immersion in a 5% NaCl solution. Top row: images taken through the microscope eye-piece under UV light; bottom row: images taken through the microscope eye-piece under natural light.....90

Figure 42. Rusted metal under the blistered area in AA1-96A sample. ....91

Figure 43. Areas in sample AA1-96A exposed to UV for a prolonged period of time (left image) and not exposed to UV (right image). Pictures were taken through microscope eye-piece under UV light. ....	100
Figure 44. FD1 (AA1-70) color change over time. ....	101
Figure 45. Color change of FD1 crystals upon exposure to UV light (350nm) (AA2-58). .....	101
Figure 46. Change in the fluorescent intensity at 580 nm (left) and color (right) of FD1 in CH <sub>3</sub> CN upon exposure to 254 nm UV light (AA2-56). ....	102
Figure 47. Sensitivity of FD1 in CH <sub>3</sub> CN to UV light and oxygen. ....	104
Figure 48. Scratched filled epoxy coating (AA1-96A, AREA2) ....	106
Figure 49. Scratched filled epoxy coating (AA1-71D) ....	107
Figure 50. Cross-sections showing metal/coating interface of samples AA1-71D (not treated with H <sub>3</sub> PO <sub>4</sub> before coating application) and AA1-96B (front and back of the sample, treated with H <sub>3</sub> PO <sub>4</sub> before coating application). Top row: images taken through the confocal microscope eye-piece (20× magnification) under natural light; bottom row: images taken through the microscope eye-piece under UV light. Insets in the bottom row pictures show the fluorescent images obtained from the confocal microscope's lambda mode. ....	111
Figure 51. FD1 in filled epoxy coating (AA2-01). Top row: top view of the coating with the scratch before and after immersion in HCl (left and right image respectively). Bottom row: cross-section of the coating before and after immersion in HCl (left and right image respectively). Images taken through the microscope eye-piece under UV light. ....	113
Figure 52. Fluorescent spectra of the FeCl <sub>3</sub> /THF solutions from experiments AA3-38A and AA3-38B (after 6 and 28 months of sample immersion in FeCl <sub>3</sub> solution respectively). $\lambda_{ex}$ =510 nm. ....	115
Figure 53. FD1 fluorescence (at 583 nm) as a function of pH; $\lambda_{ex}$ =510 nm ....	119
Figure 54. Chemical structure of iron (III) acetylacetonate. ....	132
Figure 55. Chemical structure of ferric ammonium citrate. ....	134
Figure 56. Fluorescent emission spectra of FD1/THF solution (20 M) titrated with FeCl <sub>3</sub> /H <sub>2</sub> O solution (left) and with FeCl <sub>3</sub> /THF solution (right). $\lambda_{ex}$ =510 nm. ....	136

Figure 57. Difference in color of the FD1/THF solutions upon addition of 2.2 Fe <sup>3+</sup> /FD1 equivalents from FeCl <sub>3</sub> in water (left image) and in THF (right image). .....	136
Figure 58. UV-vis absorption spectra of FD1/THF solution (20 μM) titrated with FeCl <sub>3</sub> /H <sub>2</sub> O solution (left) and with FeCl <sub>3</sub> /THF solution (right). .....	138
Figure 59. ESI-MS spectrum of FD1 in THF. ....	139
Figure 60. ESI-MS spectrum of FD1/FeCl <sub>3</sub> solution in THF (1 Fe <sup>3+</sup> /FD1 equivalent). .	140
Figure 61. Enlarged area around the <i>m/z</i> = 622.05 peak from the Figure 60 (top spectrum). Bottom spectrum shows the simulated isotopic distribution of [FD1+Fe(III)+2Cl] <sup>+</sup> .....	141
Figure 62. Enlarged area around the <i>m/z</i> = 1280.77 peak from Figure 59 (top spectrum). Bottom spectrum shows simulated isotopic distribution of [2*(FD1+Fe(III)+2Cl)+Cl] <sup>+</sup> cluster. ....	142
Figure 63. Enlarged area around the <i>m/z</i> = 730.92 peak from the Figure 59 (top spectrum). Bottom spectrum shows the simulated isotopic distribution of [(FD1+Fe(III)+2Cl) + (Fe+Cl+O)] <sup>+</sup> . ....	143
Figure 64. <sup>1</sup> H NMR spectra of (A) FD1 in THF- <i>d</i> <sub>8</sub> , (B) solution from spectrum A upon addition of FeCl <sub>3</sub> in THF and (C) solution from spectrum B upon addition of cyclen (in mixed solvent system THF- <i>d</i> <sub>8</sub> /CDCl <sub>3</sub> ). ....	145
Figure 65. ESI-MS spectrum of FD1/THF upon addition of aqueous FeCl <sub>3</sub> solution (1 Fe <sup>3+</sup> /FD1 equivalent). ....	146
Figure 66. ESI-MS spectrum of FD1/THF upon addition of aqueous FeCl <sub>3</sub> solution (6 Fe <sup>3+</sup> /FD1 equivalents). ....	147
Figure 67. <sup>1</sup> H NMR spectra of (A) FD1 in THF- <i>d</i> <sub>8</sub> , and (B) the mixture of FD1/Ga(NO <sub>3</sub> ) <sub>3</sub> xH <sub>2</sub> O. ....	149
Figure 68. Fluorescent emission of FD1 solution in CH <sub>3</sub> CN (20 μM) upon addition of HCl solution (up to 1.8 H <sup>+</sup> /FD1 equivalents) when excited at 510 nm. Right: color change of FD1 in CH <sub>3</sub> CN upon addition of HCl under UV and visible light. ....	150
Figure 69. Proposed FD1 structure upon addition of acid (protonation). ....	151
Figure 70. <sup>1</sup> H NMR spectra of (A) FD1 in THF- <i>d</i> <sub>8</sub> , as well as the mixtures of (B) FD1/H <sub>2</sub> SO <sub>4</sub> and (C) FD1/H <sub>2</sub> SO <sub>4</sub> /NaOH in THF- <i>d</i> <sub>8</sub> /D <sub>2</sub> O mixed solvents. ....	152

Figure 71. ESI-MS spectrum of FD1/THF upon addition of aqueous HCl solution (6 H <sup>+</sup> /FD1 equivalents). .....	154
Figure 72. Proposed mechanism of FD1 fluorescence at low pH. ....	154
Figure 73. <sup>1</sup> H NMR spectra of (a) FD1 and (b) RBH in THF-d <sub>8</sub> , as well as the mixtures of (c) FD1/HCl and (d) RBH/HCl in THF-d <sub>8</sub> /D <sub>2</sub> O mixed solvents. The huge water peak in (c, d) was due to HCl. ....	156
Figure 74. Fluorescent emission of RBH solution in CH <sub>3</sub> CN (20 μM) upon addition of HCl solution (up to 2.4 H <sup>+</sup> / FD1 equivalents) when excited at 510 nm. ....	157
Figure 75. Potential reaction between RBH and epoxy ring from DGEBA. ....	159
Figure 76. <sup>1</sup> H NMR spectra of (A) RBH, (B) DGEBA, (C) mixture of RBH/DGEBA and (D) mixture of RBH/DGEBA after 2 h reflux at 115°C. Letter T represents peaks for toluene-d <sub>8</sub> . ....	161
Figure 77. UV-vis absorption of the solutions of RBH and DGEBA in THF and the THF solution after extraction and wash of the cured RBH/DGEBA/TEPA sample. ....	163
Figure 78. Images of Al 1052 coated with a FD1-containing, clear epoxy coating (AA2-54) after (a) 2 days and (b) 3 days of exposure to 3.5 % NaCl solution. Top row: digital camera images taken through the confocal microscope eyepiece under UV light. Bottom row: images of the same areas taken through the confocal microscope eyepiece under natural light. ....	172
Figure 79. Images of Al 2024-T3 coated with FD1-containing filled epoxy coating (AA3-06F) after (a) 21 days and (b) 27 days of exposure to 3.5 % NaCl solution at 70 °C. Top row: digital camera images taken through the confocal microscope eyepiece under UV light. Bottom row: images of the same areas taken through the confocal microscope eyepiece under natural light. ....	174



# ABSTRACT

## IN-SITU EARLY DETECTION OF METAL CORROSION VIA “TURN-ON” FLUORESCENCE IN “SMART” EPOXY COATINGS

by

Anita Augustyniak

University of New Hampshire, September, 2011

Organic coatings (e.g., epoxy coatings) have been widely used to protect metal and metal alloys against corrosion. However protective coating fails with time, leading to corrosion of the metal substrate. When localized corrosion occurs, without being detected, it can result in disastrous failure of the metal structure. The purpose of this thesis is to develop a “smart” epoxy coating system that detects early stages of metal corrosion via indicators molecules embedded in the coating that fluoresce when triggered by ions liberated from corrosion. This fluorescence can be easily and non-destructively detected and thus further material damage can be prevented by providing necessary maintenance. In this thesis a spiro lactam, [1H-isoindole-1,9’-[9H]xanthen]-3(2H)-one, 3’,6’-bis(diethylamino)-2-[(1 methylethylidene) amino] (FD1), was successfully used to sense early stages of metal corrosion, when embedded in the epoxy coating, via “turn-on” fluorescence. Despite that we unambiguously confirmed that FD1 forms a fluorescent complex with  $\text{Fe}^{3+}$  in a nonaqueous solution by using electrospray ionization mass spectrometry (ESI-MS), the predominant mechanism that FD1 is capable of detecting early metal corrosion is due to its acid-catalyzed hydrolysis to fluorescent protonated Rhodamine B hydrazide, as the

consequence of the local pH decrease at the anodic sites of both steel and aluminum corrosion (water is always present). The “turn-on” FD1 fluorescence was easily, non-destructively detected under UV light before any visible sign of corrosion appeared. In addition, only a low FD1 concentration (0.5 wt%) in the coating was needed for effective corrosion detection. FD1 did not prematurely interact with the coating formulation components and was able to “report” early corrosion even when embedded in the filled epoxy coating in the presence of pigments.

## CHAPTER 1

### INTRODUCTION

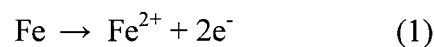
**Summary.** In the introduction of this thesis, the corrosion process is explained with focus on steel and aluminum. A general description of corrosion protection via organic coatings is presented including coating failure mechanisms that result in corrosion of the underlying metal. A short introduction to “smart” polymeric coatings for corrosion protection is given. Early corrosion detection methods, including *in-situ* early corrosion detection via indicator molecules, and their significance are then discussed. Finally an overview of the content of this thesis is presented.

## **1.1 Background of Corrosion and its Consequences**

Corrosion is a chemical or electrochemical reaction between a metal or metal alloy and its environment (ex. oxygen or water) that produces deterioration of the material and its properties. As a result of this reaction various corrosion products are formed that are in fact similar or identical to the minerals that the metal was extracted from in the first place (ex. oxides) [1, 2]. Corrosion, when undetected and untreated, can cause serious metal failure and can result in economic and safety implications. In 2001 CC Technologies Laboratories, Inc. with support from the U.S. Federal Highway Administration (FHWA) and NACE estimated that direct cost of losses due to corrosion is \$276 billion annually [3]. For the Navy, the maintenance cost related to corrosion was estimated to be \$6.14 billion/year in 2006 [4].

In general electrochemical corrosion reactions can be described using iron as an example. An iron (or steel) corrosion cell (i.e. region where corrosion occurs) is schematically illustrated in Figure 1 and described below. It includes four essential components:

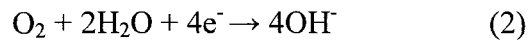
1. An anode, where metal is oxidized and dissolved (Equation 1):



2. An electrolyte solution (such as salt water), where oxidized metal is dissolved and where the transport of ions between anode and cathode occurs. This transport is

necessary to maintain electroneutrality in the cell so no charge is accumulated by corroding metal

3. A cathode, where reduction reactions take place. The main reaction for any type of atmospheric corrosion in neutral and acidic solution is reduction of dissolved oxygen (Equation 2):



4. A path for electron conduction between the anode and the cathode (through the conducting metal) [1, 5]

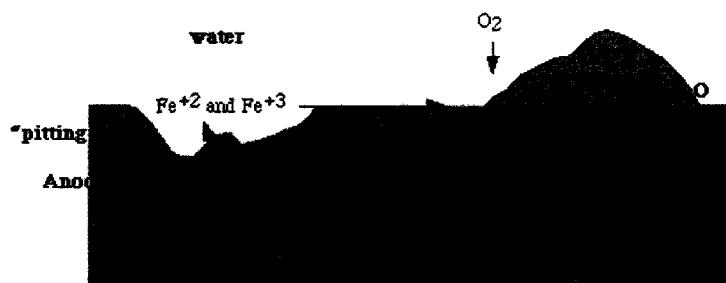


Figure 1. Scheme of iron corrosion.

The electrons liberated by the anodic reaction are consumed at the cathode as shown in Equation 1 and Equation 2. The driving force for the reactions described above is potential difference between anode and cathode which may arise from differences in the constituent phases of the metal itself, from variations in surface deposits or coatings on the metal, or from variations in the electrolyte or oxygen concentrations (different aeration cells are formed). The anode and the cathode can be located physically close to each other or at distant sites in the same metal. In some cases the anode can be the

surface of one component (metal) and the cathode can be the surface of another component in contact with it, as in the case of galvanic corrosion. All metals are arranged in the galvanic series (or electropotential series) with the noblest metals (least easily oxidized), that serve as a cathode, at one end and easily oxidized, active metals that form an anode and corrode preferentially, at the other end. A galvanic series applies to a particular electrolyte solution (e.g. seawater) thus for each specific solution it will have a different order [1, 6].

The corrosion process can be stopped by eliminating any of the four corrosion cell components mentioned above [5].

Corrosion is influenced by many factors such as:

- Alloy composition (due to possibility of galvanic corrosion between two dissimilar metals with different corrosion potential)
- Electrolyte chemistry (e.g. chloride ions or oxidizing agents in water accelerate corrosion)
- pH (acidic pH accelerates corrosion by supplying hydrogen ions that react with electrons at the cathode)
- Temperature (in general corrosion rate increases with increasing temperature)
- Oxygen content (water with high oxygen content tends to be more corrosive)
- Presence of biological organisms (that can accumulate at the metal surface and accelerate crevice attack) [1, 2].

### 1.1.1 Types of corrosion

Corrosion can be classified based on these three factors [2]:

1. Nature of the corrodent:
  - “wet” corrosion where a liquid or moisture is necessary
  - or “dry” corrosion involving reaction with high-temperature gases
2. Mechanism of corrosion:
  - electrochemical
  - or direct chemical reactions
3. Appearance of the corroded metal:
  - uniform, when metal corrodes at the same rate over the whole surface
  - or localized when only small areas are affected

Based on the appearance of the corroded metal, eight forms of wet corrosion can be distinguished [2]:

- uniform or general corrosion
- pitting corrosion
- crevice corrosion that includes corrosion under tubercles or deposits, filiform corrosion, and poultice corrosion
- galvanic corrosion
- erosion-corrosion that includes cavitation erosion and fretting corrosion
- intergranular corrosion that includes sensitization and exfoliation

- dealloying that includes dezincification and graphitic corrosion
- environmentally assisted cracking, including stress-corrosion cracking (SCC), corrosion fatigue, and hydrogen damage

Some of the most common types of corrosion are schematically illustrated in Figure 2 [2, 6].

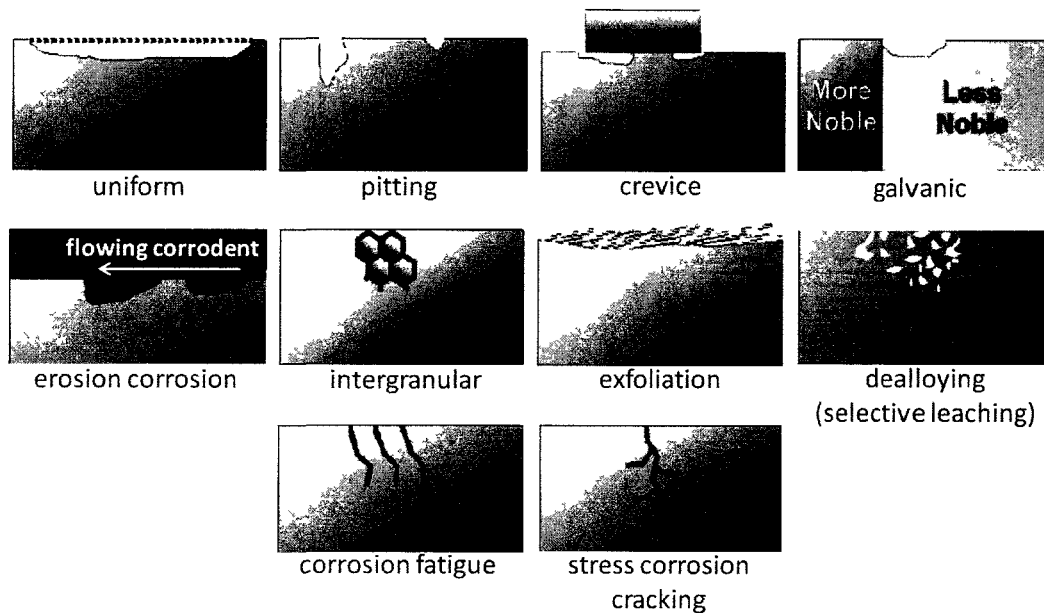


Figure 2. Schematic illustration of the common forms of corrosion [2, 6].

Localized corrosion can be divided into two groups:

- Microscopic local attack where visible metal damage is minute and the considerable corrosion can occur before it is observed by the naked eye, and
- Macroscopic form of corrosion that affects larger areas and is generally visible to the naked eye [2]



This division is illustrated in Figure 3.

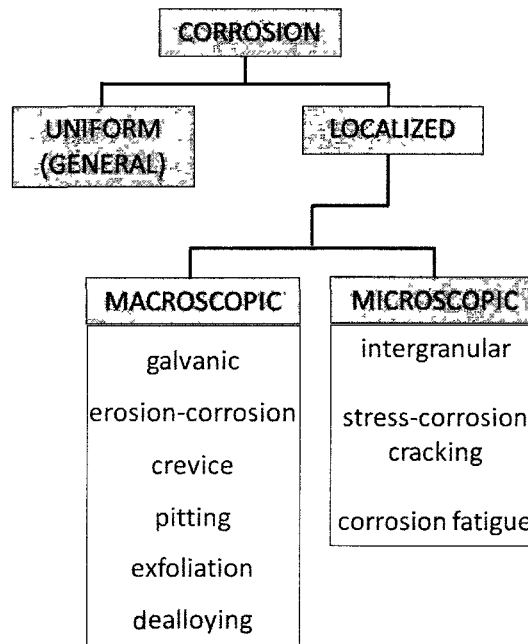


Figure 3. Forms of localized corrosion [2].

It has been reported that localized corrosion mechanisms are responsible for about two thirds of all structural failures, while uniform corrosion is responsible for less than one fourth. A large fraction of the localized corrosion failures occurs by pitting [7]. **Pitting** (Figure 2) is one of the most dangerous types of localized corrosion. It is hard to detect by visual inspection since the pits and cavities formed during the process propagate deep into the metal causing rapid metal dissolution without significant changes observable on the surface and with only a small percent weight loss of the entire structure. Additionally, pits can act as notches or cracks and trigger more damage when the metal structure is under stress (fatigue and stress corrosion cracking (SCC) can initiate at the base of corrosion pits). Therefore pitting corrosion usually leads to replacement of the entire

structure [1, 2]. Marine environment is the most favorable for pitting corrosion. For pitting to occur, the metal has to be in a passive form (i.e. an oxide film being present on the surface). Engineering alloys such as aluminum or stainless steel form passive films, which makes them highly resistant to uniform corrosion. However when the passive film is damaged metals become prone to pitting [2].

### **1.1.2 Marine Corrosion**

Seawater, which covers 70% of earth's surface, is known to be quite corrosive due to the high concentration of chloride ions (almost 55% of total dissolved solids) that make sea water a very efficient electrolyte. Chloride is also the most aggressive ion in sea water because it can penetrate and destroy the passive oxide surface of metals and accelerate their corrosion. Other factors contributing to high corrosion rates in coastal and ocean seawater are variable temperatures, dissolved oxygen contents, biological organisms and pollutants [1, 8]. At a NaCl concentration of around 3.5%, the corrosion rate of iron in an aerated solution was found to be at its maximum due to high conductivity of water and sufficient solubility of dissolved oxygen [1]. At a higher dissolved salt concentration solubility of dissolved oxygen is decreased and the corrosion rate subsequently decreases. For this reason 3.5% NaCl solution is often used to simulate seawater in laboratory. Since seawater is considered a very aggressive environment, a material exhibiting a satisfactory corrosion resistance in seawater is considered sufficient for major industrial applications and water transportations systems [8].

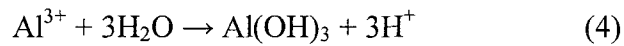
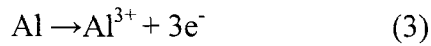
### 1.1.3 Corrosion of Construction Metals and Alloys

**Iron and steel** are the most widespread materials for construction applications. However their usefulness is not due to their corrosion resistance but due to their availability, mechanical properties, low price and ease of fabrication. **Carbon steel** is the most commonly used material for service in seawater. It is used in vast applications in ships and shipping industry [8]. Carbon steels are alloys of iron and 0.05-1% carbon, as a main constituent added as a strengthening element, and other alloying elements such as copper, nickel or chromium [1, 8]. **Cast irons** include a large family of ferrous alloys. Their carbon content is between 2 and 4 % and silicon content (for better corrosion resistance) 1% or more. Iron and steel corrode in many media including most outdoor atmospheres. Different kinds of steel corrode at different rates depending on their composition and on the presence of mechanical stresses. Iron corrodes uniformly over its entire outside surface (general corrosion). To prevent these materials from corroding, protective coatings are applied. However, their failure can lead to localized or undercoating steel corrosion (as described in section 1.2.2). **Stainless steels** on the other hand are generally very corrosion-resistant in corrosive media at atmospheric and elevated temperatures due to a protective passive oxide layer. This layer is formed on the surface in oxidizing atmospheres. However it shows susceptibility to pitting and crevice corrosion and stress-corrosion cracking in seawater and similar environments containing aggressive chloride ions that can penetrate the passivated layer. Stainless steel is an iron-based alloy containing at least 12% chromium for better corrosion resistance (forms protective

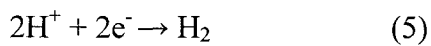
chromium oxide). There are 5 main types of stainless steel: ferritic, martensitic, austenitic, precipitation hardening and duplex [1, 8].

**Aluminum** and its alloys are another extremely useful and abundant group of materials. They are used extensively for architectural trim and window and door hardware, automotive trim [1], sidings and other building materials. Due to its light weight, aluminum and its higher-strength alloys are also widely used for structural components in aircrafts and aerospace vehicles [1, 8]. **Aluminum** is a very thermodynamically active metal, however this reactivity provides its natural corrosion resistivity. Similarly to stainless steel, a dense, inert protective aluminum oxide layer forms rapidly when the metal is exposed to an oxygen-containing environment (e.g. air, water) and protects the metal surface from corroding since it is more thermodynamically inactive. Even when the oxide layer is damaged (e.g. by a scratch), new oxide forms immediately on the bare metal [1, 9]. However the protective oxide film can be destabilized and thereby corrosion can occur. The oxide is not stable in acidic ( $\text{pH} < 4$ ) or alkaline ( $\text{pH} < 9$ ) solutions or in the presence of aggressive ions (such as chlorides, fluorides) that might locally attack the oxide and cause pitting [1]. Corrosion resistance of **aluminum alloys** varies depending on alloying components. Most of the alloying elements decrease corrosion resistance and improve mechanical properties. Corrosion on aluminum alloys is essentially a microgalvanic process between intermetallic phases and the matrix alloy due to the difference in their potential. Each alloy class is specified by the first of a four-digit designation. Alloys within each class are specified by the other three digits (xxx) [1]. The **1xxx alloys** consist of commercially pure aluminum with only residual impurities and

alloying elements that gives them excellent corrosion resistance but generally low strength. Thus, these alloys have limited commercial use. The **2xxx series** (such as Al 2024-T3) contain copper as the main alloying element. Because of their high strength and low density they are extensively used in aerospace and other industrial applications. However, they are the least corrosion resistant of all aluminum alloys and usually are used only when protected by alclading or painting (e.g. with epoxy coatings). Since copper is more noble in the galvanic series (less active) than aluminum it serves as a cathode and the surrounding aluminum matrix serves as an anode and undergoes localized attack when the protective oxide is attacked by aggressive chloride ions; in this situation pitting might occur. Pits are initiated at weak sites in the oxide and propagate according to the anodic reactions:



The cathodic reactions involve reduction of dissolved oxygen at the intermetallic particles according to Equation 2 and hydrogen evolution (in the absence of all other reduction reactions) (Equation 5):



During pit propagation, pH inside the pit decreases according to Equation 4. Also chloride ions will migrate to the pit to balance the positive charge. As a result HCl is

formed that further dissolves the metal and accelerates pit propagation [1, 8]. The pH in the pit can be as low as 3.5 [10]. Around the cathodic intermetallic particles an alkaline environment is formed due to  $\text{OH}^-$  formation (reduction reaction) and an oxide layer that is not stable in this environment will dissolve in that area forming alkaline pits. These processes are described in Figure 4 [9].

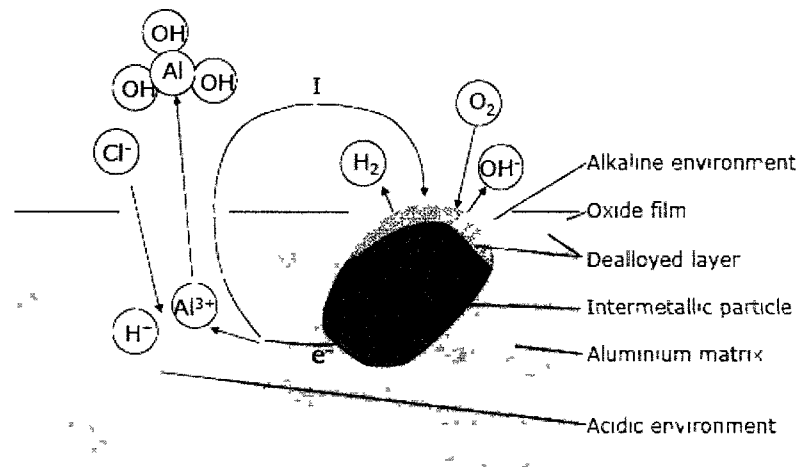


Figure 4. Pitting corrosion on aluminum alloys [9]

Other aluminum alloys contain various alloying elements, such as manganese, magnesium, chromium, silicon or zinc. Their corrosion resistance and strength depends on the composition.

## **1.2 Corrosion Protection by Organic Coatings**

One of the oldest and most convenient ways to protect metal surfaces from aqueous corrosion is the application of a protective organic coating. This coating serves not only

as a physical barrier against aggressive species present in the metal environment (such as oxygen or protons and chloride ions) but more importantly inhibits the formation of an electrolytic path, one of the corrosion cell's components necessary for the corrosion process to occur [11, 12, 13]. This barrier can be simply due to properties of the polymer (i.e. low electrical conductivity) or due to the presence of inert pigments that increase the diffusion path through the coating [13].

### **1.2.1 Corrosion Protection by Epoxy Coatings**

One of the most widely used protective coatings on metal surfaces are epoxy coatings due to their exceptional adhesion to metal surfaces, excellent chemical, acid and water resistance, better alkali resistance than most other types of polymeric paints, dielectric and insulation properties, low shrinkage at cure, thermal stability and superior mechanical strength [14, 15, 16]. Epoxies are cured products of an epoxy resin and a curing agent (sometimes called hardener). Diglycidyl ether of bisphenol-A (DGEBA, DGEBA or BADGE) is a typical commercial epoxy resin. It is formed by the condensation polymerization (step-growth polymerization) of epichlorohydrin and bisphenol A (or rather its sodium salt) that produces a linear prepolymer with an epoxide group at each end (Figure 5) [17].

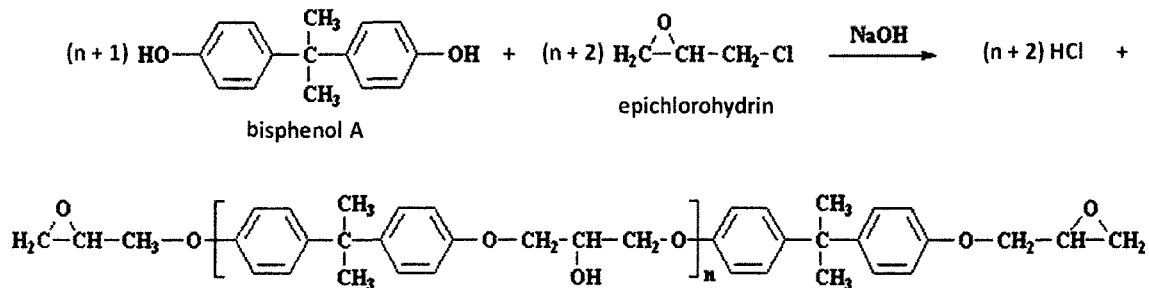


Figure 5. Condensation polymerization of epichlorohydrin and bisphenol A [17].

The molecular weight of DGEBA is controlled and liquid (with degree of polymerization,  $n=1$ ) or solid ( $2 < n < 30$ ) prepolymers are formed. Epichlorohydrin can also be prereacted with a variety of hydroxyl, carboxy and amino compounds, to form monomers with two or more epoxide groups, before reacting with bisphenol A. Various coreactants are used to cure epoxy resins either through the epoxide or hydroxyl groups. Polyamines are the most common curing agents. The curing reaction involves ring-opening addition of the amine to the epoxy [17]. Both more reactive primary and less reactive secondary amines are used. A variety of multifunctional amines (i.e. containing multiple nitrogen-hydrogen reactive bonds) are used as crosslinking agents including diethylene triamine, triethylene tertamine and polyaminoamides (e.g. the diamide formed from diethylene triamine and a dimerized or trimerized fatty acid) [17]. The curing reaction between an epoxy and a tetrafunctional diamine is shown in Figure 6. As a result of this reaction a crosslinked network is formed.



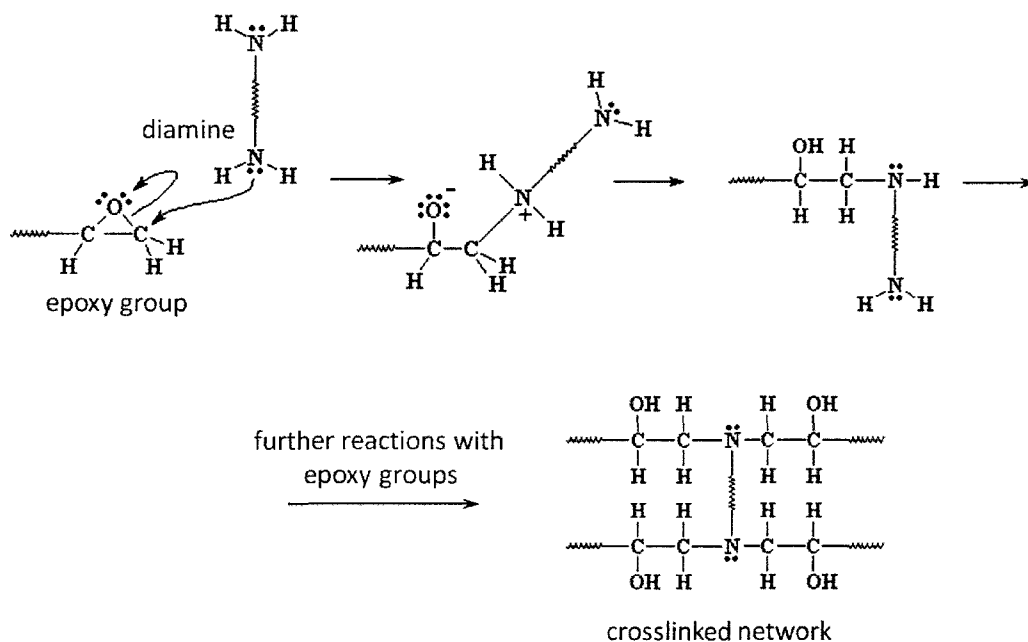


Figure 6. Curing of epoxy resin with tetrafunctional primary amine [18].

Other curing agents such as polythiols, dicyandiamide and phenolic prepolymers have also been used to cure epoxy resins via the epoxide group. Some of these compounds require weak bases (e.g. tertiary amines or imidazole derivatives) to accelerate the curing reaction. If the prepolymers have low epoxide group content then crosslinking can also be accomplished through hydroxyl groups of the repeat unit. The most common curing agent used in this case is phthalic anhydride. Another way to cure epoxy resin is by ring-opening polymerization of epoxide groups using Lewis acids or Lewis bases.

Most epoxy coating formulations contain various additives such as diluents, reinforcement materials, fillers and pigments, and toughening agents [17].

### **1.2.2 Protective Coating Failure Mechanisms and Corrosion of Coated Metals**

All organic coatings are water permeable to some extent and over time their protectiveness can decrease due to prolonged exposure to the environment or mechanical damage. The corrosive species (electrolytes) can eventually penetrate the coating, accessing the metal surface, and undercoating corrosion can take place. Also the presence of the inevitable microscopic or macroscopic defect in the protective film (such as pinholes, voids, and mechanical scrapes and scratches) allows the environment to reach the metal faster [1, 19]. There are a few steps that lead to coating degradation (Figure 7) and failure that result in exposing the metal to corrosive environment. In the case of a defect-free coating, first the conductive pathway has to be formed. Hydrophilic regions in the coating allow water uptake and interconnection of these regions (Figure 7a). When defects are present, such as air bubbles, poor wetting between pigment and binder, or mechanical damage, these connections are formed easier. After the pathway is formed water, oxygen and ions can be transported to the metal surface from the environment (Figure 7b). When soluble materials such as salts are present on the metal surface water uptake can be increased due to osmosis and blisters can form under the coating. In this case, corrosion is accelerated since all the corrosion parameters are present [19].

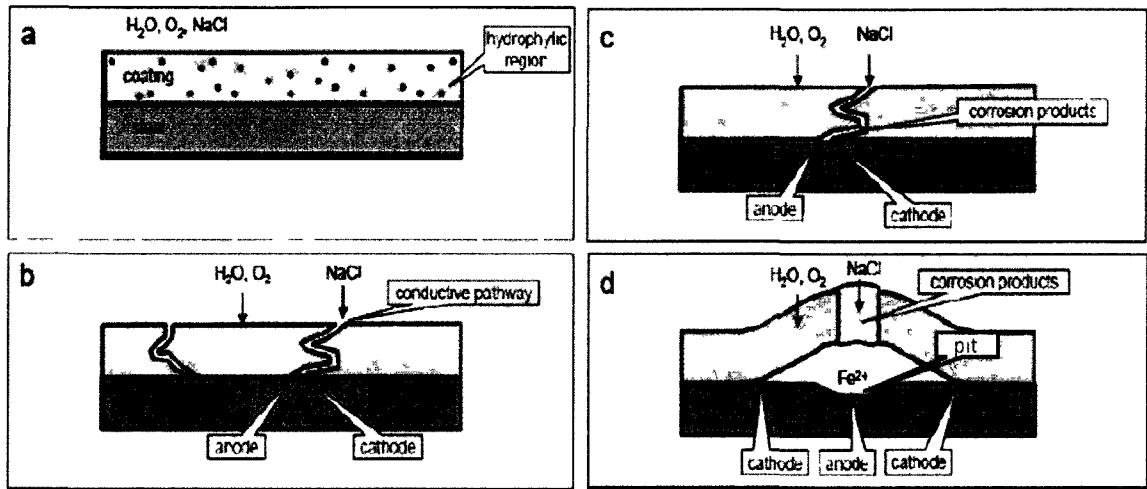
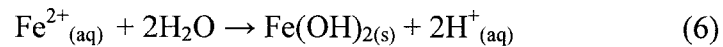


Figure 7. Stages of coating degradation and undercoating corrosion (adapted from [19]).

In the next step, the corrosion cell is formed near the conductive pathway or defect (Figure 7c). The anode forms at the bare metal at the base of the pathway. Due to hydrolysis of metal ions produced at the anodic site, a decrease in local pH is observed (iron used as an example) (Equation 6).

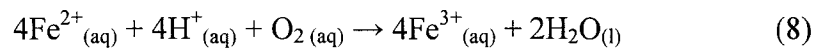


In the marine environment also aggressive ions such as  $\text{Cl}^-$  will flow to the anode (i.e. corrosion initiation site) to preserve electroneutrality (Equation 7):



This reaction starts pitting corrosion that develops when the anodic area is small relative to cathodic area (Figure 7d). As a result of reduction in pH, autocatalytic mechanism of

pit growth is created where HCl solution in the pit accelerates anodic metal dissolution and increases chloride concentration in the pit. Insoluble loose porous hydrated iron(III) oxide (Fe(OH)<sub>3</sub>) forms at the pit mouth when OH<sup>-</sup> from the cathodic site combines with ferric ions that are formed when ferrous ions diffuse out of the acid pit interior and further react with hydrogen ion from water and dissolved oxygen and are oxidized (Equation 8) .



Fe(OH)<sub>3</sub> slowly transforms into red-brown Fe<sub>2</sub>O<sub>3</sub>·H<sub>2</sub>O, commonly known as “rust”. In the same time, the cathode is formed under the coating near the defect or conductive pathway (Figure 7c). As shown in Equation 2 electrons produced at the anodic site are consumed at the cathode which results in formation of hydroxyl ions [1, 2]. OH<sup>-</sup>, besides combining with metal ions, can also react with cations that diffused through the coating (such as Na<sup>+</sup> from the salt water) and increase in local pH is produced. In case of a degraded or not well adhered coating, the pathways of ion exchange between cathode and anode are formed more easily and corrosion rates are higher. The increase in pH together with osmotic forces reduces bonding between the metal and the organic coating. As a result the coating is disbonded at its interface with the metal (Figure 7d). Two main reasons why this alkalinity causes such failure are saponification of the coating (for coating formulations containing ester bonds) and dissolution of the oxide layer at the interface that is responsible for metal/coating adhesion [13, 19]. In some coatings blisters are formed that can grow in size and eventually coalesce resulting in total delamination that

exposes metal to its environment and corrosion can progress in an uninhibited way [1, 19]. This coating degradation mechanism is called **cathodic disbondment or cathodic delamination** and usually applies to steel substrates [20].

**Anodic undermining** is another mechanism for propagation of undercoating corrosion. Aluminum substrates are especially susceptible to anodic undermining. In this case loss of adhesion between the metal substrate and organic coating is caused by anodic dissolution of the metal or its oxide [19, 21]. Unlike in cathodic delamination mechanism, the anodic reactions in this case happen at the blister edge. Anodic undermining can be caused by coating defects such as scratches but in most cases it relates to a corrosion sensitive area under the coating such as from impurities from cleaning or blasting procedures [20, 21]. Once the corrosive environment has penetrated to the metal surface this area becomes active and metal corrodes. Initially the corrosion rate is low but an osmotic pressure, caused by buildup of soluble corrosion products, encourages blister growth. From then on the blister grows due to an anodic crevice corrosion mechanism. The basic driving force for crevice corrosion is a differential aeration cell (Figure 8) (corrosion is driven by potential differences between the aerated and oxygen depleted regions). As the amount of liquid in the blister increases, local conditions cause an imbalance in the oxygen. The diffusion of oxygen into the cavities at the edge of the blister is impeded and results in these areas becoming anodic. The surrounding metal that has an easy access to oxygen becomes the cathode. Metal ions formed in these cavities migrate outside to react with the hydroxide ions at the cathode and corrosion products are

formed at the mouth of the cavity. As the process progresses metal corrodes away and detaches from the coating that is pushed up by forming corrosion products.

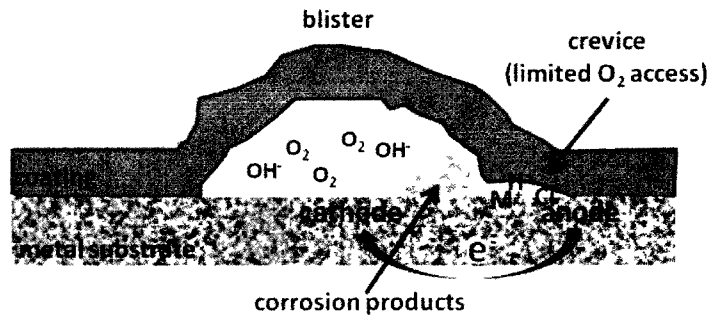


Figure 8. Crevice corrosion of the metal substrate under the protective coating.

The mechanism of crevice corrosion is similar to pitting corrosion and in the presence of Cl<sup>-</sup> has autocatalytic character. As a result filiform corrosion can occur that represents a specialized form of anodic undermining [19, 20]. Filiform corrosion has been observed under thin organic coatings on steel, aluminum, magnesium and zinc (coated on steel) [1, 20]. This type of corrosion propagates from the initiation site (edge of the blister) as narrow 0.05-3 mm-wide thread-like filaments under the coating (right image in Figure 9). Filiform corrosion penetrates the metal only superficially and causes mainly a cosmetic problem [1]. The filaments consist of actively corroding anodic head and inactive cathodic tail filled with corrosion products (left image in Figure 9).

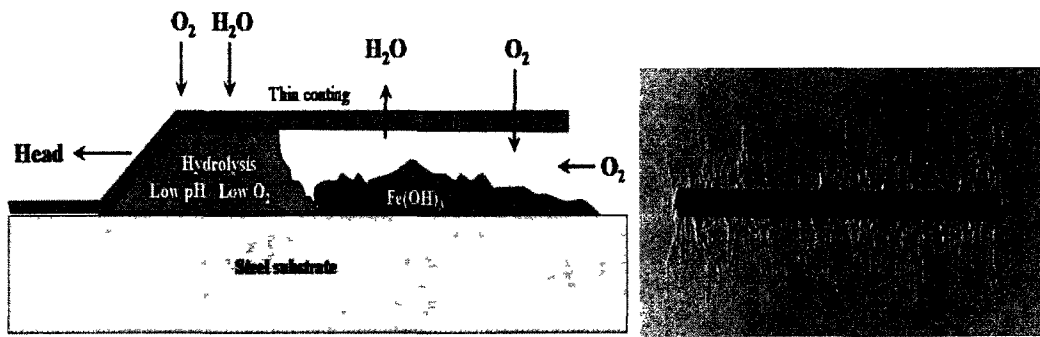


Figure 9. Corrosion filament (left image) [22] and filiform corrosion on aluminum panel coated with polyester paint (right image) [23].

Due to metal dissolution followed by hydrolysis and  $H^+$  liberation (Equation 6) pH as low as 1 is generated at the head. Atmospheric constituents such as soluble chlorides or sulfides ions assist acidification and speed up the corrosion rate [1, 20]. Delamination of the coating takes place at the active head. As the head moves, the filiform grows in length.

### 1.2.3 “Smart Polymeric Coatings” for Corrosion Protection

Polymeric coatings, in addition to their passive protecting and aesthetic functions, are increasingly being designed to serve active roles in response to internal/external stimuli as so-called “smart coatings” [24]. One widely studied application of these types of materials is in metal-corrosion protection. Autonomous self-healing films, for example, have received great attention recently [24, 25, 26], where physical damage in a coating is self repaired to recover barrier properties before metal corrosion occurs. Another stimuli-responsive approach is the use of inhibitors incorporated within the coating that are released “on demand” when corrosion occurs [27, 28, 29, 30], to effectively halt further

damage. The two approaches described above function to extend the useful lifetime of the coating by attempting to prevent or minimize the impact of the corrosion reaction. However, one strategy of particular significance that has not yet been adequately addressed, especially for epoxy-based coatings on metal, is the ability for a coating to detect and report early stage of metal corrosion under the coating or at the coating's defects before any visible sign of it can be seen. A coating that reports the onset of corrosion could, consequently, signal when maintenance should be performed to prevent further metal damage.

### **1.3 Early Corrosion Detection Methods and its Significance**

Obvious results of metal corrosion (e.g. rust), than can be easily observed after the coating fails (e. g. blistered, cracked or chipped coating,) are the latter stage of a complex and dynamic process that begins at the microscopic level under the coating or in the flawed areas of the coating. One of the ways to prevent catastrophic failure of the material and to increase the lifetime of the structures made of this material is to assess the early stages of corrosion. Therefore corrosion progress can be monitored and further material damage prevented by providing maintenance on a needs basis when it is relatively inexpensive.

Many methods have been used to detect undercoating metal corrosion before it becomes severe. Especially desired ones are so called “nondestructive testing and evaluation methods (NDT&E)” that do not require removing the coating from the metallic surface as



opposed to “tear down” inspections. Both microwave [31] and millimeter wave [32, 33] nondestructive methods were used successfully to detect both steel and aluminum corrosion under the paint by sensing the differences in dielectric properties of the coating when corrosion layer is present at the metal/coating interface. Also infrared thermography method [34] was applied using infrared camera to detect carbon steel corrosion by monitoring the temperature differences at the surface after heating the metal plate. Another NDT&E method to detect aluminum undercoating corrosion is eddy current testing [32] that uses electromagnetic induction to detect cracks, discontinuities or pits in the metal. For steel surfaces also X-ray techniques [35] were applied to evaluate corrosion beneath the organic coating by detecting and indentifying corrosion products. Even though all these methods were successfully applied to assess undercoating corrosion in a practical application they all require the detecting systems to be “delivered” to the inspected areas. Desired corrosion detection system then should incorporate both NDT&E methods with *in-situ* detection.

### **1.3.1 *In-situ* Early Corrosion Detection Methods**

Fiber optics were used as an example of *in-situ* non-destructive technique for monitoring steel corrosion in concrete [36]. In this case fiber optics bundles were simply detecting the brown color of rust formed on steel, which is formed in a later stage of corrosion. Another method involves use of small piezoelectric wafer active sensors (PWAS) [37] that can record and monitor corrosion in aluminum pipelines. Even though the above mentioned *in-situ* sensors can be potentially embedded in the coating, they require

positioning them in the right spot otherwise corrosion can be missed since undercoating corrosion tends to be localized. In addition, all the NDT&E methods stated above require the use of often complex and expensive equipment and hardware. Another challenging matter when using these sensing systems involves proper and fast data interpretation.

#### 1.3.1.1 In-situ Early Corrosion Detection via Indicator Molecules Embedded in Protective Organic Coating

A perfect corrosion sensing method will be both non-destructive and *in-situ* detection where the sensor is incorporated into the whole coating or the coating itself serves as a sensor and data output is easy to interpret and analyze. This can be realized by incorporating indicator molecules into coating formulations that detect the onset of corrosion because of their interaction with ions generated during corrosion reactions. As a result of this interaction, the color or fluorescence change of the indicator can be observed or recorded. A simple detection method based on this concept was reported by Zhang and Frankel [38] utilizing high pH-sensitive compounds in an acrylic coating applied on an aluminum substrate, which change their color or fluorescence as a result of an increase in the pH at cathodic areas of corrosion. A similar approach was also reported by Calle and Li [27], in which they used pH responsive microcapsules that release an indicator in polyurethane coatings at the alkaline cathodic areas of corrosion. For metal substrates, however, the widely used protective coatings are epoxy-based. Although the alkaline pH-sensing approach seemed to work well in acrylic and polyurethane coating systems, it proves to be very challenging in epoxy coatings. Johnson and Agarwala

attempted the use of fluorescein in an epoxy primer coating applied onto an aluminum plate and reported that the indicator became “prematurely fluorescent” in the epoxy coating [39]. If alkaline pH-sensitive compounds can be ionized prematurely by coating formulation components (such as the alkaline amine hardener in epoxy coatings) they will not be able to sense corrosion by the same trigger mechanism. An alternative corrosion-sensing approach involves the interaction of an indicator with metal ions liberated during the corrosion reaction or low pH at the anodic site of corrosion, where actual metal dissolution happens, resulting in a change in the fluorescence of the probe. By using a fluorescent indicator, better sensitivity can be achieved since the detection limits in solution for fluorescence are lower by factors of  $10^2$ - $10^4$  than for color changing species [40]. Different compounds, that change their fluorescent characteristics depending on pH or upon interaction with metal ions, have been attempted for corrosion detection on aluminum substrates [39, 40, 41, 42]. Although success of various extents was reported in the detection of aluminum corrosion, no success has been reported, to the best of our knowledge, describing such an indicator in an epoxy coating detecting steel corrosion.

#### 1.3.1.2 The Ideal In-situ Corrosion Indicator

A desired fluorescent probe for corrosion detection should interact with ions liberated during corrosion ( $\text{OH}^-/\text{H}^+$  or metal ions) resulting in “turn-on” fluorescence, in contrast to quenching reactions that are more common with fluorescence probes. The “turn-on” approach is more practical and useful since it is simply easier to see small areas that

fluoresce (when the background does not) than to see a slight decrease in overall fluorescence as in case of quenching reactions. The initially nonfluorescent indicator, after incorporated into the epoxy coating, would ideally become highly fluorescent in areas where corrosion occurs before any obvious sign of metal damage can be observed by the naked eye. Also, an ideal fluorescent indicator suitable for epoxy coatings should not become prematurely fluorescent when mixed with precursor components (i.e. epoxy resin or hardener) during the preparation of the coating.

#### **1.4 Objective and Outline of this Thesis**

The objective of this thesis is to design a smart indicator/epoxy coating system to detect early stages of metal corrosion. This smart coating, in addition to its passive protecting function, would serve an active role and *in-situ* detect early stages of metal corrosion via the indicator molecules embedded in the coating. These sensing molecules would become fluorescent, due to their interaction with ions released at the corrosion site, and their “turn-on” fluorescent response would be easily and nondestructively detected.

In chapter 2, the possibility of using acid-based indicators, embedded in the epoxy coating, to sense increase in local pH at the cathodic site of corrosion is explored. It is shown that these types of molecules are challenging to utilize as corrosion sensors in the epoxy coating due to their interaction with the matrix components and the possibility of premature indicator response. Chapter 3 describes the use of the FD1 molecule as a steel corrosion sensor due to its ability to selectively sense  $\text{Fe}^{3+}$  ions. This molecule, when

embedded in the epoxy coating, has proven to be an effective early corrosion indicator for steel. In chapter 4 the stability of FD1 in the epoxy matrix is explored. It is shown that FD1 is slightly sensitive to photooxidation but does not prematurely interact with epoxy components. It will also be illustrated that FD1 embedded in the epoxy matrix is capable of sensing corrosion even after prolonged exposure to an aqueous solution. Chapter 5 focuses on the FD1 sensing mechanism. FD1 is shown to form a fluorescent complex with  $\text{Fe}^{3+}$  ions in non-aqueous solution, however in an aqueous solution of  $\text{Fe}^{3+}$  the low pH of the ferric salt solution will be shown to be responsible for FD1 “turn-on” fluorescence. In chapter 6, FD1 is explored as an early corrosion indicator for aluminum due to its sensitivity to low pH. The effectiveness of FD1 as an aluminum corrosion sensing molecule in an epoxy matrix will be shown. In chapter 7, overall conclusions from the work comprising this thesis are described and a future outlook will be presented.

## CHAPTER 2

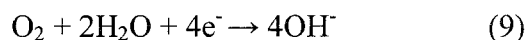
### CORROSION DETECTION BASED ON HIGH pH SENSING

*Summary.* In this chapter, the possibility of using acid-base indicators embedded in an epoxy matrix to sense increase in local pH at the cathodic site of corrosion is described. The behavior of two different chromophoric acid-base indicators, phenolphthalein and Alizarin Yellow R sodium salt, in an epoxy matrix (both commercial and model) was explored. These types of indicators were found to be prematurely activated by the epoxy components during coating formulation. As a result of this interaction, the indicator color changes and it is not able to respond to alkaline pH. More importantly, after the color of the indicator fades with time, the epoxy matrix is no longer responsive to high pH. Due to the high reactivity of both components of the matrix (epoxy resin and amine hardener), and the possibility of premature response, these type of molecules are excluded from further investigation as corrosion sensors when embedded in epoxy based coatings.

## **2.1 Introduction and Literature Review**

### **2.1.1 Phenolphthalein as a Chromophoric Acid-Base Indicator for Detection of Cathodic Corrosion Reaction**

As described in chapter 1 (section 1.2), at the cathodic site of a corrosion cell, due to reduction of dissolved oxygen, OH<sup>-</sup> ions are produced according to Equation 9:



As a result of this reaction an increase in the local pH occurs. An acid-base indicator, for example **phenolphthalein**, with pKa 9.3, is often used to observe this change in pH on metal surfaces [43]. This chromophore in its undissociated, protonated form is colorless. In pH solutions higher than 8, phenolphthalein changes color to bright pink (magenta) due to deprotonation and delocalization of electrons in the whole molecule (longer wavelength of light can be absorbed). If the pink solution of phenolphthalein is allowed to stand in the presence of excess base, the color gradually disappears [44]. These changes in the molecule's structure are illustrated in Figure 10. Color change for phenolphthalein depending on pH is shown in Figure 11.

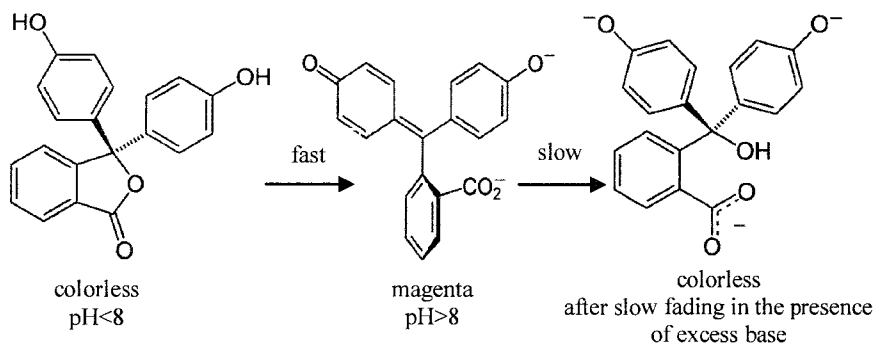


Figure 10. Different forms of dissociation of phenolphthalein [44].

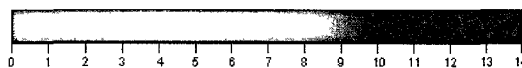


Figure 11. Change in color of phenolphthalein in different pH solutions.

A mixture of phenolphthalein together with  $K_3[Fe(CN)_6]$  (potassium ferricyanide) is known as a ferroxyl indicator and is often used in simple school experiments to show iron corrosion [43, 45]. An iron nail is immersed in a solution of water or neutral electrolyte (e.g. NaCl), an indicator and a stiffening agent (such as gelatin or agar to minimize ion diffusion and preserve the colors formed). When the corrosion starts potassium ferricyanide reacts with  $Fe^{2+}$  ions in acid solution producing insoluble blue pigment, Prussian blue, indicating metal dissolution at the anodic sites. At the same time, phenolphthalein turns pink at the cathodic sites of corrosion where the metal remains intact (Figure 12).



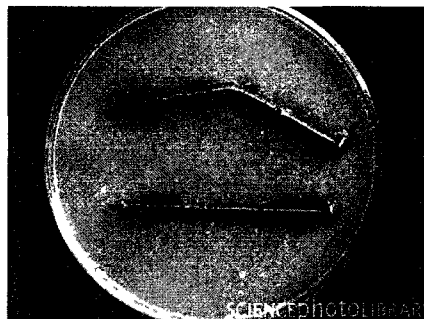


Figure 12. Corrosion of iron nails immersed in agar containing ferroxy indicator [46].

### **2.1.2 Fluorescent Acid-Base Indicators**

Alkaline pH at the cathodic site of corrosion can also be sensed using fluorescent compounds. Fluorescent molecules tend to be organic molecules with a rigid structure and delocalized electrons. These molecules after reaching an excited state, due to the absorption of energy of a specific wavelength, are able to re-emit some of the absorbed energy at a different (but equally specific) wavelength and return to its ground state. Since the emitted photon has lower energy than the absorbed photon the emission wavelength is longer than the absorption wavelength. This energy difference is called the Stokes shift [47, 48]. The emission spectrum is usually a mirror image of the absorption spectrum. Fluorophores absorb a range of wavelength of light energy and also emit a range of wavelength. Within these ranges are excitation maximum ( $\lambda_{ex,max}$ ) and emission maximum (or wavelength of maximum fluorescent intensity;  $\lambda_{em,max}$ ).  $\lambda_{em,max}$  can shift to a shorter wavelength (blue-shifting) or a longer wavelength (red-shifting) depending on the environment. The other important experimental parameters describing fluorescent materials are the fluorescent emission intensity at a particular wavelength, the fluorescent quantum yield and the fluorescent lifetime. Quantum yield describes the emission

efficiency of a given fluorescent material and can be defined as the ratio of photons emitted over photons absorbed through fluorescence. Fluorescent lifetime is a measure of the lifetime of the excited state (i.e. it is the average time the molecule stays in the excited state before emitting a photon and returning to the ground state). Fluorescent emission intensity, quantum yield and fluorescent lifetime can be altered depending on the local environment [47, 48].

The advantage of using fluorescent species, over chromophores, to sense alkaline pH at the cathodic site of corrosion, is that they show better sensitivity [40]. Similar to chromophores, pH-sensitive fluorescent compounds show different fluorescent intensity depending on their ionization state. As an example of this type of molecule, fluorescein is shown in Figure 13. The deprotonated form of fluorescein (at high pH) exhibits fluorescence (middle and right structures in Figure 13), while the protonated species does not (left structure in Figure 13) [49].

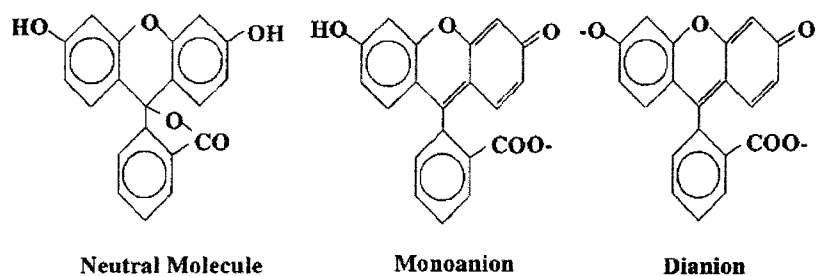


Figure 13. Different ionic forms of fluorescein occurring in aqueous solution at pH's exceeding 3.3. The dianion is highly fluorescent [49].

pH-sensitive fluorescent dyes such as -methylumbelliferone, -naphthol and fluorescein were applied directly on aluminum- and gold- metalized integrated circuit (IC) devices to

detect pH changes associated with corrosion reaction [50]. Solution of fluorescein was also applied directly on aluminum alloys (6061 and 2024) to indicate pH changes and surface chemistry over and around corrosion active sites [51]. These experiments were performed to investigate localized corrosion directly on metal surfaces.

### **2.1.3 *In-situ* Early Corrosion Detection at Cathodic Site of Corrosion via Indicators Embedded in Protective Organic Coating**

Since it was proved that pH-sensitive chromophores and fluorophores can be successfully used to sense the cathodic site of corrosion, there were also a few attempts to use them as *in-situ* early corrosion indicators by incorporating them into protective organic coatings. Frankel et al. [38] incorporated pH sensitive chromophores (phenolphthalein and bromothymol blue) and fluorophores (7-hydroxycoumarin and coumarin) into a clear acrylic coating to sense corrosion. These indicators were chosen because they change color (chromophores) or become fluorescent (fluorophores) in alkaline pH. The indicating paint mixed with phenolphthalein (2.4 wt%) was coated on the surface of aluminum alloy samples (Al 2024-T3) and subsequently immersed in a corrosive 1.0 M NaCl solution. After only 4 h of immersion red-colored spots appeared in the sample. After 9 h, pits developed in the vicinity of the red-colored areas (Figure 14) proving that the acrylic-phenolphthalein coating can sense localized increase in pH that accompanies pitting corrosion. This sensing system was also successful in detecting crevice corrosion [38]. Frankel et al. also were able to detect corrosion via fluorescing compounds at at

least an order of magnitude lower concentration compared to the color responding indicator.

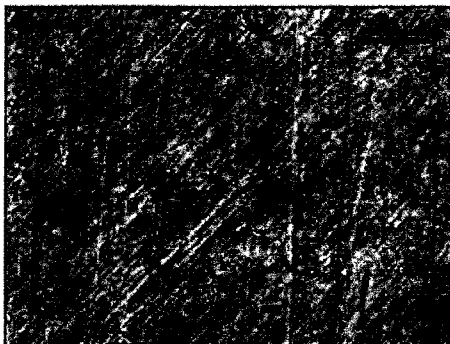


Figure 14. Optical micrograph of Al 2024-T3 coated with acrylic-phenolphthalein (2.4 wt%) after immersion in 1 M NaCl for 9 hrs [38].

Phenolphthalein was also used in a system where it could be released from pH-sensitive microcapsules embedded in a clear or light-colored polyurethane coating, at the cathodic site of localized corrosion [27]. Although use of pH-sensitive compounds in different clear or lightly colored organic coatings has been proposed to detect increase in local pH at the cathodic site of corrosion, no reports of successful use of these compounds in epoxy coatings can be found.

Johnson and Agarwala [39] attempted the use of pH-sensitive fluorescein in an epoxy primer coating applied onto an aluminum plate and reported that the indicator became “prematurely fluorescent”. This phenomenon can be ascribed to the premature chemical reaction between fluorescein and the reactive components of the epoxy coating itself. If pH-sensitive molecules can be ionized prematurely by coating components they will not be able to sense corrosion by the same trigger mechanism.

## **2.2 Objectives of this Chapter**

In this chapter the possibility of using pH indicators in epoxy based coatings to sense cathodic reactions of metal corrosion was investigated. The amines used as hardeners in epoxy coating formulations are bases with pKa values in the 9-11 range. Thus the potential interaction between hardener and the indicator that will result in color change of the indicator was expected when formulating the coating. However once the epoxy is fully cured, the assumption is that the pH of the matrix will have dropped below the pKa of the indicator as the amine groups will have been reacted. A question is, at this lower matrix pH, how long will the initial premature response of the indicator persist before returning to its protonated/colorless state? How will the rigidity of the now cured matrix impact the indicator's ability to return to the protonated state? Once incorporated in the cured epoxy and back in the protonated state, will the indicator be able to be ionized again in a new alkaline environment and return to the colored state to report corrosive conditions? The work described in this chapter attempts to answer these questions.

In the preliminary experiments of this chapter chromophoric acid-base indicators were used since their response is easier to observe by the naked eye, especially when embedded in a clear matrix, as compared to changes in fluorescence. Ultimately, the use of pH-sensitive fluorophores, due to their higher sensitivity, was planned.

## **2.3 Experimental Section**

### **2.3.1 Reagents and Materials**

Phenolphthalein was purchased from Acros Organics. Alizarine Yellow R, sodium salt (AYR), 96%, pure, was purchased from Sigma-Aldrich. Commercial Clear Epoxy-Polyamide coating, MIL-DTL-24441C, type III, was purchased from NCS Coatings, Inc. D.E.R.<sup>TM</sup> 332 Epoxy Resin (high purity diglycidyl ether of bisphenol A, DGEBA) was purchased from The Dow Chemical Company. 2,2'-(ethylenedioxy)bis(ethylamine), 97% (EBE) was purchased from Alfa Aesar. Triethanolamine (TEA), 99% was purchased from Pfaltz&Bauer. Sodium hydroxide (NaOH), reagent ACS, pellets, 97+% was purchased from Acros Organics. Solutions with different pH (9 and 10) were prepared by dissolving appropriate amount of NaOH pellets in DI water. Ethyl alcohol (ethanol), 95%, ACS/USP grade, was purchased from Pharmco-AAPER and commercial alcohols.

### **2.3.2 General Sample Preparation in this Chapter**

In the experiments with the commercial clear Epoxy-Polyamide coating (AA1-06), component A (hardener) and component B (epoxy resin) were mixed as suggested by the producer (1:1 volume ratio). The indicator was first mixed with component A and component B was subsequently added. Phenolphthalein content was 1 wt% based on the whole mixture. In the experiments with the model clear epoxy coating (AA1-16B, AA1-

17B, AA1-18B, AA1, AA1-39A, AA1-39B, AA1-20, AA1-21 and AA1-22) the indicators were first mixed with EBE (phenolphthalein content was 1 wt% and AYR was 0.06 wt% based on the whole mixture) and then DGEBA was added to the mixture. To obtain different matrix rigidity (by crosslinking), the ratio of epoxy groups (from DGEBA) to hydrogen from amine (EBE) varied depending on the sample. Additional details on other experiments are shown in the text.

## **2.4 Characterization Methods**

Glass transition temperature ( $T_g$ ) was determined using differential scanning calorimetry (TA Instruments Q2000 temperature-modulated DSC) with an overall heating rate of 3 C/min, an amplitude of +/-2 C, and a period of 60 s. Samples were first pre-heated in the DSC to 110 C to produce stable and uniform contact of the sample with the DSC pan. The temperature range of data collection was from 10 C to 120 C and two cycles were recorded for each sample.

Visual color change of the samples with time after mixing with the matrix coating was monitored with the naked eye. The pictures of the samples were taken with a digital camera.

## 2.5 Results and Discussion

### 2.5.1 Experiments with Phenolphthalein

The first choice for testing the concept of using an acid-base indicator in the epoxy matrix to sense cathodic corrosion reaction was a chromophore, phenolphthalein. This indicator was chosen because its color change (from colorless to magenta) occurs at alkaline pH as shown in Figure 11.

.

#### 2.5.1.1 Experiments with Phenolphthalein in Clear Commercial Epoxy Matrix

In my first experiment (AA1-06) I mixed phenolphthalein (1 wt%) with commercial clear epoxy coating (MIL-DTL-24441C, type III). This coating consists of two components: component A (amidoamine resin in 1-butanol with additives) and component B (epoxy resin with additives). After mixing of all of the components, the color of phenolphthalein in the epoxy matrix changed with time as shown in Figure 15.

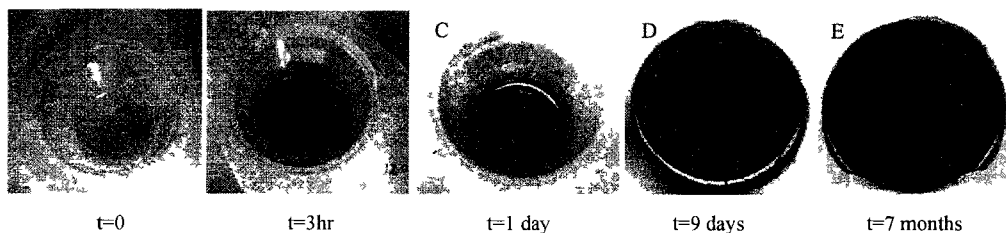


Figure 15. Color change of commercial clear epoxy coating with 1 wt% phenolphthalein (AA1-06)



Initially, the cloudy yellow mixture changed color to pink-red after 3 h (system not fully cured, Figure 15B). Then the color become more intense after 1 day (system fully cured, Figure 15C) and subsequently slightly faded with time (Figure 15E). Thus it is obvious that phenolphthalein after embedding in a commercial epoxy matrix cannot sense high pH related to corrosion because of its premature response and color change to magenta, followed by a very slow fading of that color. A further question was, in the case that the initial color would eventually fade, whether the indicator's ability to sense a new increase in pH would be recovered. To confirm that the color change of the indicator is due to the basic character of the hardener, component A (amidoamine resin) was mixed with phenolphthalein. Initial color of this mixture was slightly pink but changed to a more intense hue after 1 day as seen in Figure 16A and B. Surprisingly however, the intensity of the color was not as high as in the case where both components were mixed with the indicator (Figure 15C), even though the concentration of phenolphthalein was the same in both cases. This fact would suggest that the epoxy resin itself influences the indicator's response as well. After 9 days color seemed to fade and changed to orange (Figure 16C). This color change can be ascribed to the fact that phenolphthalein color fades when it is allowed to stand in the presence of excess base for an extended period of time [44]. This fading did not occur in the cured matrix as fast probably due to the fact that there is no base excess present in the system anymore after the coating is cured.

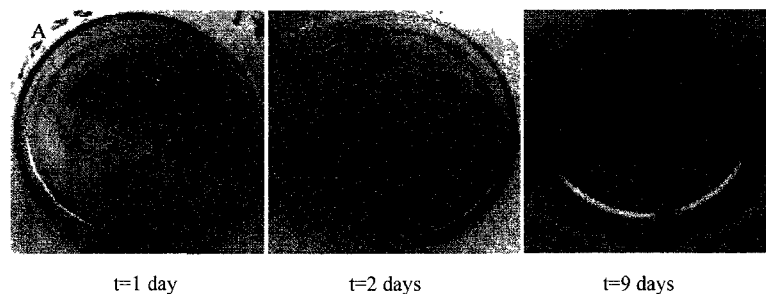


Figure 16. Color change of component A of commercial clear epoxy coating after mixing with 1 wt% phenolphthalein.

When the component B (epoxy resin) was mixed with phenolphthalein no color change was observed. Thus it was concluded that not only the component A causes indicators color change, as expected, but also the component B influences phenolphthalein's chromophoric response, but only when in the mixture with the component A. This finding required further investigation. In order to understand the interactions between the indicator and both of the epoxy coating components at different matrix rigidity we chose to move to a model epoxy system.

#### 2.5.1.2 Experiments with Phenolphthalein in Clear Model Epoxy Matrix

In order to more systematically evaluate the mechanism of color change of pH responsive indicators in an clear epoxy matrix, and to assess their ability to be reprotonated to a colorless form in that polymeric environment, I decided to move to a simple model epoxide/amine system without any additives that could potentially influence the color response. For the model epoxy system, diglycidyl ether of bisphenol A (DGEBA) was chosen as an epoxy resin and 2,2'-(ethylenedioxy)bis(ethylamine) (EBE) as the amine hardener. Chemical structures of these compounds are shown in Figure 17.

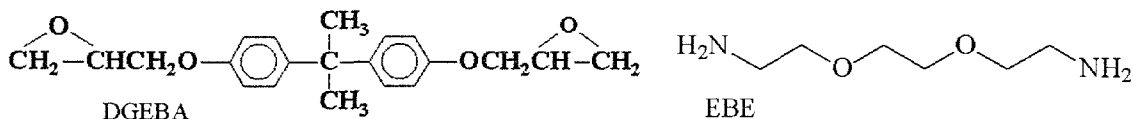


Figure 17. Chemical structures of DGEBA and EBE.

EBE has only 4 hydrogen atoms able to react with DGEBA which results in less crosslinked structure of the matrix (lower glass transition temperature,  $T_g$ ) and thus diffusion of the molecules and their interactions are expected to occur faster than in the case of the commercial system. The reduction in amine groups usually increases hydrophobicity of the system. However for the indicator to work and to sense increase in pH, coating has to absorb some water, thus the two ether groups in the amine structure will help increase the hydrophilicity and by that plasticize the epoxy. Thus by using EBE, both reduction in the matrix rigidity and satisfactory hydrophilicity of the system can be accomplished.

To systematically study the effect of matrix rigidity as well as relative component concentrations of reactants on the indicator's color change, I prepared samples with different ratios of epoxide ring from DGEBA to hydrogen from the EBE ( $\nabla \text{NH}$ ). The phenolphthalein content was 1 wt% in all cases. Sample AA1-16B was the most rigid one since  $\nabla \text{NH}$  ratio was 1:1 (fully cured,  $T_g = 75^\circ\text{C}$ ). Sample AA1-17B was softer ( $\nabla \text{NH}$  ratio of 3:2,  $T_g = 40.5^\circ\text{C}$ ) and AA1-18B was the softest epoxy matrix ( $\nabla \text{NH}$  ratio of 2:1,  $T_g = 28^\circ\text{C}$ ). First EBE was mixed with phenolphthalein resulting in appearance of the light pink color. Then DGEBA was added and color became clear after

mixing all of the components. However with time a pink color with different intensity developed again in all samples. The color change of the samples is shown Figure 18.

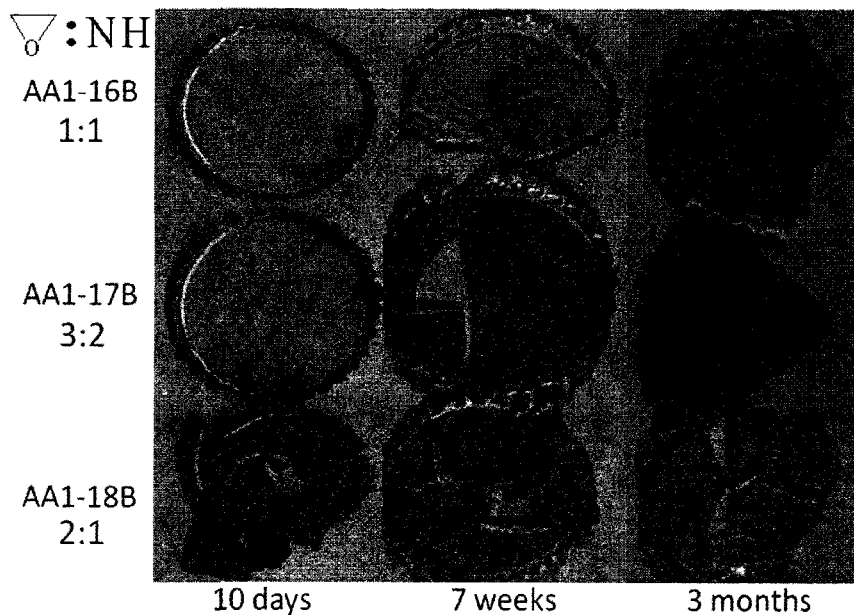


Figure 18. Color change of clear model epoxy matrix with different rigidity mixed with 1 wt% of phenolphthalein.

As it can be seen in the Figure 18 color of the softest sample (AA1-18B) developed the fastest but then faded with time. This proved that the color change is diffusion controlled process and depends on the matrix rigidity. This finding was confirmed when the samples were placed at elevated temperature (60°C, experiments AA1-31 and AA1-32). In case of the more rigid AA1-16B sample, color became more intense with time at 60°C but did not fade even after 1 month. This lack of fading can be explained by the fact that there is not enough mobility in this rigid matrix even at elevated temperatures to complete the reactions between the matrix and the indicator. In case of the medium rigidity AA1-17B, color developed to bright pink only after 15 minutes at 60°C and then faded to colorless after 2 days. The least rigid AA1-18B became colorless after only 2 hr in the oven. The

ability of the AA1-18B sample to sense alkaline pH after the indicator's color fading was examined by putting it in an aqueous NaOH solution (pH 9.5). Color of the solution turned light pink probably due to leaching of the unreacted phenolphthalein and its ionization in alkaline solution. However color of the sample did not return to pink even after 3 weeks at both, room temperature and elevated temperature, in NaOH solution. This experiment proved that phenolphthalein when embedded in epoxy matrix is not able to sense increase in pH after its initial color disappearance.

As mentioned above, just mixing phenolphthalein with EBE resulted in the appearance of a slight pink color. However when water was added to that mixture, bright magenta color appeared since more phenolphthalein was deprotonated. Thus the change in color intensity in AA1-16B, AA1-17B and AA1-18B samples with time could be explained by the fact that water is absorbed more rapidly in the softer matrices (AA1-17B and AA1-18B) and thus the intense color in less rigid samples appears faster due to ionization of the indicator by the amine. However the softer matrices had an excess of DGEBA that should cause full EBE conversion to a tertiary amine. I investigated the ability of the cured matrix (after 1 month of curing) to change color of the phenolphthalein in experiment AA1-30; sample without the indicator but with the same DGEBA-EBE content as in AA1-18B (sample AA1-18A) was placed in water-ethanol solution of phenolphthalein at 60°C (to speed up the indicator diffusion into the matrix). Color change of the sample to magenta was observed especially at the edges of the sample after only 15 minutes. This color was persistent even after 1 month in solution. At this point all EBE in this sample should be reacted to tertiary amine. Thus the color response of the

indicator can be explained only by 1) its interaction with tertiary amine that is present after and during the curing reaction, or by 2) the reaction between the indicator's phenol group and DGEBA's epoxide ring in the presence of the tertiary amine. However the color of the indicator did not fade with time as in case of AA1-17B and AA1-18B samples. Perhaps at this point the matrix is cured to the point where molecular mobility (diffusion) is restricted and the reactions and thus fading can not be completed.

Yet if the color change from magenta to colorless (as observed in AA1-17B and AA1-18B samples) is only due to indicator being exposed for extended period of time to excess of amine, then when the faded sample is placed in low pH solution it should be able to slowly reprotonate to magenta color (as shown in Figure 10). In experiment AA1-38 I placed a piece of faded, colorless AA1-18B sample in aqueous solution of HCl (pH 1) at 60°C. Color of the sample remained clear even after 4 hr in this low pH solution which indicates that the indicator was not reprotonated to its pink form. Thus it was concluded that the indicator fading must be due to reaction with DGEBA in the presence of tertiary amine. This reaction is possible because phenolphthalein (similarly to other acid-base indicators) has phenol group with active hydrogen that is able to react with the epoxy ring in the presence of a weak base such as tertiary amine [17]. The magenta color appears because the indicator is ionized in the first stage of the reaction. Then color goes away as the indicator molecule is built into the DGEBA structure and the delocalization of electrons in the whole molecule (that is responsible for the chromophoric response) is not possible any more. This explanation of the indicator's response in the epoxy matrix was confirmed in experiment AA1-40. In this experiment DGEBA was mixed with

phenolphthalein and a drop of triethanolamine (tertiary amine) in a capped vial (colorless mixture). The mixture was placed in the oven at 70°C to speed up molecular diffusion. No water absorption was possible since the sample was in a sealed container. Initially colorless mixture turned into light magenta after 2 hr and then to bright magenta after 6 hr. After 1 day this color disappeared. These color changes are illustrated in Figure 19, vial 3. It was also clearly seen that the viscosity of the sample changed significantly due to polymerization of DGEBA. It was clearly evident that phenolphthalein reacts with DGEBA in the presence of a tertiary amine causing color change to magenta, since DGEBA mixed with the indicator separately does not change its color (Figure 19, vial 2). Also phenolphthalein mixed with triethanolamine results only in a very light pink color that does not change to colorless even after 24 hr in 70°C (Figure 19, vial 1).

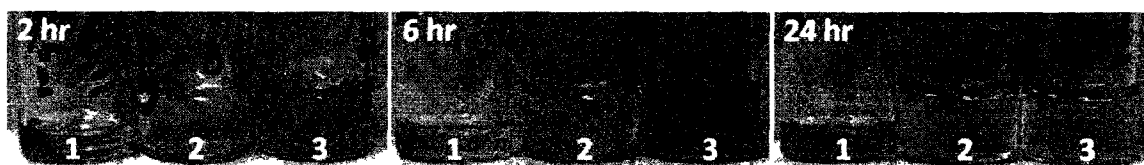


Figure 19. Color change of: TEA and phenolphthalein (vial 1), DGEBA and phenolphthalein (vial 2) and DGEBA with phenolphthalein and a drop of TEA (vial 3) with time at 70°C.

When I added NaOH solution to the faded DGEBA- phenolphthalein- TEA mixture (pH 10), color did not change similarly to the AA1-18B sample after fading. When DGEBA-phenolphthalein mixture was placed in the same NaOH solution, bright pink color appeared instantly in the solution.

To further confirm that DGEBA is the main component responsible for phenolphthalein color change in the epoxy matrix two samples of DGEBA-EBE-phenolphthalein mixtures

were prepared, but this time with the amine in excess; sample AA1-39A ( $\nabla$  NH ratio was 2:3) and AA1-39B ( $\nabla$  NH ratio was 1:2). After mixing, color of the samples was clear and after 7 days only AA1-39B changed to very light pink (AA1-39A remained clear). In both samples after curing, all epoxy rings should be reacted with the amine excess and not able to react with phenolphthalein. Thus it is expected for samples with larger amine excess (AA1-39B) to have more intense color just due to the presence of the amine. Both samples were placed in NaOH solution (pH 9) for 4 days to test the indicator's ability to sense alkaline pH. AA1-39B changed its color immediately to bright pink and sample AA1-39A became slightly pink after some time. Also color of the solutions changed to light pink. This difference in the color response could be due to the rigidity of the matrix (sample AA1-39A is much softer thus diffusion occurs faster). Similar response was observed when samples were placed in DI water due to the further indicator ionization. Even though in these epoxy systems the indicator was able to respond to high pH, they cannot be used in practical applications since they are not fully cured.

Overall response of all model clear epoxy systems with the indicator (EBE + DGEBA+ phenolphthalein) to high pH is shown in (Figure 20). The chromophoric response of the indicator embedded in the epoxy matrix to alkaline pH was only possible in the lightly colored samples (AA1-17B, AA1-16B, AA1-39A and AA1-39B) that did not fade. Sample AA1-18B did not respond to high pH after its color faded. However in the case of the samples with amine excess (AA1-39A and AA1-39B) similar response was observed also in neutral water due to the further indicator ionization after water absorption.



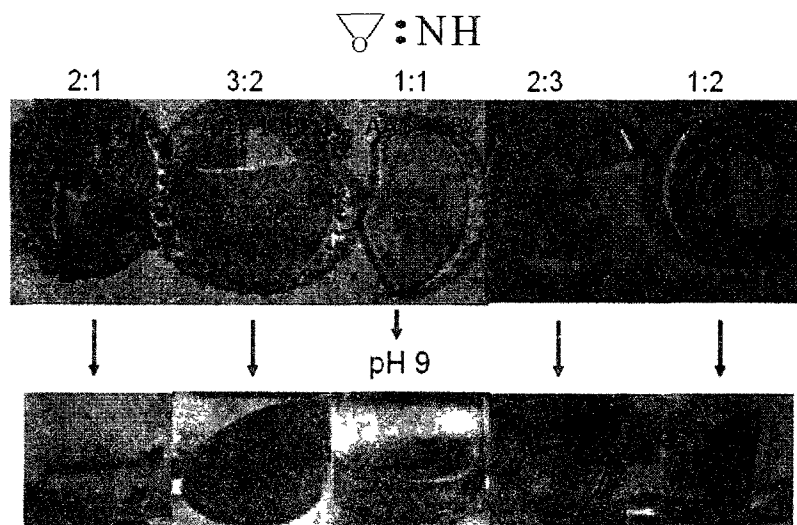


Figure 20. Response of clear model epoxy coatings with phenolphthalein to pH 9 solution.

The overall conclusion from this series of experiments is that phenolphthalein simply mixed with an epoxy coating cannot be used as an alkaline pH-sensing system because both components (primary amine and DGEBA) can react with the indicator causing its color change (indicator is “prematurely activated”). Moreover, even when the color of the indicator fades with time in the soft epoxy matrix, the coating is not able to sense alkaline pH any more. The degree of the interaction between phenolphthalein and the epoxy coating components (and thus a chromophoric response) depends on the formulation, temperature and time (diffusion controlled process).

## 2.5.2 Experiments with Alizarin Yellow R

To further explore the interactions between acid-base indicators and an epoxy matrix I decided to use a different indicator with a higher pKa for color change than phenolphthalein. These experiments were performed to examine whether any pH sensitive indicator would have the potential for interacting with the epoxy matrix preventing them from being used in this type of coating without some sort of protection (e.g. encapsulation). I chose Alizarin Yellow R (AYR) (Figure 21) since its pH range for color change is 10.1-12.0 (Figure 22).

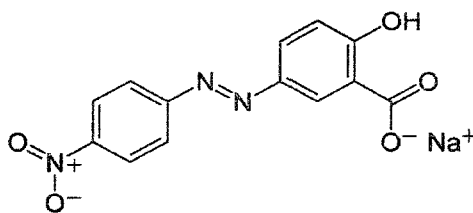


Figure 21. Chemical structure of Alizarin Yellow R sodium salt.

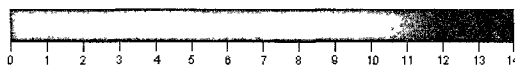


Figure 22. Change in color of Alizarin Yellow R in different pH solutions.

It was expected that AYR would not change to red color when reacted with EBE due to its high pKa, thus will still be able to sense high pH after the coating is formed and in response to alkaline corrosion sites, in the case where the color change of the indicator happens only due to reaction with the amine.

### 2.5.2.1 Experiments with Alizarin Yellow R in Clear Model Epoxy Matrix

AYR in the solid state is in a form of rusty-orange crystals. When mixed with EBE it gave orange color proving that EBE itself does not ionize this indicator. However after water addition, color of this mixture changed to bloody red.

Similarly to the experiments with phenolphthalein I also prepared samples with different ratios of epoxide ring from DGEBA to hydrogen from the EBE ( $\nabla^{\circ} \text{NH}$ ) (samples AA1-20, AA1-21 and AA1-22 with the  $\nabla^{\circ} \text{NH}$  ratios identical as in AA1-16B, AA1-17B and AA1-18B respectively). The AYR content was 0.06 wt% (based on the whole mixture) for all the samples. The results were identical to those obtained when phenolphthalein was used as an indicator. Instantly after mixing all of the samples had a bright orange color that developed to red after different times depending on the matrix rigidity ( $T_g$ ). Also the softest matrix color (sample AA1-22) faded with time from dark red (after 1 month) to orange-red (after 3 months). The changes in the color of the samples are shown in Figure 23.



Figure 23. Color change of clear model epoxy matrix with different rigidity mixed with 0.06 wt% of Alizarin Yellow R.

## 2.6 Conclusions

The experiments involving acid-base indicators, phenolphthalein and AYR, embedded in the commercial (phenolphthalein) and model (phenolphthalein and AYR) epoxy systems, proved that independent of the pKa of the indicator there is a possibility of its interaction with an epoxy matrix. As a result of this interaction, the indicator is prematurely activated and thus not able to respond, at least with the same sensitivity, to alkaline pH. More importantly, when the color of the indicator fades with time, the epoxy matrix is no longer responsive to high pH. Unexpectedly, not only the amine hardener is responsible for the color change of the indicator, but also epoxy rings from the epoxy resin, in the

presence of a weak base (such as tertiary amine), can react with the phenol groups of the sensing molecule. The most probable scenario explaining these interactions is that:

First, the weak base opens the epoxy ring.

The ion formed this way is able to abstract active hydrogen from the phenol group of the indicator which causes its ionization (magenta color appears for phenolphthalein and red color for AYR).

Then the ionized indicator is built into the structure of DGEBA through an ether bond.

That causes changes in the indicator's molecule form to the unionized state (colorless for phenolphthalein and yellow for AYR).

Since in the commercial epoxy coatings tertiary amines are always present, either added to the formulation as an accelerators (or catalysts) or produced on consumption of the primary and secondary amine, there is always a potential for pre-mature color change of the indicator.

Thus, it was concluded that acid-base indicators should be excluded from further investigation as corrosion sensors when embedded in epoxy based coatings due to the high reactivity of both components of the matrix (epoxy resin and amine hardener) and the possibility of premature indicator response and in some cases inability of the indicator to re-respond after fading of the premature response.

## CHAPTER 3

### EARLY DETECTION OF STEEL CORROSION\*

**Summary.** In this chapter, the successful application of spiro[1*H*-isoindole-1,9'-[9*H*]xanthen]-3(2*H*)-one, 3',6'-bis(diethylamino)-2-[(1-methylethylidene)amino] ("FD1") as a smart indicator in epoxy-based coatings for the early detection of steel corrosion is described. This indicator was chosen as a corrosion sensing molecule due to its claimed ability to selectively sense Fe<sup>3+</sup> ions (that are produced at the anodic site of steel corrosion) and its desirable chemical structure that assures no interaction with the epoxy matrix. The molecule was synthesized in our lab and its response to FeCl<sub>3</sub> was explored. FD1, in solution and embedded in epoxy coating, showed "turn-on" fluorescence upon addition of FeCl<sub>3</sub> solution. Moreover it was successfully utilized as an early steel corrosion detector in model (clear) epoxy coating and more importantly in commercial (filled) epoxy coatings in the presence of pigments. The "turn-on" fluorescence was observed, even at low FD1 concentration (0.5 wt%), by confocal fluorescent microscope and by, more conveniently, an optical microscope with UV light,

---

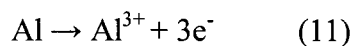
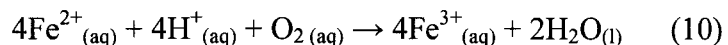
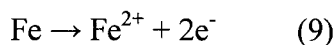
\* Portions of this chapter have been published: Augustyniak, A.; Tsavalas, J.; Ming, W. Early detection of steel corrosion via "turn-On" fluorescence in smart epoxy coatings. *ACS Applied Mater. Interface* **2009**, *1*(11), 2618-2623 (DOI: 10.1021/am900527s). That publication was highlighted by *Chemical & Engineering News* (American Chemical Society weekly magazine) in the October 26, 2009 issue, and was also highlighted in *Tribology & Lubrication Technology* in the February 2010 issue.

which allows easy and non-destructive early corrosion detection of steel before any visible sign of corrosion appears.

### **3.1 Introduction and Literature Review**

#### **3.1.1 New Requirements for an Ideal *In-situ* Corrosion Indicator in Epoxy Based Coatings**

Since the acid-base indicators were excluded as potential corrosion sensors when embedded in an epoxy coating matrix, efforts were shifted to look for a new potential sensing molecule candidate with an appropriate chemical structure. This time, the search was focused on a molecule that is able to sense metal ions (i.e. ferrous/ferric and aluminum ions) produced at the anodic site of corrosion where metals are dissolved according to the following reactions (Equations 9, 10 and 11):



Besides the requirements regarding the ideal *in-situ* corrosion indicator for an epoxy coating discussed in section 1.3.1.2 of chapter 1 (i.e. corrosion sensing via “turn-on” fluorescence), several additional requirements have to be fulfilled to obtain a robust smart corrosion-sensing indicator epoxy system (i.e. an indicator that can be incorporated into



any type of epoxy system independent of formulation). Namely, the new corrosion indicator cannot possess any functional groups that can be ionized by epoxy components (as in the case of acid-base indicators as described chapter 2) or any other reactive groups (such as  $\text{-NH}_2$ ) able to be built into the epoxy structure during curing. Thus there would be no risk of altering the indicator molecule's fluorescence behavior after mixing with epoxy components or interfering with the curing of epoxy coatings.

### 3.1.2 In-situ Fluorescent Aluminum Corrosion Sensing via Complexation with $\text{Al}^{3+}$

Different fluorescent compounds have been attempted for corrosion detection on aluminum substrates due to increase in their fluorescence upon complexation with metal ions. Upon this interaction, chelation enhanced fluorescence (CHEF) effect is produced [40]. As an example, lumogallion (shown in Figure 24) was used to detect  $\text{Al}^{3+}$  ions during aluminum corrosion [40].

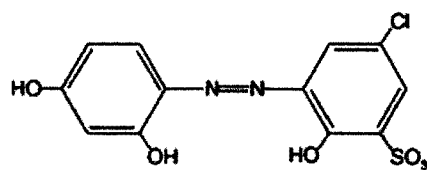


Figure 24. Structure of lumogallion [42].

This probe was mixed with an epoxy/polyamide coating and applied onto a 2024-T3 aluminum alloy to sense  $\text{Al}^{3+}$  ions [42]. The coating showed some initial blue fluorescence background when illuminated by UV light. With time of exposure to 0.5 M

NaCl solution, white spots were observed on the epoxy primer surface. After longer exposure to the corrosive solution, dark spots or circles appeared in the bright area. The authors ascribed these changes in fluorescence to the corrosion process on the aluminum alloy surface [42].

Another fluorescent probe, showing CHEF when complexing with  $Al^{3+}$ , morin (Figure 25 [52]), was proposed as a corrosion sensor for 7075 aluminum panels [39].

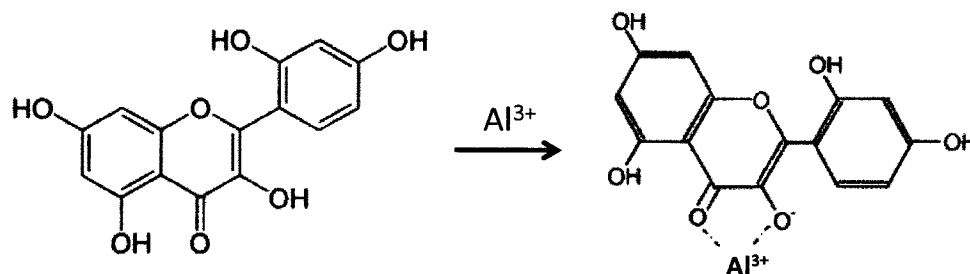


Figure 25. Morin complexation with  $Al^{3+}$  [52].

Epoxy coated aluminum coupons were aged in a 1 wt% NaCl solution and then placed in the 4 ppm morin solution. The coupons were photographed in UV light showing strong fluorescence. The authors claimed that morin combined with aluminum from corrosion and produced a fluorescent complex. However in this case the indicator was not further explored for its effectiveness to sense aluminum corrosion when embedded in the protective coating [39].

Bryant et al. [40] also reported using a CHEF fluorescent probe, 8-hydroxyquinoline-5-sulfonic acid (Figure 26), for sensing aluminum corrosion. The solution of this  $Al^{3+}$  complexing agent was directly deposited as a primer layer on the aluminum test panels

and after drying the epoxy coating was applied on top of this sensing primer layer. The coating was scored by a scalpel and exposed to a salt spray. The corrosion indicated by fluorescence was observed on the panel under UV light where the coating had been scored and where bubbles were present in the coating. These authors however tended to deposit a solution with sensing compound directly onto the metal surface. That elongates the coating application process and might have an influence on adhesion between the metal surface and the protective coating. The sensing molecule was also not explored by directly embedding it into the main epoxy coating as a smart corrosion-sensing system. Since this fluorescent probe contains functional group with active hydrogen (phenol group) it can potentially interact with the epoxy components and change its fluorescent properties.

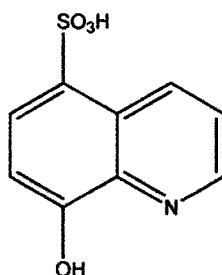


Figure 26. Chemical structure of 8-hydroxyquinoline-5-sulfonic acid hydrate [40].

### **3.1.3 “Turn- on” Fluorescent Sensing via Complexation with Fe<sup>2+</sup>/Fe<sup>3+</sup>**

Although success of various extents was reported in the detection of aluminum corrosion via fluorescent sensor molecules (section 3.1.2) , no success has been reported, to the best

of my knowledge, describing such an indicator detecting steel corrosion by sensing ferric or/and ferric ions.

Most of the known sensors for iron ions, which could be potentially used as corrosion indicators, are based on a chelation enhanced fluorescence quenching mechanism (CHEQ). Ferric and ferrous ions act as efficient fluorescence quenchers due to their paramagnetic nature [53, 40]. However, in recent years, many studies have focused on the development of “turn-on”  $\text{Fe}^{3+}$  sensing molecules due to the biological and environmental importance of this heavy metal ion [54]. Many of these chemosensors are derived from Rhodamine B. This fluorescent dye is widely used as a fluorescent labeling agent due to its excellent photophysical properties [55]. Kim et al. [56] recently published a review describing the application of rhodamine derivatives in sensing heavy metal ions such as lead, mercury, copper and ferric ions as well as acidic solution. These derivatives are non-fluorescent and colorless in their ring-closed, spirocyclic form. Yet acidic solution or the presence of metal ions causes the opening of the spirocyclic ring and, as a result, strong orange fluorescent emission occurs together with pink or red color as seen in Figure 27.

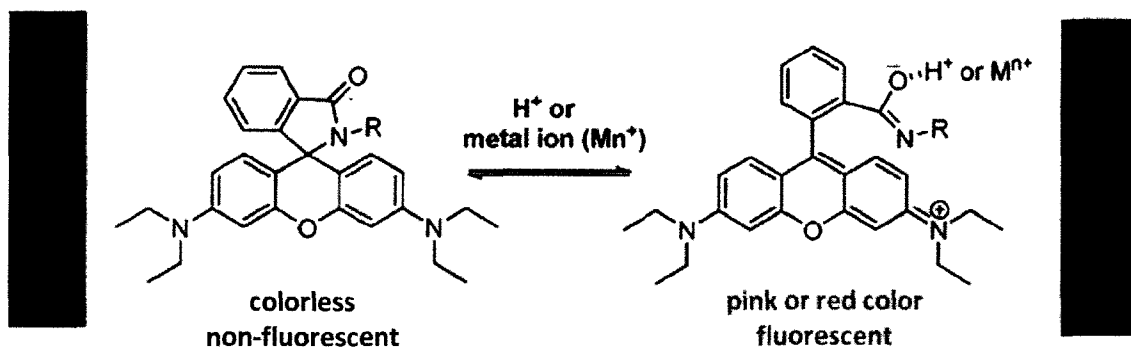


Figure 27. Spirolactam ring-opening reaction of a rhodamine derivative [56].

Some of the rhodamine derivatives were claimed to be selective “turn-on” chemosensors to ferric ions [53, 57, 58, 59], which makes them very attractive as potential steel corrosion sensors, and others were shown to also sense other transition metal ions such as  $\text{Zn}^{2+}$ ,  $\text{Fe}^{2+}$ ,  $\text{Pb}^{2+}$ ,  $\text{Hg}^{2+}$  [60] along with  $\text{Fe}^{3+}$ . Even though some of the molecules were claimed to be “turn-on” sensors for  $\text{Fe}^{3+}$  ions, only one inorganic/organic polymer hybrid system was shown to be highly selective to  $\text{Fe}^{2+}$  ions so far [61]. However since this sensing system includes a polymeric molecule it would be undesirable to incorporate it into the sensing epoxy matrix since it could potentially influence the coating properties.

### 3.1.4 Rational for choice of FD1 as a Steel corrosion Indicator

After investigating potential candidates for sensing iron ions at the anodic site of steel corrosion, when embedded in an epoxy based matrix, spiro[1H-isoindole-1,9'-[9H]xanthen]-3(2H)-one, 3',6'-bis(diethylamino)-2-[(1 methylethylidene) amino] (FD1) molecule described by Zhang et al. [57] was selected for preliminary experiments. This

rhodamine derived molecule was claimed to be a highly selective and sensitive “turn-on” fluorescent sensor for  $\text{Fe}^{3+}$ .

The fluorescent response of FD1 (10  $\mu\text{M}$ ) to various amounts of  $\text{Fe}^{3+}$  (from an aqueous solution of  $\text{FeCl}_3$ ) were investigated by Zhang et al. [57] under excitation at  $\lambda_{\text{ex}}=510\text{nm}$  (Figure 28). Each fluorescent emission spectrum was obtained in a  $\text{CH}_3\text{CN}$  solution diluted 20 times with HEPES buffer (20 mM, pH 7) after  $\text{Fe}^{3+}$  addition for 5 minutes. No obvious fluorescent emission was observed in the FD1 solution in the absence of  $\text{Fe}^{3+}$ . When  $\text{Fe}^{3+}$  (0-80  $\mu\text{M}$ ) was introduced into the FD1 solution, an obvious visible fluorescence peak and red-orange color were observed and also enhanced upon further addition of  $\text{Fe}^{3+}$  [57].

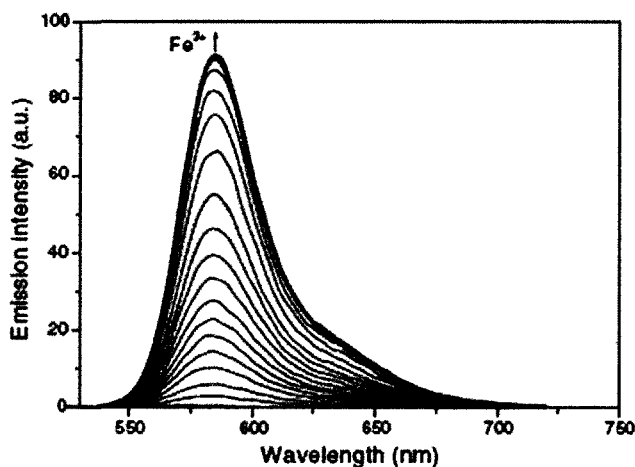


Figure 28. Fluorescence response of FD1 (10  $\mu\text{M}$ ) upon the addition of  $\text{Fe}^{3+}$  at 25°C [57].

This increase in fluorescence of FD1 upon addition of ferric ion solution, according to Zhang et al. [57], was due to formation of the fluorescent ring opened form of FD1 upon coordination with  $\text{Fe}^{3+}$  as illustrated in Figure 29 [52].

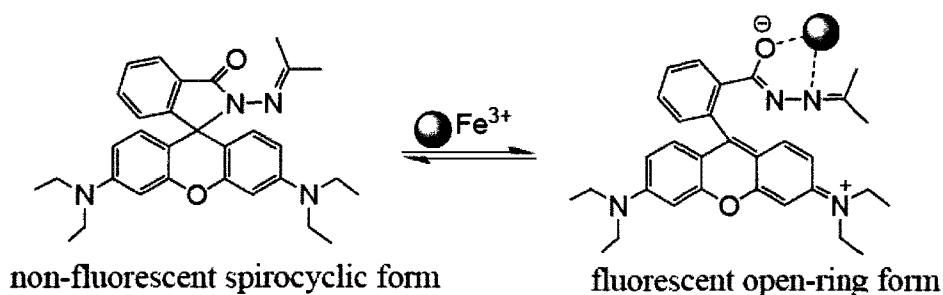


Figure 29. Proposed coordination between FD1 and  $\text{Fe}^{3+}$  ion resulting in the fluorescence enhancement [57].

The selectivity of FD1 to  $\text{Fe}^{3+}$  sensing was proved by performing the selective coordination studies with heavy, transition, and main group metal ions in aqueous solutions by fluorescence spectroscopy. Upon the addition of excess of metal ions, a very mild fluorescence enhancement in FD1 solution was observed only for  $\text{Cu}^{2+}$ , while  $\text{Na}^+$ ,  $\text{K}^+$ ,  $\text{Cu}^+$ ,  $\text{Ag}^+$ ,  $\text{Ca}^{2+}$ ,  $\text{Cd}^{2+}$ ,  $\text{Co}^{2+}$ ,  $\text{Cr}^{2+}$ ,  $\text{Zn}^{2+}$ ,  $\text{Mg}^{2+}$ ,  $\text{Mn}^{2+}$ ,  $\text{Ni}^{2+}$ ,  $\text{Pb}^{2+}$ , and  $\text{Fe}^{2+}$  showed very weak response [57].

Additionally, FD1 does not possess any reactive functional groups that can potentially interact with the epoxy matrix when embedded in the coating to sense steel corrosion. The molecule can be synthesized from commercially available Rhodamine B Base (Figure 30). Moreover FD1 can also be easily synthesized from Rhodamine B Hydrazide, that is also commercially available, and in doing so the use of toxic  $\text{POCl}_3$  can be omitted. Thus this selective, “turn-on” chemosensor for  $\text{Fe}^{3+}$  appeared to be a good candidate as an indicator for the detection of steel corrosion at the anodic site.

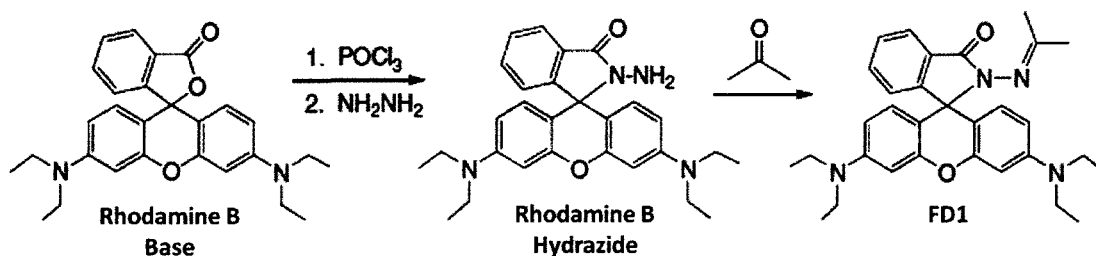


Figure 30. Synthesis of FD1 [57].

### 3.2 Objectives of this Chapter

In this chapter the experiments utilizing FD1 as a corrosion sensor for steel, due to its ability to bind  $\text{Fe}^{3+}$  ions that are produced at the anodic site of corrosion, will be shown. Since FD1 is not commercially available it had to first be synthesized in our lab. The sensing molecule's ability to respond to  $\text{Fe}^{3+}$  (as claimed by Zhang et al. [57]) when in solution also had to be confirmed. Given that FD1 was chosen to serve as a corrosion indicator for epoxy based coatings, the following questions had to be addressed: 1) is FD1 effective as a  $\text{Fe}^{3+}$  sensor when embedded in the epoxy matrix (both clear and filled, where pigments are present and could potentially dampen the FD1 fluorescent response) and 2) is FD1 a sensitive enough sensor to be able to detect early stages of steel corrosion (when the ferric ions are produced at the cathodic site of corrosion at the metal/coating interface)? It also had to be confirmed that FD1 does not prematurely interact with the epoxy coating components as predicted due to its structure.



### **3.3 Experimental Section**

#### **3.3.1 Reagents and Materials**

FD1 was synthesized from Rhodamine B Hydrazide (purchased from Fluka Chemical Corp. or synthesized in our lab). Acetone (HPLC grade), acetonitrile (HPLC grade), tetrahydrofuran (THF) (HPLC grade), methanol (HPLC grade), dichloromethane, ethyl acetate, sodium chloride (NaCl), ferric chloride, anhydrous ( $\text{FeCl}_3$ ), anhydrous sodium sulfate and hydrochloric acid (ACS grade, 36.5–38.0%) were purchased from EMD chemicals. Ferric chloride hexahydrate ( $\text{FeCl}_3 \times (\text{H}_2\text{O})_6$ ) was purchased from Mallinckrodt. Acetic acid (glacial, ACS grade) was purchased from VWR Scientific Products. Rhodamine B Hydrazide was synthesized from Rhodamine B Base (purchased from Aldrich) or from Rhodamine B (pure, purchased from Acros Organic) in our lab. Ethyl alcohol (ethanol), 190 proof, 95%, ACS/USP grade, was purchased from Pharmco-AAPER and commercial alcohols. Hydrazine Hydrate 100% (Hydrazine, 64%) was purchased from Acros Organic. Sodium hydroxides (NaOH), reagent ACS, pellets, 97+% and potassium phosphate, monobasic ( $\text{KH}_2\text{PO}_4$ ) were purchased from Acros Organics. Commercial Epoxy-Polyamide coatings: clear MIL-DTL-24441C, type III and Haze Gray MIL-DTL-24441C, type III, Formula 151, were purchased from NCS Coatings, Inc. Carbon steel coupons (AISI 1018 grade, edge ground and sand blasted to SPPC SP-5) with dimensions: 9.7 cm  $\times$  15 cm  $\times$  0.3 cm were purchased from KTA-Tator Inc. Tetraethylenepentamine (TEPA), technical grade, was purchased from Acros Organics.

D.E.R.<sup>TM</sup> 332 Epoxy Resin (high purity bisphenol A diglycidylether, DGEBA) was purchased from The Dow Chemical Company.

### **3.3.2 Sample Preparation**

#### **3.3.2.1 FD1 Synthesis**

FD1 was synthesized first from Rhodamine B hydrazide (RBH) (experiment **AA1-49**). 0.1 g of RBH was dissolved in 15 ml of acetone. The orange-pink mixture was refluxed for 1.5 hr. After that time solvent was evaporated with a rotary evaporator. The remaining residue had an orange color. The starting material and the product were analyzed with thin layer chromatography (TLC) (dichloromethane/methanol 5:1, v/v). There was no difference between the two materials thus the reaction was performed again (**AA1-50**) but this time a drop of hydrochloric acid was added as a catalyst after the reflux. Also, in this second method, there was no difference between the starting material and the product. The synthesis was performed in a third manner with acetic acid as a catalyst (**AA1-51** and **AA1-70**). RBH (0.1 g) was dissolved in 12.5 ml of acetone. A trace amount of acetic acid was added as a catalyst and the whole mixture was refluxed for 5 h. After solvent removal under reduced pressure, the residue was redissolved in chloroform. The chloroform solution was washed with DI water and dried over anhydrous sodium sulfate. After chloroform was removed under reduced pressure, the light orange-pink obtained residue was recrystallized from ethanol to give an almost colorless powder. This time TLC showed that the product was synthesized successfully; Yield: 0.0835 g (83.5%). The

product was characterized with  $^1\text{H-NMR}$  and  $^{13}\text{C-NMR}$  (in  $\text{CDCl}_3$ ) and matched that reported by Zhang et al. [57]. FD1 was also synthesized in the same way as described above from RBH synthesized in our lab (experiments described below) in experiment **AA1-92** and **AA2-26**. Also in experiment **AA2-27**, FD1 was synthesized by simply placing RBH (synthesized in experiment **AA2-25**) in a solution of acetone for 3 days under argon atmosphere and in the dark at room temperature. After washing the residue with acetone and filtration, the light orange crystals were dried in air; Yield 73%.  $^1\text{H-NMR}$  (in  $\text{CDCl}_3$ ) matched that reported by Zhang et al. [57]

### 3.3.2.2 Rhodamine B Hydrazide (RBH) Synthesis

RBH was first synthesized from Rhodamine B base (RBB) according to the modified reference [62] (**AA1-72**). 1 g of RBB was dissolved in 25 mL of ethanol. Then 0.16 g of hydrazine hydrate was added (1:1.5 excess). The mixture was refluxed for 24 hr. Then 1 M HCl solution was added to remove the residual hydrazide followed by 1M NaOH solution to bring the pH back up to 9-10. The solvent was evaporated with a rotary evaporator. The residue had a pink color. TLC showed that the product was synthesized successfully.  $^1\text{H-NMR}$  (in  $\text{CDCl}_3$ ) matched that reported by Soh et al. [62]. RBH was synthesized again according to the reference [63] from Rhodamine B (RB) (experiments **AA1-85**, **AA1-90**, **AA1-94** and **AA2-25**). 1 g of RB was dissolved in 37.5 ml of methanol. Then 1.25 ml of hydrazine hydrate was added and the mixture was refluxed until the pink color disappeared (24 hr). After reflux, the solution had an orange-red color. The cooled reaction solution was poured into DI water and extracted with ethyl

acetate. Then the combined extracts were dried with sodium sulfate anhydrous, filtered and solvents evaporated with a rotary evaporator. The product was in a form of orange crystals. TLC (ethanol/dichloromethane 0.1:9.9 v/v) showed that the product was successfully synthesized.  $^1\text{H-NMR}$  (in  $\text{CDCl}_3$ ) matched that reported by Yang et al. [63].

### **3.3.3 FD1 Response to $\text{Fe}^{3+}$ in Solution.**

**AA1-66A**; 0.2 ml of FD1 in  $\text{CH}_3\text{CN}$  solution (0.0014 M) was diluted with 2.5 ml of  $\text{NaOH}/\text{KH}_2\text{PO}_4$  buffer solution (pH 7). Solution of  $\text{FeCl}_3$  (in DI water, 0.003 M) was added dropwise to the solution of FD1. **AA1-66B**; Similar to AA1-66A, solution of  $\text{FeCl}_3$  (in DI water, 0.003 M) was titrated to a solution of FD1 in  $\text{CH}_3\text{CN}$ . **AA2-19**: 3 ml of FD1 solution in  $\text{CH}_3\text{CN}$  (20 M) was titrated with  $\text{FeCl}_3$  (in  $\text{CH}_3\text{CN}$ , 0.004 M). The changes in solution fluorescence were observed on a spectrofluorometer with excitation 510 nm.

### **3.3.4 Preparation of FD1-Embedded Clear-Epoxy $\text{Fe}^{3+}$ -Sensing Films (AA1-62)**

A  $\text{Fe}^{3+}$ -sensing clear epoxy film (free from any substrate) was prepared in order to test the efficacy of the indicator within a clear epoxy matrix. 0.0032 g of FD1 was first dissolved in THF and then combined with both components of a clear commercial epoxy-polyamide coating (MIL-DTL-24441C, 2.14 g). FD1 content was 1.5 wt% based on the wet coating (before solvent evaporation). After mixing, the whole mixture was poured into a rectangular shaped silicone mold and cured at room temperature under nitrogen

atmosphere for a few days. After 7 months a small piece of the sample was cut off and placed in an aqueous  $\text{FeCl}_3$  solution for 24 hr. The fluorescent response of FD1 in the freestanding clear epoxy matrix to  $\text{Fe}^{3+}$  ions from the solution was observed with a confocal microscope with an excitation wavelength of 514 nm. The sample was also examined under UV light from handheld UV lamp.

### **3.3.5 Preparation of FD1-Embedded Filled-Epoxy $\text{Fe}^{3+}$ -Sensing Films (AA1-84A)**

A  $\text{Fe}^{3+}$ -sensing filled epoxy film (free from any substrate) was prepared in order to test the efficacy of the indicator within an epoxy matrix in the presence of filler pigments. The coating was prepared by mixing both the amine and epoxide components of commercially available MIL-DTL-24441C, Haze Gray Epoxy Polyamide coating with 1.5 wt% of FD1 (based on dry coating). To aid in uniform mixing with the epoxy components, FD1 was first dissolved in toluene. After mixing, the resin solution was poured into a rectangular shaped silicone mold and cured at room temperature for one week. After curing, the film specimen was cut into a 5.5 cm × 1 cm × 0.05 cm piece and placed in a vial with 0.002 M  $\text{FeCl}_3 \cdot (\text{H}_2\text{O})_6$  aqueous solution, so that half of the specimen was immersed in the solution. Fluorescent response of FD1 in the neat (no metal substrate) epoxy matrix to  $\text{Fe}^{3+}$  ions from the solution was observed with the confocal microscope with an excitation wavelength of 514 nm.

### **3.3.6 Preparation of Steel Coupons Coated with Fe<sup>3+</sup>-sensing Clear Model Epoxy Coating**

Samples **AA1-71A** and **AA1-71B** were prepared by mixing tetraethylenepentamine (TEPA, amine hardener) and epoxy resin (DGEBA) (at an NH/epoxy molar ratio of 1:0.8 to obtain full curing) with FD1 (1 wt%) and spraying this mixture (with an airbrush) onto carbon steel coupons cut into dimensions 5.3 cm × 7.3 cm × 0.3 cm. After cutting the steel samples, edges were smoothed to avoid edge effects during coating application. To aid in uniform mixing with the epoxy components, FD1 was first dissolved in toluene. Before coating application, the steel surface was washed with acetone. The back of the specimen and its edges were painted using a brush applicator with MIL-DTL-24441C, Haze Gray Epoxy Polyamide coating without FD1. The panels were cured at room temperature in a nitrogen purged atmosphere for one week. The coating thickness was approximately 50 μm for AA1-71A and 30 μm for AA1-71B. To observe the response of FD1 in the clear model epoxy coating to steel corrosion, sample AA1-71A was scribed using a razor (scribe length 1.3 mm) and partially dipped into a 0.5 M NaCl solution so the scribed area was exposed to the corrosive environment. Three different areas in the coating surface were monitored with time for changes in fluorescence intensity with the confocal microscope with an excitation wavelength of 514 nm; AREA1 was not exposed to NaCl solution, AREA2 was exposed to NaCl solution but not scribed and AREA3 was both exposed to NaCl solution and scribed to expose the steel surface and facilitate corrosion. Also pictures of the sample surface under UV light were taken using a digital camera placed on the microscope eyepiece. Sample AA1-71B was not exposed to NaCl

solution and was used as a reference. Similarly to AA1-71A and AA1-71B, sample AA2-48A2 was prepared but in this case only 0.5 wt% of FD1 was used. The mixture of TEPA/DGEBA and FD1 was applied on steel coupons using a drawdown bar at wet thickness 250  $\mu\text{m}$ . The samples were placed in an oven to cure (70°C) overnight. After drying, many defects were present in the coating most likely due to fast solvent evaporation (toluene was used to dissolve FD1). The dry coating thickness was not uniform (from 30  $\mu\text{m}$  to 130  $\mu\text{m}$ ). An open-ended glass cylinder filled with a 3.5% NaCl solution was affixed and sealed to the coated sample to expose only the contained area to the corrosive environment.

### **3.3.7 Preparation of Steel Coupons Coated with Fe<sup>3+</sup>-sensing Filled Commercial Epoxy Coating**

Sample **AA1-71D** was prepared in a similar way to samples AA1-71A and AA1-71B but in this case the filled Haze Gray Epoxy Polyamide coating (MIL-DTL-24441C, Type III) was used as an epoxy matrix for FD1 (1.5 wt% based on dry coating). The mixture of FD1 and the epoxy was applied on steel coupons using a brush applicator and cured at room temperature for 6 weeks. The coating thickness was approximately 40  $\mu\text{m}$ . To observe the response of FD1 in the coating to steel corrosion, the coated steel panels were scribed using a razor (scribe length 1.3 mm) and placed horizontally on top of a beaker containing a 0.5 M NaCl solution, exposing their scribed surface to the water vapor. After 40 h, the sample was subsequently placed in DI water for 22 h and was then submerged in a 0.5 M NaCl solution for 30 min to speed up the corrosion process. The area on the

coating surface surrounding the scribe was monitored with time for changes in fluorescence intensity with a confocal microscope with an excitation wavelength of 514 nm. Images of the sample surface under UV light were taken using a digital camera placed on the microscope eyepiece.

### **3.3.8 Preparation of Undercoating Corrosion-Sensing Panels**

Special panels were also prepared to simulate delamination to test the efficacy of the FD1-containing epoxy coating for sensing undercoating steel corrosion (**AA1-96A**). The coatings on the steel coupons were prepared by mixing MIL-DTL-24441C, Haze Gray Epoxy Polyamide coating with 0.5 wt% of FD1 (based on dry coating). Prior to mixing with the epoxy components, FD1 was first dissolved in toluene. Before applying the coatings in this case, the steel coupons (ANSI 1018 grade, edge ground and sand blasted, with dimensions 5.3 cm × 7.3 cm × 0.3 cm) were treated with 10% phosphoric acid to remove any possible corrosion products (pickling process), washed a few times with acetone and then dried with compressed air. To mimic a coating defect, a small drop of silicone oil was applied onto the steel surface (to deteriorate coating adhesion to the metal surface and induce a weak point that is susceptible to undercoating corrosion). The filled epoxy coating containing FD1 was then applied onto the steel coupon using an air brush applicator. The panel was cured at room temperature for one week. The coating thickness was approximately 30 μm. To initiate the undercoating corrosion, an open-ended glass cylinder was affixed and sealed to the part of the coated panel containing defects. The cylinder was filled with a 5 wt% NaCl solution so only this circular portion of the sample



was exposed to the corrosive environment. The surface of the defect area was monitored with the confocal microscope at different times and temperatures of exposure to the NaCl solution for changes in fluorescence intensity. Also pictures of the sample surface under UV light were taken using a digital camera placed on the microscope eyepiece.

### **3.4 Characterization Methods**

$^1\text{H}$  NMR spectra were recorded on a Varian *Mercury* 400 MHz NMR with autosampling capabilities. Fluorescence emission spectra were obtained with a Cary Eclipse fluorescence spectrofluorometer with an excitation wavelength of 510 nm. The examined solutions were placed in a 3 ml quartz cuvette. Fluorescence imaging was conducted on a Zeiss LSM 510 Meta Laser Scanning Confocal Microscope with an Axio Imager M1 platform. In all experiments, a 514 nm ArMultiLine laser was used as the excitation source. An EC Plan-Neofluar 10 /0.30 M27 objective was used to observe the sample surface. The fluorescent emission wavelength was obtained from the lambda mode function (using Meta detector with selected emitted fluorescence range 520-660 nm with 10.7 nm step). To compare the laser excited images to those obtained by more practical end-use conditions, the confocal microscope's 100 W mercury lamp was used as a broad wavelength UV light source. Visual inspection of the samples was also performed under UV light using a handheld UV lamp (Model UVGL-25, MINERALIGHT<sup>®</sup>) with an excitation wavelength of 365 nm. The coating thickness was measured with a CHECK-LINE<sup>®</sup> coating thickness tester, model DAC-1KS.

## **3.5 Results and Discussion**

### **3.5.1 FD1 and Rhodamine B Hydrazone Synthesis**

FD1 synthesis was first attempted by performing only the second step of the reaction shown in Figure 30 since Rhodamine B hydrazone (RBH) was commercially available. By synthesizing FD1 directly from RBH, the usage of toxic phosphoryl chloride ( $\text{POCl}_3$ ) was avoided. However when RBH was simply refluxed in acetone, FD1 was not properly synthesized. This probably happened because there was no acid catalyst in this system that might be necessary for this nucleophilic addition reaction to take place. In reference [57], traces of acid were probably still present from the previous reaction steps which allowed FD1 synthesis. When a catalytic amount of acetic acid was introduced to the RBH/acetone mixture, FD1 was successfully obtained (AA1-51); (see section 3.3.2.1). RBH was also synthesized in our lab (since it was no longer commercially available) utilizing two methods, described in reference 62 and 63 from Rhodamine B base (RBB) and Rhodamine B (RB) respectively. Neither of these methods required usage of  $\text{POCl}_3$  but only hydrazone. Moreover FD1 was also simply synthesized in high yield (73%) by placing RBH in acetone (AA2-27) for 3 days in the case when RBH is synthesized from RB (AA2-25) since traces of acid (from RB) were probably still present in the system. Thus use of acetic acid as a catalyst was not necessary.

### **3.5.2 FD1 Response to Fe<sup>3+</sup> in Solution**

In order to confirm that FD1 forms a fluorescent complex due to binding with Fe<sup>3+</sup> as claimed by Zhang et al. [57] series of experiments were performed.

In experiment AA1-66A, when a solution of FD1 in CH<sub>3</sub>CN (0.0014 M, clear solution) was diluted 12.5 times with pH 7 buffer (NaOH/KH<sub>2</sub>PO<sub>4</sub>) a white precipitate was formed. The pH 7 buffer was used to mimic the conditions in the experiment with FD1 performed by Zhang et al. [57]. The precipitation was probably formed because FD1 does not dissolve in water and addition of a large amount of aqueous solution caused FD1 precipitation. This solution showed no fluorescence when excited at 510 nm. FeCl<sub>3</sub> aqueous solution was used as Fe<sup>3+</sup> source similarly to the Zhang et al. experiment [57]. When a drop of FeCl<sub>3</sub> aqueous solution (0.003 M) was added to the FD1-buffer solution no increase in fluorescence was observed. Also further FeCl<sub>3</sub> addition did not change the fluorescence of the solution. This is not surprising, since as mentioned above, FD1 probably precipitated out of solution and was not able to sense Fe<sup>3+</sup>. To prevent FD1 precipitation, the experiment was repeated (AA1-66B) but no aqueous buffer was added to the FD1 solution. Initially, the solution of FD1 in CH<sub>3</sub>CN showed almost no fluorescence. However, the addition of only one drop of FeCl<sub>3</sub> caused a pink-red color to appear. In addition, the high intensity fluorescence was observed to peak at 583 nm. Further FeCl<sub>3</sub> addition caused an increase in the fluorescence intensity. This experiment proved that FD1 was able to sense Fe<sup>3+</sup> in solution. A more careful experiment was subsequently performed with known concentration of FD1 and Fe<sup>3+</sup> (AA2-19). The

fluorescent emission spectrum of the 20  $\mu\text{M}$  solution of FD1 in  $\text{CH}_3\text{CN}$  upon addition of 6 equivalents of  $\text{Fe}^{3+}$  from  $\text{FeCl}_3$  (in  $\text{CH}_3\text{CN}$ ) is shown in Figure 31.

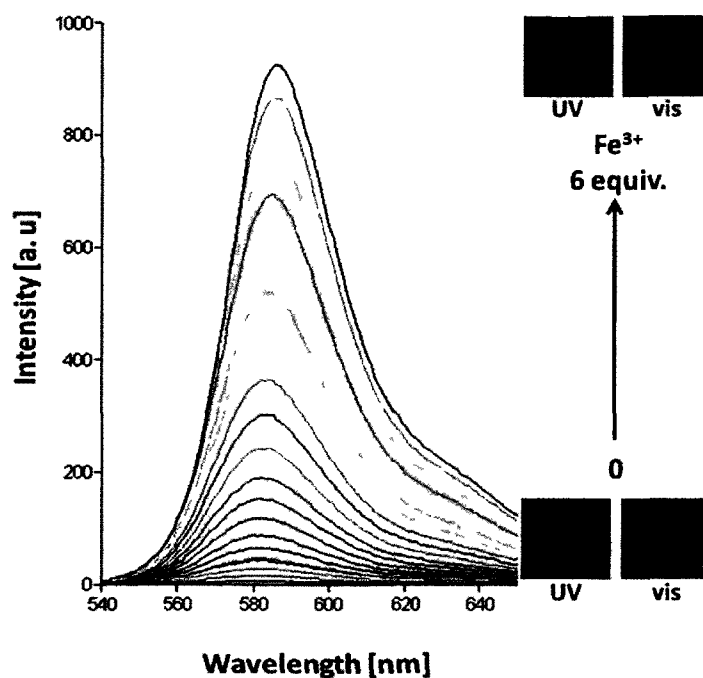


Figure 31. Fluorescent response of FD1 (solution in  $\text{CH}_3\text{CN}$ , 20  $\mu\text{M}$ ) to  $\text{FeCl}_3$  solution in  $\text{CH}_3\text{CN}$  (0 to 6 equiv.) ( $\lambda_{\text{ex}} = 510 \text{ nm}$ ). Right: color change of FD1 in  $\text{CH}_3\text{CN}$  on  $\text{FeCl}_3$  addition under UV and visible light.

The initially colorless and non-fluorescent solution of FD1 changed to bright pink-red and fluorescent orange (under UV) with  $\text{FeCl}_3$  addition (inset in Figure 31). As can be seen in Figure 31, the maximum fluorescent intensity ( $\lambda_{\text{em,max}}$ ) was shifting from 580 nm at lower intensities to 582 nm (3  $\text{Fe}^{3+}$  equivalents) and reached a maximum of 586 nm at 6.3  $\text{Fe}^{3+}$  equivalents (red-shifting). After addition of higher  $\text{Fe}^{3+}$  equivalents fluorescent intensity was over ranged.

These preliminary experiments proved that FD1 is able to sense FeCl<sub>3</sub> in solution as claimed by Zhang et al. However in my experiments when buffered solution was used (pH 7) no fluorescence was observed upon FeCl<sub>3</sub> addition. This is further explored in chapter 5 of this thesis where the FD1 sensing mechanism will be discussed in detail.

### **3.5.3 FD1 Ability to Sense Fe<sup>3+</sup> when Embedded in Commercial Clear Epoxy**

#### **Matrix**

The ability of FD1 (1.5 wt% based on wet coating) to respond to FeCl<sub>3</sub> solution when embedded in a clear epoxy coating (MIL-DTL-24441C, type III) was examined in experiment AA1-62. A piece of the FD1-epoxy sensing film was placed in aqueous FeCl<sub>3</sub> solution for 24 h. After this time orange color was observed under a UV lamp (smaller piece in the middle image in Figure 32). The broader range of excitation wavelengths from the UV source does not excite FD1 at its maximum (maximum excitation wavelength for FD1/FeCl<sub>3</sub> solution in CH<sub>3</sub>CN is 510 nm), yet the fluorescence emission is still visible by eye (at a lower intensity). Using a handheld UV lamp to excite the FD1 fluorescence allows easy and fast examination of the samples and can be conveniently utilized in a practical field application. Under visible light the color change was not seen (left image in Figure 32). This proves that the fluorescent response can be observed much earlier than the chromophoric response.

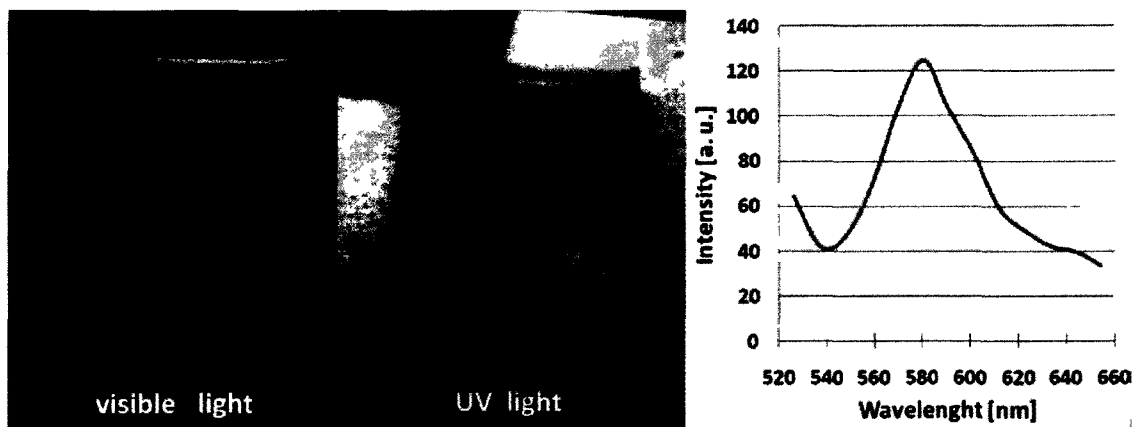


Figure 32. Fluorescent response of FD1 embedded in the clear commercial epoxy coating (AA1-62) to aqueous  $\text{FeCl}_3$  solution after 24 h of immersion (smaller piece of film in the left and the middle images). The large piece was not immersed in  $\text{FeCl}_3$ , for comparison. Far right: fluorescent emission intensity of the small piece immersed in  $\text{FeCl}_3$  solution for 24 h (data transformed from the lambda mode).

The sample was also investigated with a confocal microscope when excited with a 514 nm ArMultiLine laser ( $\lambda_{ex}$ ), which is essentially the maximum excitation wavelength for FD1/  $\text{FeCl}_3$  mixture (510 nm). The confocal microscope images allow quantification of the response by lambda mode analysis (e.g. maximum emission wavelength;  $\lambda_{em,max}$ ). The sample piece not exposed to  $\text{FeCl}_3$  showed no fluorescence characteristic of FD1. The piece immersed in  $\text{FeCl}_3$  for 24 h showed high intensity fluorescence with  $\lambda_{em,max} = 580$  nm (right plot in Figure 32). This value was slightly lower than the maximum emission wavelength in the FD1/ $\text{FeCl}_3$  mixture in a  $\text{CH}_3\text{CN}$  solution (Figure 31). However, the confocal microscope lambda mode collects emission spectra in 10.7 nm steps therefore the actual  $\lambda_{em,max}$  is in the  $\pm 5$  nm error range. Thus the 580 nm maximum fluorescent emission can be confidently assigned to FD1 fluorescence. These results suggested that FD1 can sense  $\text{Fe}^{3+}$  ions from the solution when embedded in a clear model epoxy film. As a result of this interaction, fluorescence is observed in the sample. It is also important to note that the sensor does not show fluorescence characteristic of FD1 when simply

embedded in the clear epoxy coating (and not exposed to  $\text{FeCl}_3$  solution) even after 7 months (no premature response).

#### **3.5.4 FD1 Ability to Sense $\text{Fe}^{3+}$ when Embedded in Commercial Filled Epoxy**

##### **Matrix**

The ability of FD1 (1.5 wt% based on dry coating) to respond to  $\text{FeCl}_3$  solution when embedded in a filled epoxy coating (Haze Gray MIL-DTL-24441C, type III) was proved in experiment AA1-84A. In this system, pigments, that could dampen FD1 fluorescent response, are present. The fluorescent response of FD1-epoxy film to  $\text{Fe}^{3+}$  from  $\text{FeCl}_3$  aqueous solution was monitored by confocal microscopy. Initially no fluorescence emission of the epoxy film was observed when excited at 514 nm. After the sample film was immersed in  $\text{FeCl}_3$  aqueous solution for 24 h, a significant increase in the fluorescence emission was observed. From the confocal microscope's lambda mode function it can be seen that the maximum fluorescence emission was at 580 nm (Figure 33)

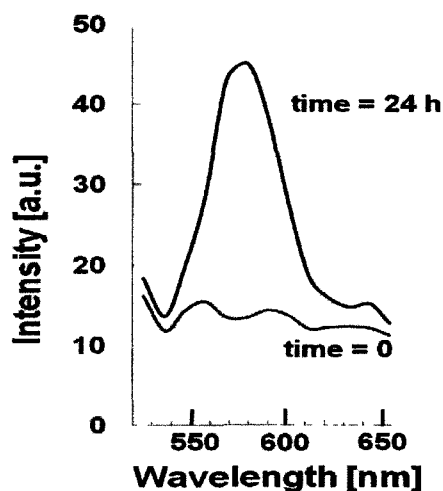


Figure 33. Change in fluorescent emission intensity of filled FD1-epoxy sensing film in  $\text{FeCl}_3$  aqueous solution ( $\lambda_{\text{ex}} = 514 \text{ nm}$ ) at time 0 and after 24 h (data was transformed from lambda mode).

Also after 2 months of immersion in  $\text{FeCl}_3$  the color of the sample changed from gray to slightly pinkish in visible light and orange under UV light. It can thus be concluded that FD1 when embedded in a filled epoxy film (i.e. in the presence of pigments) can respond to  $\text{Fe}^{3+}$  from solution by formation of a fluorescent molecule. Additionally, pink color was not observed in the  $\text{FeCl}_3$  solution suggesting that FD1 did not leach out of the matrix during this period of time.

### **3.5.5 Fluorescent Emission Response of FD1 in $\text{Fe}^{3+}$ -sensing Clear Model Epoxy Coating on Steel Coupons**

Since it was proved in the previously discussed experiments that FD1 can sense  $\text{Fe}^{3+}$  ions from a solution of  $\text{FeCl}_3$  when embedded in both clear and filled epoxy coatings, it was necessary to also determine if FD1 is able to sense  $\text{Fe}^{3+}$  released at the anodic site of steel corrosion when embedded in the epoxy matrix. First, FD1 (1 wt%) was embedded in a



model clear epoxy coating consisting of a mixture of bisphenol A diglycidylether (DGEBA, epoxy resin) and tetraethylenepentamine (TEPA, amine hardener) (at an epoxy/NH molar ratio of 0.8:1 to obtain full curing) (samples AA1-71A and AA1-71B). Sample AA1-71A was exposed to 0.5M NaCl solution to induce corrosion. Sample AA1-71B was used as a reference and was not exposed to the corrosive NaCl environment. This model epoxy system is a purposely designed “bad coating” which means that corrosion is expected to occur rapidly in the samples due to the poor anticorrosion properties of this coating. Three areas in the sample AA1-71A were examined by the confocal microscope ( $\lambda_{\text{ex}} = 514 \text{ nm}$ ) in order to observe the fluorescent response of FD1 to early corrosion. Initially no significant fluorescence was observed in AREA1 that was not exposed to the corrosive environment, in AREA2 exposed to 0.5M NaCl solution, and as well as in AREA3 that was exposed to NaCl and additionally scribed to expose metal surface. However after 2 h of exposure to NaCl solution, AREA2 showed some fluorescence around the defects that resemble air bubbles in the coating (indicated by red arrows in the bottom left image in Figure 34). Fluorescent emission recorded from the confocal microscope's  $\lambda$  mode function showed that the maximum fluorescence emission was between 570 and 580 nm depending on the area examined, which clearly indicates FD1 fluorescence. After 9 h of exposure to NaCl an obvious corrosion spots appeared in the middle of the areas where fluorescence was observed previously (indicated by red arrows in the top right image in Figure 34). This indicated that FD1 detected the early stages of steel corrosion before any obvious visual indicator (i.e. rust) was observed.

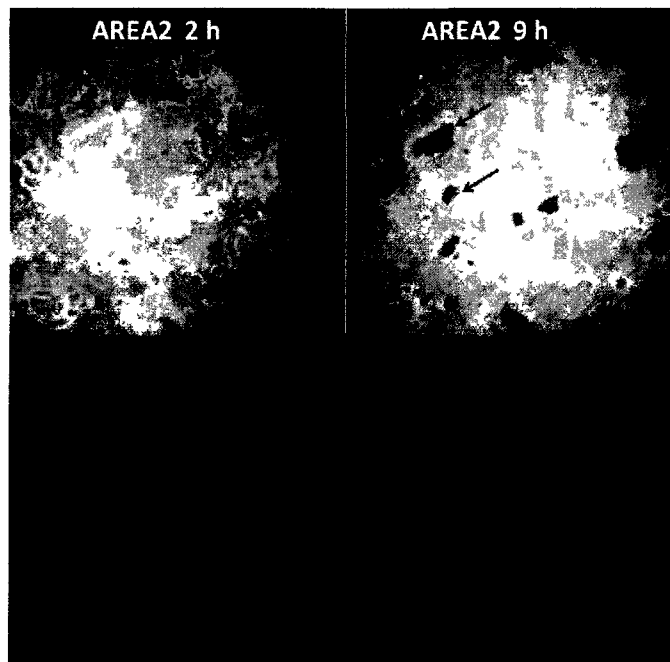


Figure 34. AREA2 in  $\text{Fe}^{3+}$ -sensing clear model epoxy coating on steel substrate (AA1-71A) after exposure to 0.5M NaCl solution. Top row: digital camera images taken through the microscope eye-piece under UV light; bottom row: fluorescent images, of the same area, taken with the confocal microscope.

A similar result was observed in AREA3 after 2 h of immersion in NaCl. In the same areas where fluorescence was observed by the confocal microscope (left image in Figure 35), a pale orange-pink color was also observed under UV light (right image in Figure 35) indicating fluorescent as well as chromophoric FD1 response.

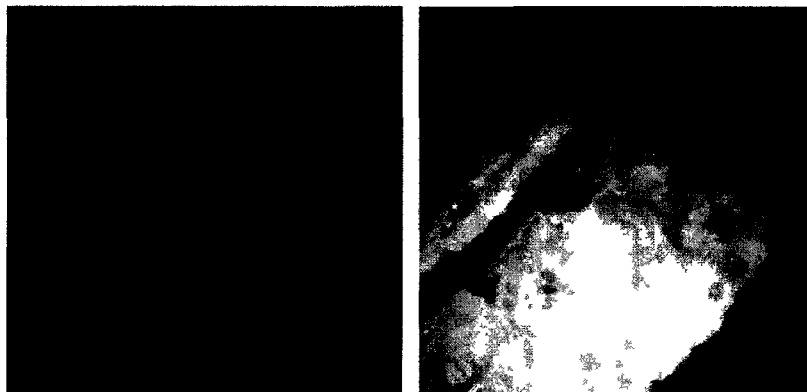


Figure 35. AREA3 in  $\text{Fe}^{3+}$ -sensing clear model epoxy coating on steel substrate (AA1-71A) after exposure to 0.5M NaCl solution for 2 h. Left: fluorescent image taken with a confocal microscope; right: digital camera image, of the same area, taken through the microscope eye-piece under UV light.

After 9 h of exposure to NaCl, corrosion was easily noticeable in the scribed areas and where the previously fluorescent spots were. AREA1 (not exposed to NaCl) showed some lower intensity fluorescent spots around the air bubbles after 9 h. With time these areas had slowly developed into small rusty spots. Even the AA1-71B reference sample (exposed only to air for 11 months) showed the same fluorescence with maximum emission peaking at 570 nm and 580 nm depending on the area examined (left image in Figure 36). Under UV light the same areas appeared light orange-pink (middle image in Figure 36) and rusty in visible light (right image in Figure 36). The appearance of corrosion in these areas is not surprising even though the sample was not exposed to the corrosive environment. The model coating probably absorbed water from air and with time it reached the metal surface. The water diffusion was further enhanced in the areas where the air bubbles were present in the coating (defects) thus corrosion occurred in these defected areas over time.

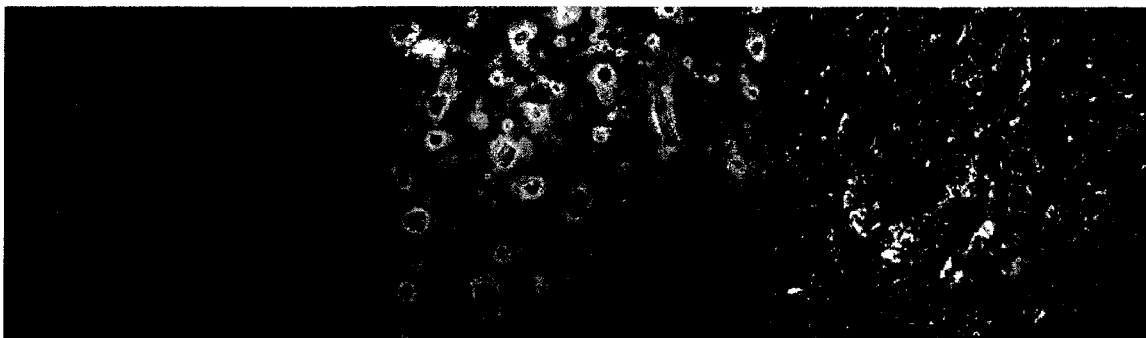


Figure 36. FD1 in model clear epoxy matrix after 11 months of exposure to air (AA1-71B, reference sample). Left: fluorescent image taken with the confocal microscope; middle: digital camera image, of the same area, taken through the microscope eye-piece under UV light; right digital image taken through the microscope eye-piece under visible light.

Similar to AA1-71A, sample AA2-48A2 was prepared in order to determine the FD1 response to steel corrosion at lower indicator concentration (0.5 wt%). Also this time the sample was observed after exposure to NaCl. After 6 h bright orange areas (under UV) appeared around the areas where air bubbles were present in the coating (top left image in Figure 37). At this time rust was also already present in the middle of these areas as can be seen in the bottom left image in Figure 37. Fluorescent emission recorded from the confocal microscope's  $\lambda$  mode function showed that the maximum fluorescence emission was at 580 nm.

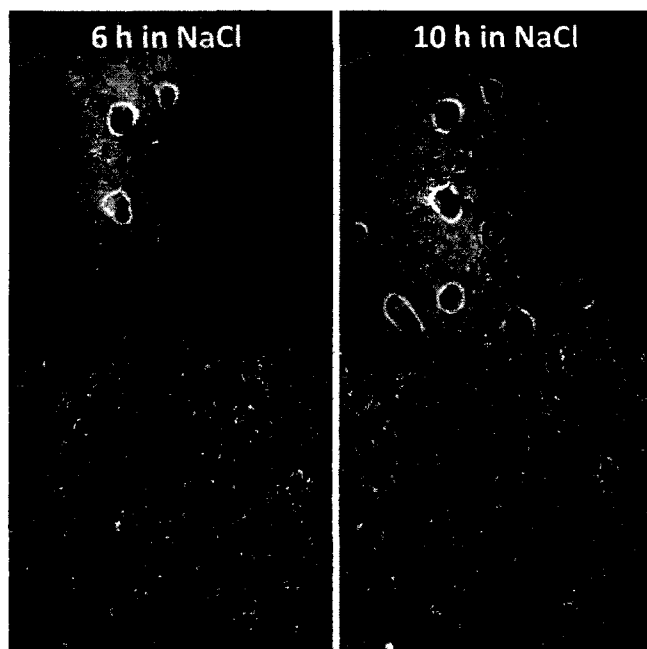


Figure 37. FD1 in model clear epoxy matrix after exposure to 3.5% NaCl solution (AA2-48A2) Top row: digital camera images taken through the microscope eye-piece under UV light; bottom row: digital camera images, of the same area, taken through the microscope eye-piece under visible light.

These results confirmed the previous conclusions that FD1 molecules embedded in a clear epoxy coating can sense steel corrosion by appearance of “turn-on” fluorescence in the corroded areas.

### **3.5.6 Fluorescent emission response of FD1 in Fe<sup>3+</sup>-sensing filled commercial epoxy coating on steel coupons**

In the previous section it was proven that FD1 can serve as an early steel corrosion sensor when embedded in the model clear epoxy coating. To explore the practical use of FD1 and its ability to sense early stages of corrosion in a commercial coating system, the indicator (1.5 wt% of FD1 based on dry coating) was incorporated into a filled, grey

commercial epoxy coating (MIL-DTL-24441C, Type III) and applied onto steel coupons (AA1-71D). After curing the coating was scribed to expose the metal surface and facilitate corrosion attack. Figure 38 shows the fluorescence images of the scribed area on the Fe<sup>3+</sup>-sensing epoxy coating on a steel coupon. The images were recorded at different times of exposure to a corrosive environment. The coated coupon was first suspended above a beaker containing a 0.5 M NaCl solution (sample not immersed in the solution) to observe slow corrosion of the scribed area due to water vapor. Initially no significant fluorescence was observed by the confocal microscope (Figure 38a, top row). Similarly under UV light, the area around the scribe looked no different from the rest of the sample (Figure 38a, bottom row). After 40 h, bright areas appeared around the scribe (Figure 38b, top row). From the lambda mode it was seen that the maximum fluorescence intensity ( $\lambda_{em,max}$ ) of these bright areas was at 570 nm and 580 nm depending on the area examined. To speed up the corrosion process, the coated coupon was then half-immersed in a beaker with DI water (images c and d in Figure 38). Finally, Figure 38e shows the sample after 30 min of immersion in the original 0.5 M NaCl solution. The FD1 indicator was reporting the onset of corrosion by the bright yellow area in the fluorescence images and the yellow-orange areas in the UV images (Figure 38b-e).

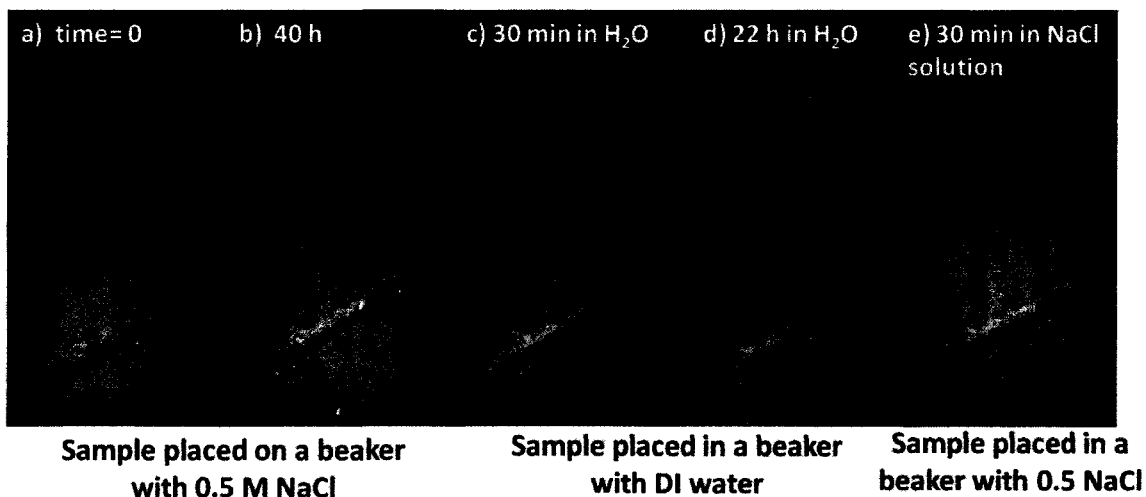


Figure 38. Scribed area on the coated steel coupon (AA1-71D) after various times of exposure to different corrosive environments: sample placed on a beaker with 0.5 M NaCl solution (a) at time 0 and (b) after 40 h, sample placed in the beaker with DI water after (c) 30 min and (d) 22 h, and (e) sample placed in 0.5 M NaCl solution after 30 min. Top row: fluorescent images taken on confocal microscope; bottom row: digital camera images of the same area, taken through the microscope eye-piece under UV light.

When compared however to the 30-min optical microscope image (Figure 39a), in which the onset of corrosion was not discernible at all to the naked eye, it was clearly evident in the FD1 fluorescence response in Figure 38e. After 2 h of immersion in NaCl solution, corrosion was finally visible to the naked eye (Figure 39b). This is very promising data indicating that the FD1 is indeed functioning as an early-detection indicator for corrosion. Moreover these promising results were obtained in commercial pigmented coating which potentially could have reduced the observable fluorescence response from FD1.

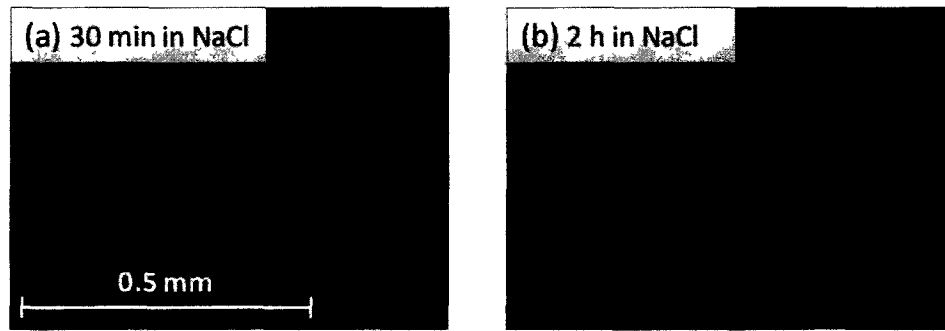


Figure 39. Optical images of the scribed area of the corrosion-sensing panel (AA1-71D) after (a) 30 min and (b) 2 h of immersion in 0.5 M NaCl. Images taken through the microscope eye-piece.

### **3.5.7 Undercoating steel corrosion sensing in a filled commercial epoxy coating**

In experiment AA1-71D the coating was scribed in order to expose the metal surface and initiate corrosion. However this mechanical damage can be also easily observed by the naked eye and thus corrosion is expected to happen in this defected area. A more important function of an effective corrosion indicator is to sense undercoating corrosion (described in chapter 1, section 1.2.2) that can cause major metal damage before it becomes obvious (i.e. coating delaminates occurs).

Sample AA1-96A was prepared to examine whether FD1 is able to sense undercoating corrosion in a filled epoxy coating. In order to mimic an undercoating defect, a small drop of silicone oil was applied onto the steel surface (to deteriorate coating adhesion to the metal surface and induce a weak point that is susceptible to undercoating corrosion) prior to coating with the filled epoxy containing FD1 (0.5 wt% based on dry coating). The application of the silicone oil drop caused visible crater-like defects to appear in the coating surface immediately after coating application. The defective areas are the weak



points in the coating. Undercoating corrosion can initiate from these weak spots and develop into blisters (as a result of osmotic action and coating delamination). Blistering is usually the first visual indication of coating failure [19].

Initially, two areas were marked on the panel surface shown in Figure 40a: AREA1 (where silicone oil was initially applied, area exposed to NaCl solution is indicated by the blue circle) and AREA2 (where no defects were observed, area not exposed to NaCl). After the coating was cured, and before the panel was exposed to the corrosive environment, no initial fluorescent emission was observed in the coating as viewed under the confocal microscope in both of the marked areas (excitation wavelength  $\lambda_{ex}=514$  nm). After one day of exposure to a 5% NaCl solution, a crater-like blister appeared (3 mm in diameter) in one of the defective areas, indicated by the red circle in Figure 40a. Nonetheless, the coating remained intact and there was no visible sign of any corrosion. When the fluorescence measurement was performed on this panel using the confocal microscope, a bright spot in the middle of the blister (Figure 40b) was observed. From the lambda mode function, we observed that the maximum fluorescence intensity in this spot was between 580 and 585 nm (Figure 40c), as expected. Also, under UV light, the same spot appeared to be bright orange. These observations clearly pointed to the *undercoating* corrosion that had occurred after one-day immersion in the NaCl solution.

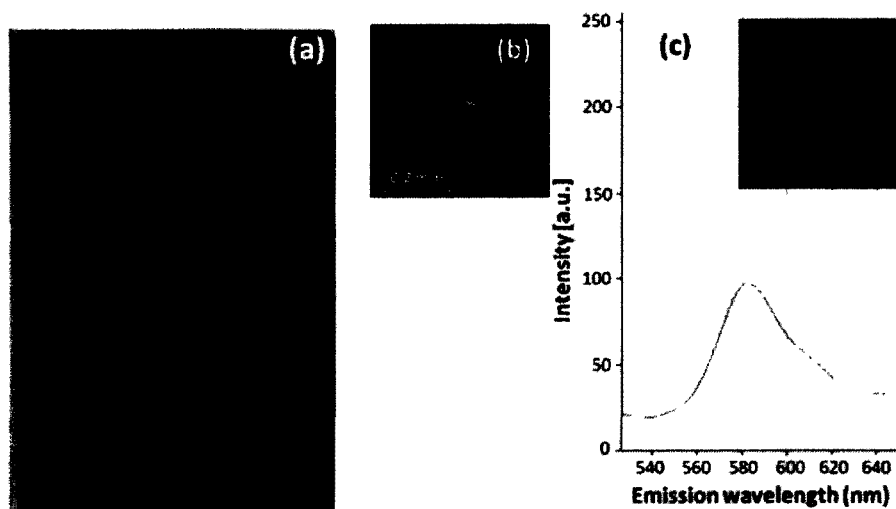


Figure 40. (a) Undercoating corrosion sensing panel (AA1-96A) after 1 day of exposure to 5% NaCl solution. Blue circle and red circle represent areas exposed to NaCl and a blister, respectively. “1” and “2” represent areas exposed to NaCl solution where silicone oil was applied and area not exposed to NaCl solution, respectively; (b) fluorescence image of the area in the red circle taken on the confocal microscope and (c) the lambda mode of the same area.

After 2 days of exposure to the 5wt% NaCl solution, other bright areas appeared within the blister (Figure 41a, top row). It is important to note that in the same area, under the microscope, in natural light, no visible signs of corrosion were observed (Figure 41a, bottom row). After 3 days, small dark spots started to appear in the bright area (Figure 41b, top row) under UV light. In natural light the same dark spot had a rusty color (Figure 41b, bottom row). After 16 days of exposure, both the dark spot (in UV light) and the rusty area (in natural light) slightly increased in size (Figure 41c). Also from lambda mode we observed a corresponding decrease in the fluorescence intensity in those areas, likely due to deposition of the corrosion products (rust). To facilitate the diffusion of the corrosive solution to the metal/coating interface the coated panel was then placed in an oven at 60 °C. After 17 h at 60 °C (and in the 5% NaCl solution) more dark precipitation was observed in the previously bright area (Figure 41d, top row). At the same time under

natural light, the rusty spot was easily observable in the same area (Figure 41d, bottom row). After 7 more days in the NaCl solution at 60 °C, the rusty areas were significantly larger and could be easily seen under both UV and natural light (Figure 41e). The coated panel was then subsequently placed at a higher temperature (70 °C) for another 5 days. After that time further increase in the size of the rusty areas in the blister was observed under the microscope (Figure 41f, bottom row). By this time, the rusty spot could also be seen by the naked eye without a microscope. Also throughout the blister some bright yellow-orange spots (under UV light) appeared. The maximum fluorescence intensity of these bright spots was the same as in the initial bright areas in the blister. Those areas are potentially new onsets of corrosion. It should also be noted that the whole area investigated under UV light (which was the same in size as the blister area) changed color intensity from bright blue to a more faded purple-blue over time during the testing. This color change might be explained by prolonged exposure to high power UV light during the imaging. This phenomenon is further investigated in the following chapter of this thesis. Over the course of this experiment, no fluorescence was observed in AREA2, as expected, confirming that corrosion only occurred in areas in contact with NaCl solution.

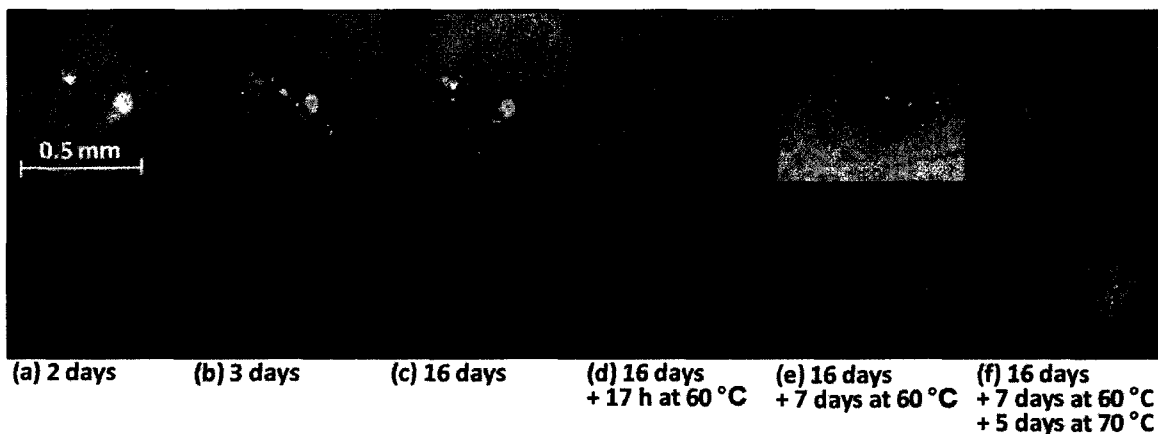


Figure 41. Images of the blister in the undercoating corrosion sensing panel (AA1-96A) after immersion in a 5% NaCl solution. Top row: images taken through the microscope eye-piece under UV light; bottom row: images taken through the microscope eye-piece under natural light.

This experiment proved that FD1 in the filled epoxy coating was able to sense undercoating corrosion, before any obvious sign of metal damage was observable, due to its reaction with ions produced at the anodic site where metal dissolution takes place. The probable scenario is that: 1) the ions produced at the anodic site of corrosion diffuse through the coating causing the appearance of intense FD1 fluorescence (Figure 41a), 2) then with time  $\text{OH}^-$  ions produced at the cathodic site combine with the metal ions from the anodic site causing the insoluble corrosion products built up, 3) the corrosion product accumulation causes coating delamination (coating breaks) and rust can be visible on the coating surface (Figure 41b-d). At the same time accumulated rust decreases the observable FD1 fluorescence (Figure 41b-d). At the end of this experiment the coating was peeled off in the blistered area revealing the rusted surface of the metal substrate (Figure 42) proving that extensive corrosion took place under the coating.



Figure 42. Rusted metal under the blistered area in AA1-96A sample.

### **3.6 Conclusions**

FD1, initially proposed as a  $\text{Fe}^{3+}$  chemosensor for biological applications [57], was easily and efficiently synthesized in our lab. FD1 solution (in  $\text{CH}_3\text{CN}$ ) showed “turn-on” fluorescence when titrated with  $\text{FeCl}_3/\text{CH}_3\text{CN}$  solution. The indicator also showed fluorescent response to  $\text{FeCl}_3$  aqueous solution when embedded in both clear and filled commercial epoxy coating. Moreover it was successfully utilized as an early steel corrosion detector in both model (clear) and commercial (filled) epoxy coatings. FD1 was very effective for indicating early corrosion of steel covered with an epoxy coating, both for areas damaged through to the substrate (scribed areas) and areas without exposure of the substrate (*undercoating* corrosion). The “turn-on” FD1 fluorescence was captured not only by confocal fluorescent microscope but also by, more conveniently, an optical microscope with UV light, which allows easy and non-destructive early corrosion detection of steel before any visible sign of corrosion appears. In addition, only a low FD1 concentration (0.5 wt%) in the coating is needed. FD1 does not prematurely interact with coating formulation components, and FD1 can “report” early corrosion even in the presence of pigments.

## CHAPTER 4

### FD1 STABILITY IN AN EPOXY COATING

*Summary.* This chapter deals with the stability of the FD1 sensing molecule in an epoxy matrix over time in order to establish the robustness of the indicator in a practical application. It is shown that the FD1 molecule itself is slightly sensitive to photooxidation, which results in change of the color of the indicator to pink and for fluorescence to appear. Nevertheless, when embedded in the clear epoxy matrix (both model and commercial epoxy system) FD1 showed stability to photooxidation over time and lack of interaction with the epoxy components. Interestingly however, a slight increase in the FD1 fluorescence over time was observed when the indicator was embedded in the filled commercial epoxy coating, only when the coating was scratched. This change in FD1 fluorescence was ascribed to the presence of the various additives in the filled coating (such as  $\text{TiO}_2$ ), which can facilitate photooxidation of an indicator. FD1 proved to be a robust corrosion indicator, when embedded in epoxy coatings, capable of sensing corrosion even after prolonged exposure (28 months) to an aqueous solution.

#### **4.1 Introduction and Objectives of this Chapter**

FD1, in order to serve as a robust corrosion indicator in a practical application, must maintain its ability to respond to the metal corrosion throughout the coating lifetime, which often means 10-15 years. Most of the anticorrosion coatings are applied to protect metal surfaces from aqueous solution (e.g. salt water) thus the FD1 molecules must reside in the epoxy matrix even after prolonged exposure to the aqueous environment to serve as an effective corrosion indicator (i.e. it should not leach out of the coating matrix). During the course of experiments, it was observed that FD1 does not dissolve in water thus it is not expected to readily leach out of the matrix when placed in the aqueous environment. However this statement has to be confirmed experimentally.

Another issue that had to be addressed in order to confirm FD1 effectiveness as a corrosion sensor when embedded in the epoxy matrix over time, was its sensitivity to oxidation or/and photooxidation that can change the indicator's fluorescent characteristics and cause undesired premature response. Since FD1 was introduced in the literature, these properties have not yet been reported for the molecule.

Thus the purpose of this chapter is to examine FD1 long-term stability and its ability to serve as a corrosion sensor in the epoxy coating over prolonged periods of time.

## **4.2 Experimental Section**

### **4.2.1 Reagents and Materials**

All the reagents and materials used in this chapter are described in section 3.3.1 of chapter 3. Additionally, deuterated tetrahydrofuran (THF-d<sub>8</sub>) was purchased from Cambridge Isotope Laboratories, Inc. Titanium dioxide (TiO<sub>2</sub>, Aeroxide<sup>®</sup> P25) was purchased from Evonik Industries.

### **4.2.2 Sample Preparation and Characterization**

#### **4.2.2.1 Measurement of FD1 Sensitivity to UV Light in a Filled Coating**

FD1 sensitivity to UV light in a filled commercial epoxy coating (Haze Gray MIL-DTL-24441C, type III, Formula 151) (sample AA1-96A described in section 3.3.8 of chapter 3) was observed on a Zeiss LSM 510 Meta Laser Scanning Confocal Microscope with an Axio Imager M1 platform. An EC Plan-Neofluar 10 /0.30 M27 objective and the microscope's 100 W mercury lamp was used as a UV light source to observe the sample surface. The fluorescent emission wavelength was obtained from the lambda mode function (using Meta detector with selected emitted fluorescence range 520-660 nm with 10.7 nm step) when a 514 nm ArMultiLine laser was used as the excitation source. The



pictures of the coating surface were taken with a digital camera through the microscope's eye-piece.

#### 4.2.2.2 Measurement of FD1 Sensitivity to UV Light in the Solid State

To determine FD1 sensitivity to UV light in the solid state, FD1 (AA2-27; synthesis described in section 3.3.2.1) in the form of almost colorless crystals was placed on a glass slide, covered with a cover glass and subsequently exposed to high power UV light from the 100 W mercury lamp from the Zeiss LSM 510 Meta Laser Scanning Confocal Microscope. The change in color under UV was observed through the microscope's eye-piece and the pictures were taken with a digital camera. The sensitivity and fluorescent response of the color changed FD1 (AA1-70, after 10 months) to  $\text{FeCl}_3/\text{CH}_3\text{CN}$  solution was tested on Cary Eclipse fluorescence spectrofluorometer with an excitation wavelength of 510 nm (experiment **AA2-28**). The examined solution was placed in a 3 ml quartz cuvette. The results from this experiment (AA2-28) were compared with the experiment AA2-19 (described in section 3.3.3).

#### 4.2.2.3 FD1 Sensitivity to UV Light in Solution

To determine FD1 sensitivity to UV light in a solution, experiment **AA2-56** was performed. A few crystals of FD1 were dissolved in 2 ml of  $\text{CH}_3\text{CN}$  and the whole solution was placed in a 3 ml quartz cuvette. The solution was then exposed to UV light (excitation wavelength 254 nm) for different periods of time by placing a handheld UV

lamp (Model UVGL-25, MINERALIGHT<sup>®</sup>) 5 cm from the cuvette containing the solution. The change in FD1 fluorescence upon exposure to UV light was monitored on Cary Eclipse fluorescence spectrofluorometer with an excitation wavelength of 510 nm. To observe the change in the chemical structure of FD1 when exposed to UV light, experiment **AA2-59** was performed. A concentrated solution of FD1 in deuterated tetrahydrofuran (THF-d<sub>8</sub>) was prepared. The solution was placed in a 3 ml quartz cuvette and then exposed to UV light (excitation wavelength 254 nm) for different periods of time. The changes in the structure of FD1 were examined using <sup>1</sup>H NMR (Varian *Mercury* 400 MHz NMR with autosampler capabilities). The fluorescence intensity change with time of exposure to UV light was monitored with the fluorescence spectrofluorometer with an excitation wavelength of 510 nm.

The influence of oxygen on FD1 UV sensitivity was determined in experiment **AA2-60**. A solution of FD1 in CH<sub>3</sub>CN ( $1.42 \times 10^{-2}$  M) was placed in four 4 ml vials. Two of the vials were purged with argon (to remove oxygen) and the remaining two were not. All the vials were capped and sealed with paraffin film. Then one vial purged with argon and one not purged were exposed to UV light (254 nm) from handheld UV lamp for total time of 8 days. The two remaining vials were wrapped in aluminum foil to protect them from light (not exposed to UV light). The color change of the solutions with exposure to UV light was observed.

#### 4.2.2.4 Investigation of FD1 Fluorescence Gradient across the Filled Epoxy

##### Coating

Preparation of samples AA1-71D and AA1-96A was described in sections 3.3.7 and 3.3.8 of chapter 3, respectively. Sample **AA1-96B** was prepared in the same way as sample AA1-96A. However in this case, the coating with FD1 was applied on both sides of the sample. During preparation of this sample, a 10 wt% phosphoric acid solution was accidentally spilled on the back of the sample immediately after coating application causing the appearance of a pink color (this accident inspired some of the interpretation of other results in this chapter). AA1-96B sample was used as a reference sample (it was not exposed to NaCl solution but left exposed to air and sunlight). Sample **AA2-01** was prepared by mixing FD1 (0.5 wt% based on the dry coating) with both components of commercial epoxy-polyamide coating (Haze Gray MIL-DTL-24441C, type III, Formula 151). FD1 was dissolved in toluene prior mixing. After mixing, the resin solution was poured into a rectangular shaped silicone mold and cured at room temperature for one week. After curing the specimen thickness was 1.8 mm.

Surfaces of the samples: AA1-96A, AA1-96B, AA1-71D, AA2-01, AA1- 62 (FD1 in clear commercial coating, described in section 3.3.4) and AA1-48A (FD1 in model clear epoxy coating applied on steel surface, described in section 3.3.6) were scribed with a metal razor blade. The samples were then investigated with the confocal microscope under UV light.

To investigate if FD1 can be photooxidized on the surface of titanium dioxide (TiO<sub>2</sub>) particles, 1 mg of the TiO<sub>2</sub> pigment was dispersed in a solution of FD1 in THF (19.5 M) (experiment **AA3-36**). The mixture was exposed to 356 nm UV light from a handheld UV lamp for 1.5 h. Color of the initially white dispersion changed to slightly pink after the UV exposure. When the solution was left to evaporate for 20 h (not exposed to UV) the color of the particles changed to bright pink.

To observe FD1 fluorescence gradient across the filled coating thickness, small pieces (with dimensions 1 cm × 1.5 cm) were cut from the corners of samples AA1-71D and AA1-96B using a diamond saw (experiment **AA1-06**) and mounted in a clear epoxy resin in such a way that the metal/coating cross-sections were viewed from above after the resin was cured. After curing for 1 day, the epoxy discs (with the embedded cross-sectioned pieces) were polished with different grading steps sand papers (starting from 180 grit and finishing with 600 grit) and aluminum oxide as a final polishing step to obtain smooth metal/coating cross-sections. The cross-sections were examined under the confocal microscope with 20× magnification (compared to all other experiments where 10× magnification was used).

#### 4.2.2.5 FD1 Leaching Tests

**AA2-87A**; TEPA (amine hardener) and DGEBA (epoxy resin) (at a NH/epoxy molar ratio of 1.0:0.8 to obtain full conversion of epoxy) were mixed with FD1 (0.5 wt%, previously dissolved in toluene). After curing for 1 week at room temperature, the sample

was placed in an aqueous solution of  $\text{FeCl}_3$  (0.125 M) for 6 months. To determine if FD1 leached out of the epoxy matrix to the aqueous solution after this time, 0.5 ml of the  $\text{FeCl}_3$  solution from this experiment was mixed with 0.5 ml THF (to fully dissolve FD1 that potentially leached out of the matrix) and placed in a 3 ml quartz cuvette (experiment **AA3-38A**). The solution's fluorescence was examined on an AMINCO-Bowman Series 2 (AB2) spectrofluorometer with an excitation wavelength of 510 nm.

The FD1 leaching after prolonged exposure to aqueous solution was also determined in experiment **AA3-38B**. After 28 months of immersion, 0.5 ml of the  $\text{FeCl}_3$  solution from experiment AA1-84A (described in section 3.3.5; FD1 (1.5 wt% based on dry coating) in the filled epoxy coating, free of substrate immersed in  $\text{FeCl}_3$  aqueous solution) was mixed with 0.5 ml of THF and placed in a 3 ml quartz cuvette. The fluorescence of this solution was determined as described in the previous experiment.

## **4.3 Results and Discussion**

### **4.3.1 FD1 Sensitivity to UV Light**

#### **4.3.1.1 FD1 Sensitivity to UV Light in a Filled Coating**

During the experiment testing the ability of FD1 to sense undercoating steel corrosion when embedded in the filled commercial epoxy coating (described in section 3.3.8, Figure 41) it was observed that the areas examined for a prolonged time under UV light

changed their color from bright blue to grayish-blue. These areas included the area in the blister (Figure 41f) and AREA 1 (left image in Figure 43). However AREA 2, which was not examined under UV as often, kept its original bright blue color (under UV light) as shown in the right image of Figure 43.

#### FD1 Sensitivity to UV Light



Figure 43. Areas in sample AA1-96A exposed to UV for a prolonged period of time (left image) and not exposed to UV (right image). Pictures were taken through microscope eye-piece under UV light.

Also, a slight fluorescence, with maximum emission ( $\lambda_{em,max}$ ) at 570, was observed by the confocal microscope in areas exposed to UV light for longer periods of time. The color change might be explained by prolonged exposure of the coating to high power UV light during the imaging. However the fluorescence that appeared with time of exposure to UV was characteristic to FD1. Thus it appears that this increase in fluorescence must be related to FD1 sensitivity to UV light that results in a slight increase in its fluorescence intensity.

#### 4.3.1.2 FD1 Sensitivity to UV Light in the Solid State

FD1 was observed to change its color (which also corresponds to an increase in fluorescence) from slightly orange-pink to bright pink when stored in a capped clear glass vial over time (Figure 44).



Figure 44. FD1 (AA1-70) color change over time.

This color change could suggest that FD1 is sensitive to oxidation or photooxidation (since the indicator was exposed to light). This finding was confirmed in experiment AA2-58 when a high power UV lamp with maximum excitation wavelength at 350 nm (from the confocal microscope) was used to induce photooxidation of solid FD1 (in powder form). In this case, color change was observed much faster as seen in Figure 45. Under visible light (after 16 min of exposure to UV light) it was obvious that FD1 crystals changed color from almost colorless to light pink.

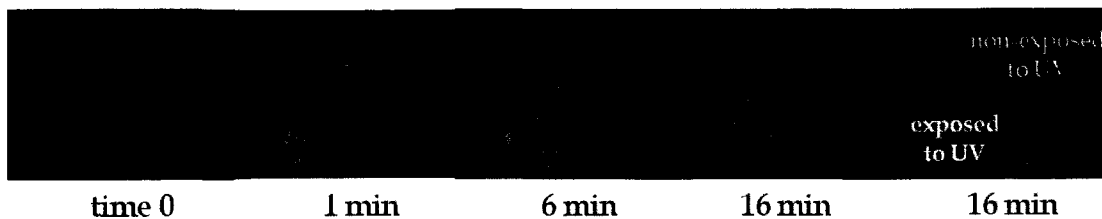


Figure 45. Color change of FD1 crystals upon exposure to UV light (350nm) (AA2-58).

It is important to note that even after the color of FD1 changed to pink after 10 months (middle image in Figure 44) the indicator's sensitivity (when dissolved in CH<sub>3</sub>CN) to FeCl<sub>3</sub>/CH<sub>3</sub>CN (AA2-28) was not changed as proved by comparison of the fluorescent emission spectra to that of experiment AA2-19.

#### 4.3.1.3 FD1 Sensitivity to UV Light in Solution

The FD1 sensitivity to UV light when in solution was investigated in experiment AA2-56. Solution of FD1 in CH<sub>3</sub>CN was exposed to UV light (254 nm) for a total time of 71 h. The fluorescent emission of the solution at 580 nm (when excited with 510 nm) was found to increase with time of exposure to UV as shown on the graph in Figure 46. In addition, the color of the solution changed from colorless to slightly orange-pink and more intense orange-pink with longer exposure time (right images in Figure 46).

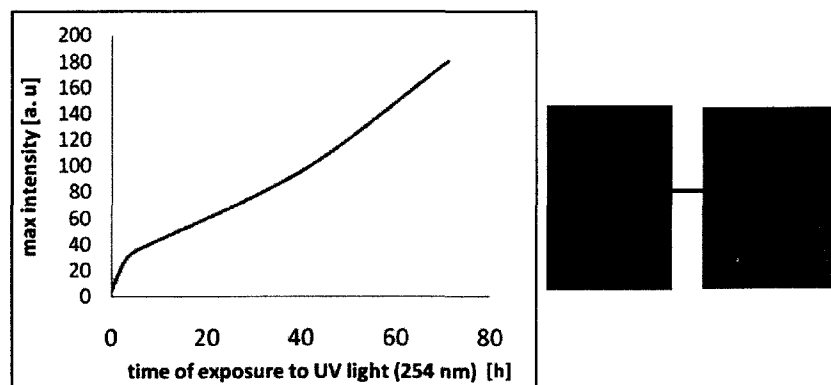


Figure 46. Change in the fluorescent intensity at 580 nm (left) and color (right) of FD1 in CH<sub>3</sub>CN upon exposure to 254 nm UV light (AA2-56).

This experiment confirmed that FD1 fluorescence (and color) increases slightly when the molecule is exposed to UV light.



To determine how and to what extent UV influences the chemical structure of FD1, experiment AA2-59 was performed. A concentrated solution of FD1 in THF-d<sub>8</sub> was prepared and examined using <sup>1</sup>H NMR after different times of exposure to UV light (254 nm for 8 days and 354 nm for additional 13 days). The total exposure time was 21 days. In this case THF was used to dissolve FD1 to facilitate higher concentrations more suited to higher resolution <sup>1</sup>H NMR spectra (THF is a better solvent than CH<sub>3</sub>CN). Even though the color of the solution changed with UV exposure from colorless to pink-red (and its fluorescent intensity with maximum emission at 583 nm increased) no significant changes in the <sup>1</sup>H NMR spectra were observed even after 21 days of exposure to UV light. This result suggested that even minute changes in the chemical structure of FD1 (not detected by <sup>1</sup>H NMR) due to prolonged exposure to UV light can noticeably change the molecule's fluorescent (and chromophoric) behavior.

The influence of oxygen on UV sensitivity (sensitivity to photooxidation) of FD1 solution in CH<sub>3</sub>CN was determined in experiment AA2-60. As can be seen in Figure 47, samples not exposed to light (vials 3 and 4) remained colorless over time. The sample exposed to both oxygen and UV light (254 nm) changed color to light pink after only 24 h (vial 1 in the left image in Figure 47). The intensity of the color increased with UV exposure and reached pink-red after 8 days (vial 1 in the right image in Figure 47). The sample exposed to only UV light (and not to oxygen) also showed change in color from faint pink (vial 2 in the left image in Figure 47) to more intense pink-red (vial 2 in the right image in Figure 47). This could be caused by the oxygen eventually reaching the

sample causing slow color change. This change however was much slower than observed for vial 1. Both solutions (vial 1 and 2) that showed color change in visible light were also fluorescent orange under UV light.

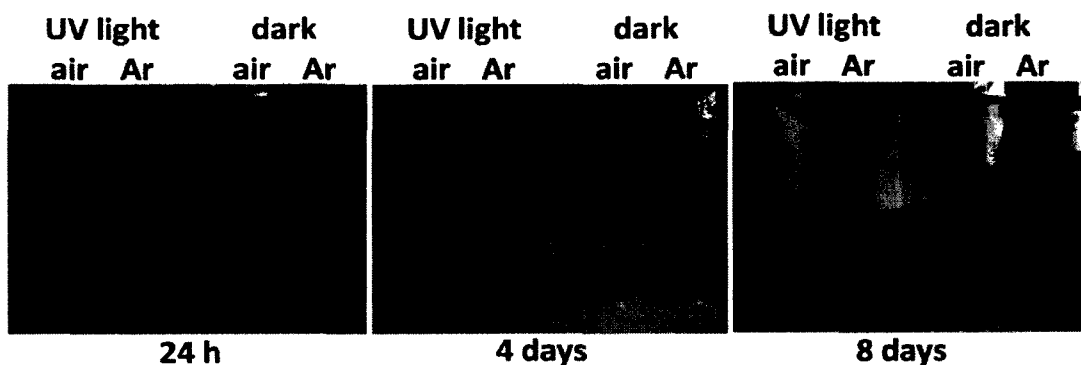


Figure 47. Sensitivity of FD1 in CH<sub>3</sub>CN to UV light and oxygen.

The results of this experiment showed that the color change of FD1 (and its fluorescence) is influenced by both oxygen and UV light suggesting that FD1 is sensitive to photooxidation. However only prolonged exposure to UV light and oxygen caused color change of the FD1 solution. This finding was confirmed by observation of the FD1 solutions during storage. The solution of FD1 (in THF or CH<sub>3</sub>CN) exposed only to sunlight showed no color change even after months of storage in a glass vial (non-permeable to oxygen). On the other hand when the FD1 solution (in CH<sub>3</sub>CN) was stored in polyethylene bottles (that allow oxygen diffusion) the pink color (and low intensity fluorescence) appeared in the solution after a few months of storage. However FD1 embedded in the highly crosslinked epoxy coating is expected to be significantly more resistant to photooxidation due to slower oxygen diffusion in the crosslinked matrix than in solution. Thus the sensitivity of FD1 to photooxidation might not be an issue in a

practical application where the molecule is used as a corrosion sensor when embedded in the epoxy coating. This topic is addressed in the next section of this chapter.

### **4.3.2 FD1 Stability in the Epoxy Coating**

#### **4.3.2.1 Fluorescence of FD1 in Epoxy Coating when Scratched**

Even though FD1 seemed not to interact with the clear commercial epoxy coating (as shown in section 3.5.3), and did not change its fluorescence as a result of this interaction, a puzzling phenomenon was observed when FD1 was embedded in the filled commercial epoxy coating (Haze Gray MIL-DTL-24441C). In the AA1-96A sample (described in section 3.5.7) in AREA2 (not exposed to NaCl solution) the surface of the filled coating with embedded FD1 applied on steel showed no significant fluorescence, as observed by the confocal microscope under UV light (left image in Figure 43), even after a few months after coating application. However, when the coating surface was slightly scratched with a razor, some low intensity fluorescence was revealed with maximum emission at 570 nm (left image in Figure 48).

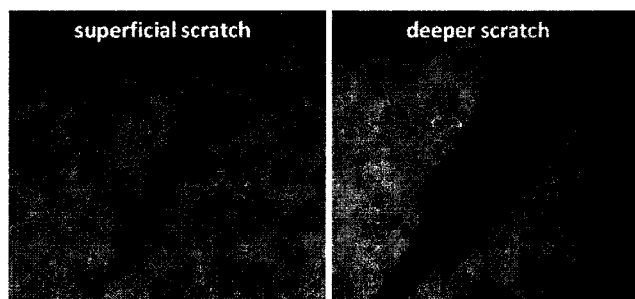


Figure 48. Scratched filled epoxy coating (AA1-96A, AREA2)

This value is lower than the value reported for areas where early corrosion was detected (580 and 585 nm, section 3.5.7). The lower wavelength could suggest that the fluorescence is much less intense in the scratched area (as described in section 3.5.2 at lower emission intensities the wavelength at which the maximum emission is observed shifts to a lower value). Similar phenomenon was observed in the samples: AA1-71D (FD1 in filled epoxy coating applied on the steel surface; described in section 3.5.6), AA1-96B (prepared in the same way as AA1-96A but not exposed to NaCl; used as a reference) and in sample AA2-01 (free standing filled epoxy film with FD1, not applied on a metal surface); the coating revealed some low intensity fluorescence when scratched. As an example, the scratch on sample AA1-71D is shown in the left image in Figure 49.

When the coating was scratched deeper to the metal surface in samples AA1-96A and AA1-96B, even more intense orange fluorescence was observed (right image in Figure 48) with  $\lambda_{em,max} = 580$  and 585 nm. However that was not the case for samples AA1-71D (right image in Figure 49) and AA2-01 in which the fluorescence was the same even when the scratch was much deeper.

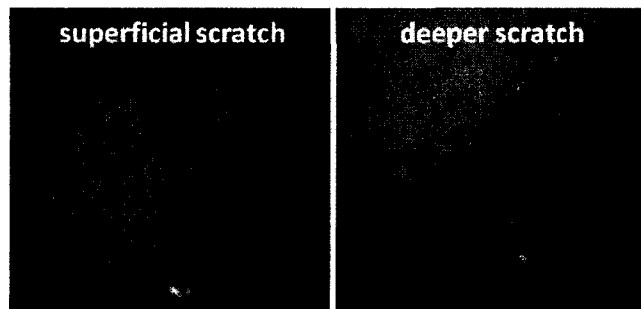


Figure 49. Scratched filled epoxy coating (AA1-71D)

These results suggested that there is some FD1 fluorescence gradient through the coating thickness for all of the samples (i.e. fluorescence is not observed on the top of the coating but only when scratched) in which the indicator is embedded in the filled coating. This fluorescence gradient was investigated and will be described in more detail in the next section of this chapter.

The surprising fact was that only samples AA1-96A and AA1-96B showed significant increase in the fluorescent intensity when the coating was scratched deeper to the metal surface and that this fluorescence was not observed on the top of the sample. However it was proven (in section 3.5.7 of the previous chapter) that FD1 in the filled coating was able to sense undercoating corrosion and its fluorescent response to the early corrosion was easily observable when the top of the coating was examined under UV (Figure 41). Perhaps in the case when high intensity fluorescence occurs only close to the metal/coating interface (as shown when AA1-96A and AA1-96B was scratched deeper to the metal surface), and not in the other parts of the coating closer to the top, it is not strong enough to be detected on the top of the coating. This dampening of the

fluorescence can be caused by 1) excitation light cannot reach that deep into the filled coating (i.e. the pigments in the coating can absorb the light so it does not reach the fluorescent molecule at the interface) or 2) emitted light of the excited fluorophores can not reach the top of the coating (for the same reasons).

In the case when corrosion occurs under the coating, the ions released during the process can diffuse into the coating and interact with FD1 causing its fluorescence to appear in the coating layers closer to the top. For this reason the light emitted by the sensor can be seen on the top of the coating. Thus the coating thickness seems to play a big role in the detection of fluorescence in the case of filled coating and this factor has to be included in the design of the corrosion sensing systems.

When the same “scratch” experiment was performed for clear epoxy coatings with embedded FD1 (samples in AA1- 62; FD1 in clear commercial coating, described in section 3.3.4 and sample AA1-48A; FD1 in model clear epoxy coating applied on steel surface, described in section 3.3.6) no fluorescence was revealed even months after sample preparation. These results suggested that FD1 shows slight fluorescence only in the deeper layers of the filled coating. This could be caused by the pigments (e.g. titanium dioxide,  $\text{TiO}_2$ ) and other additives that are present in this commercial coating that might influence the fluorescent behavior of FD1 (e.g. facilitate its photooxidation). The photoactivity of  $\text{TiO}_2$  pigment has been reported since the early 20<sup>th</sup> century. UV absorption of  $\text{TiO}_2$  produces active oxygen species on the pigment’s surface [64]. These active species could oxidize FD1 (also absorbed on the surface) causing its fluorescence.

Since the clear coatings do not contain this pigment (or any other pigments) the change in FD1 fluorescence over time was not observed in the case where FD1 was embedded in the clear coating. In this case, the photooxidation was significantly slowed down due to the highly crosslinked epoxy matrix, thus the change in color and fluorescence did not take place in these systems.

The ability of TiO<sub>2</sub> to photooxidize FD1 was tested in experiment AA3-36. In this experiment, a solution of FD1 in THF was mixed with TiO<sub>2</sub> powder and exposed to UV light (365 nm) for 1.5 h. After this short time of UV exposure an obvious light pink color was observed in the powder. When the mixture was left for 20 h to evaporate the solvent, a bright pink color appeared in the powder proving that FD1 was photooxidized to its fluorescent form. The actual product of FD1 photooxidation was not determined at this time since it was out of the scope of the current study

#### 4.3.2.2 Change in FD1 Fluorescence across the Coating Thickness

To investigate the change of FD1 fluorescence across the coating thickness, experiment AA1-06 was performed. The cross-sections of samples AA1-96B, AA1-71D and AA2-02 were investigated by confocal microscope (with 20× magnification for samples AA1-96B, AA1-71D and 10× magnification for sample AA2-01). Surprisingly the cross-section of sample AA1-71D showed no fluorescence gradient across the coating thickness (as seen in the left image in Figure 50). It is worth mentioning however that one area at the metal/coating interface showed some indication of superficial corrosion. In

addition, fluorescence was observed near this area under UV (orange color as seen in the bottom left image in Figure 50) and on the fluorescent image from the confocal microscope's lambda mode (yellow areas in the inset of the bottom left image in Figure 50 with  $\lambda_{em,max}$  at 580 and 585 nm). At this point, early corrosion stages were missed (since the rust can be already seen) however FD1 was still fluorescent near the corroded area proving its ability to sense corrosion. In this case, the sample was not exposed to the corrosive environment (i.e. NaCl solution) however uncoated steel corrodes readily even when only exposed to air. Thus the occurrence of the corrosion was not surprising since the metal was unprotected.

Unlike AA1-71D, the front of the reference sample AA1-96B (not exposed to NaCl) showed variations in the fluorescence across the coating thickness. Some bright orange fluorescent areas (under UV, bottom middle image in Figure 50) were observed across the whole metal/coating interface. They showed  $\lambda_{em,max}$  at 580 and 585 nm (yellow areas in the inset of the bottom middle image in Figure 50). However no indication of corrosion was observed near these areas. Also the back of the sample was investigated. The top layer of the coating appeared slightly pink under natural light (top right image in Figure 50) and bright orange under UV (bottom right image in Figure 50).



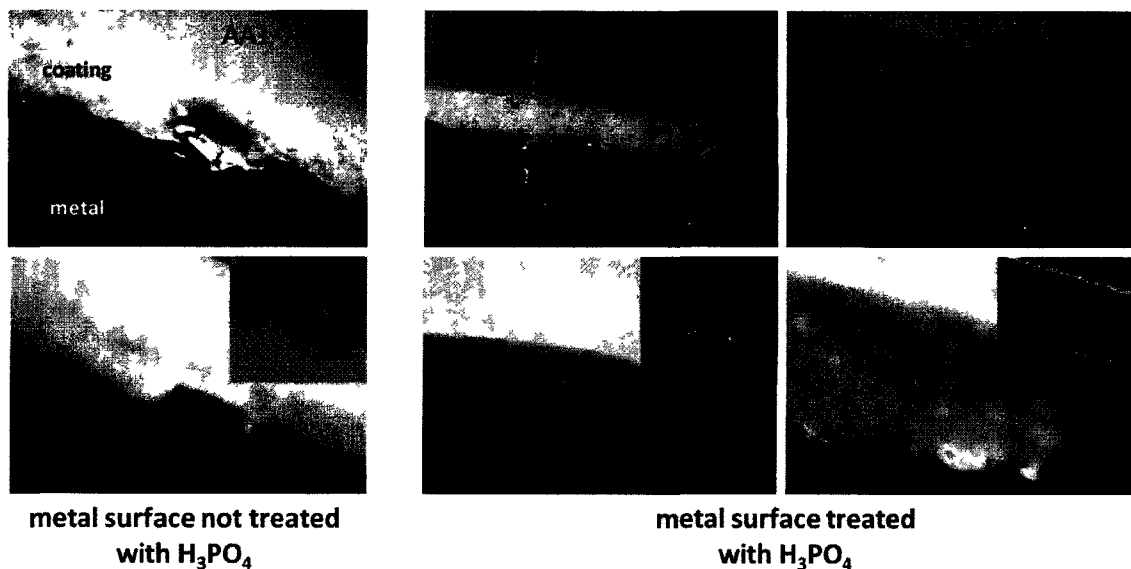


Figure 50. Cross-sections showing metal/coating interface of samples AA1-71D (not treated with  $H_3PO_4$  before coating application) and AA1-96B (front and back of the sample, treated with  $H_3PO_4$  before coating application). Top row: images taken through the confocal microscope eye-piece ( $20\times$  magnification) under natural light; bottom row: images taken through the microscope eye-piece under UV light. Insets in the bottom row pictures show the fluorescent images obtained from the confocal microscope's lambda mode.

The fluorescence in the top bright layer (in Figure 46, bottom right) was identical to the one for the bright areas at the metal/coating interface. The pink color on the back of the AA1-96B sample was observed even before the sample was examined on the confocal microscope. It appeared when a solution of 10 wt% phosphoric acid ( $H_3PO_4$ ) was accidentally spilled on the sample right after the coating application. This occurrence suggested that the steel surface pre-treatment with  $H_3PO_4$  (to remove any impurities and corrosion products from the substrate surface) before epoxy coating could have also influenced the fluorescent areas at the metal/coating interface; the pre-treatment was performed on both samples AA1-96A and AA1-96B. In closer inspection of the work by Zhang et al. [57] (that originally proposed the FD1 molecule as a  $Fe^{3+}$  chemosensor), the supporting information reported that FD1 is also sensitive to changes in pH and becomes fluorescent with decreasing pH. The fact that the maximum fluorescent intensity was the

same in both the top surface and at the metal/coating interface suggested that the bright spots at the metal/coating interface were probably due to residual  $\text{H}_3\text{PO}_4$  that was used to clean the steel surface. As a result, the FD1 corrosion sensing mechanism and its response to acidic solution was more closely investigated and will be described in detail in the following chapter of this thesis.

With this result, it was then clear as to the reason the deeper scratch revealed brighter fluorescence in the samples AA1-96A (Figure 48) and AA1-96B (steel surface treated with  $\text{H}_3\text{PO}_4$  before coating application) and not in the sample AA1-71D (Figure 49, steel surface not treated with  $\text{H}_3\text{PO}_4$  before coating application). However the cross-section experiment did not explain why low intensity fluorescence was only observed when the coating was scratched and not from the top of the coating. Perhaps the coating was too thin to be able to observe this subtle change in fluorescence. Thus the thicker (1.8 mm) free standing sample of filled commercial epoxy coating with embedded FD1 (0.5 wt% based on the dry coating) was prepared (AA2-01) and observed under the confocal microscope after 1 year after curing. Before scratching the coating no fluorescence characteristic for FD1 was observed. When the coating was scratched, low intensity fluorescence ( $\lambda_{\text{em,max}} = 570$  and 580 nm) and light orange color (under UV light) were revealed (top left image in Figure 51). When the cross-section of this coating was examined, it was clear that there is a fluorescence gradient across the coating thickness (as seen in the bottom left image in Figure 51). The outer layer of the sample showed no significant fluorescence. However, deeper in the sample some light orange spots were

clearly seen indicating low intensity FD1 fluorescence. This observation explained why the fluorescence was observed only when the coating was scratched.



Figure 51. FD1 in filled epoxy coating (AA2-01). Top row: top view of the coating with the scratch before and after immersion in HCl (left and right image respectively). Bottom row: cross-section of the coating before and after immersion in HCl (left and right image respectively). Images taken through the microscope eye-piece under UV light.

This gradient in fluorescence across the coating thickness was even more obvious when the sample was immersed in a 0.1M HCl solution for 1 day (as indicated above, it was known by this point that FD1 responds to low pH) (right images in Figure 51). Thus it was concluded that FD1 appears to stay away from the coating/air interface. The underlying reason could be the difference in surface energy between FD1 and epoxy components. FD1 may not have a higher surface energy than the amine hardener, but its surface energy is very likely higher than the epoxy component, which is why FD1 tends to “shy away” from the top surface. This may explain why fluorescence of FD1 is revealed only when the coating is scratched. This experiment also proved that slightly fluorescent FD1 (after being embedded in the filled coating for 1 year) can still be highly responsive to low pH.

#### 4.3.2.3 FD1 Leaching Test

To determine if FD1 leached out of the epoxy matrix after 6 months of immersion in the aqueous solution, experiment AA3-38A was performed. FD1 was embedded in the clear model DGEBA-TEPA coating (0.5 wt%) (sample AA2-87A). After curing, the sample was placed in an aqueous solution of  $\text{FeCl}_3$  (0.125 M) for 6 months. The bright pink color and fluorescence (under UV light) of the sample was easily observed after this immersion time. The solution from this experiment was collected after 6 months and mixed with THF to fully dissolve FD1 that potentially leached out of the matrix (1:1 v/v). If there was any FD1 present in that mixture it should give a fluorescent response upon reaction with  $\text{FeCl}_3$ . When this mixture was examined by a spectrofluorometer with an excitation wavelength of 510 nm, no fluorescence was observed (red curve in the spectra in Figure 52) proving that FD1 did not leach out of the epoxy matrix after 6 months of immersion in the aqueous solution.

A similar experiment was performed to determine if FD1 would leach out from the epoxy matrix after prolonged exposure to an aqueous solution (experiment AA3-38B). FD1 embedded in the filled epoxy coating (1.5 wt% based on dry coating; experiment AA1-84A described in section 3.3.5) was immersed in the  $\text{FeCl}_3$  aqueous solution for 28 months. After this time, 0.5 ml of the  $\text{FeCl}_3$  solution from this experiment was mixed with 0.5 ml of THF. This mixture showed some low intensity fluorescence when examined by a spectrofluorometer with an excitation wavelength of 510 nm (blue curve

in the spectra in Figure 52). However the maximum emission intensity ( $\lambda_{em,max}$ ) was observed at around 570 nm which indicates that the intensity of this fluorescence was very low (maximum emission intensity for highly fluorescent FD1 species is at 580 nm and higher). This experiment showed that a minute amount of FD1 eventually diffused out of the epoxy matrix to the aqueous environment after prolonged time of 28 months. It is worth mentioning however that the sample AA1-84A after immersion in the  $FeCl_3$  aqueous solution for 28 months still showed pink color and fluorescence (as examined under UV light) proving that the remaining FD1 in the sample was still responsive to  $FeCl_3$  solution.

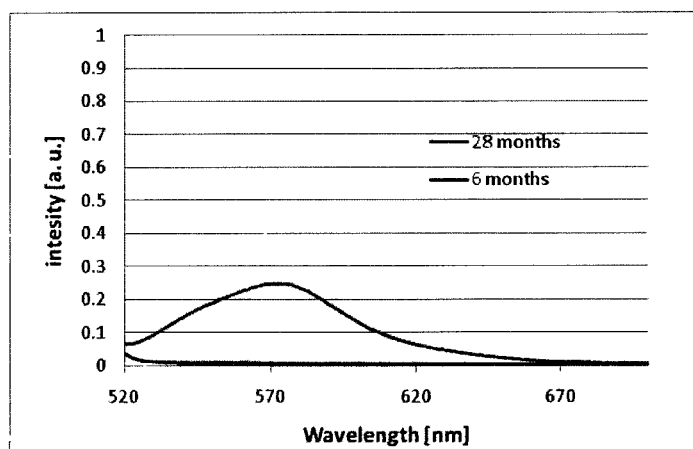


Figure 52. Fluorescent spectra of the  $FeCl_3$ /THF solutions from experiments AA3-38A and AA3-38B (after 6 and 28 months of sample immersion in  $FeCl_3$  solution respectively).  $\lambda_{ex} = 510$  nm.

#### **4.4 Conclusions**

FD1 in the solid state, as well as in solution, showed a slight sensitivity to photooxidation. However, only prolonged exposure to UV light and oxygen caused

significant color and fluorescence of the indicator to appear. Even after color change to pink, due to photooxidation, FD1 was still highly responsive to a  $\text{FeCl}_3/\text{CH}_3\text{CN}$  solution. Moreover, FD1, when embedded in the clear epoxy matrix (both model and commercial epoxy system), even months after sample preparation, showed no change in its fluorescence proving its stability to photooxidation in the epoxy matrix over time and lack of interaction with the epoxy components. Interestingly when the indicator was embedded in the filled commercial epoxy coating, over time a slight increase in the FD1 fluorescence was observed when the coating was scratched. This change was most likely caused by the presence of the various additives in the coating, such as  $\text{TiO}_2$  (that itself can facilitate FD1 photooxidation). FD1 did not leach out of the epoxy matrix after immersion in the aqueous  $\text{FeCl}_3$  solution for 6 months. After 28 months however, some minute traces of FD1 were detected in the aqueous solution indicating that FD1 slowly diffused out of the epoxy matrix. The remaining FD1 was still responsive to  $\text{FeCl}_3$  proving that even after prolonged exposure to the aqueous solution enough FD1 is still in the coating to be capable of sensing corrosion.

## CHAPTER 5

### EXPLORATION OF FD1 SENSING MECHANISM<sup>†</sup>

**Summary.** In this chapter, the ability and mechanism of FD1 sensing early stages of steel corrosion via “turn-on” fluorescence is explored. Three potential mechanisms causing FD1 fluorescent response due to corrosion are considered: namely, FD1/Fe<sup>3+</sup> complexation, FD1 oxidation to a fluorescent form, and FD1 sensitivity to acidic pH. It is shown that at low pH (which is observed at the anodic site of corrosion) FD1 undergoes hydrolysis, catalyzed by acid, to fluorescent protonated Rhodamine B hydrazide (RBH). It has been also confirmed that FD1 forms a fluorescent FD1/Fe<sup>3+</sup> complex in a non-aqueous solution. However when an aqueous solution of ferric salt is titrated to the FD1 solution, the “turn-on” fluorescence is due to acidity of the solution and not due to the FD1/Fe<sup>3+</sup> complex formation. It is also proposed to explore RBH itself as a corrosion indicator due to its “turn-on” fluorescence at low pH and due to the fact that it can be covalently bonded to a polymeric network without losing its responsiveness to low pH, which eliminates the possibility of the molecule leaching out of the epoxy matrix.

---

<sup>†</sup> Portions of this chapter have been published: Augustyniak, A.; Ming, W. Early detection of aluminum corrosion via “turn-on” fluorescence in smart coatings. *Prog. Org. Coat.* **2011**, 71, 406-412 (doi:10.1016/j.porgcoat.2011.04.013).

## **5.1 Introduction and Objectives of this Chapter**

In sections 3.5.5, 3.5.6 and 3.5.7 of chapter 3, the FD1 molecule was proved to sense early stages of steel corrosion when incorporated into an epoxy matrix via “turn-on” fluorescence.

This molecule was chosen as a corrosion indicator due to its ability to selectively sense  $\text{Fe}^{3+}$  ions, as claimed by Zhang et al. [57]. Those authors used FD1 for sensing metal concentrations within living cells for bioimaging. Here in the work of this thesis, the FD1 molecule was chosen to sense  $\text{Fe}^{3+}$  ions that are produced during the corrosion of steel. Even though the structure of a potential FD1- $\text{Fe}^{3+}$  fluorescent complex was proposed by Zhang et al. (Figure 29), no experimental evidence confirming the actual chemical structure of the complex formed was shown in their manuscript. Other authors also claimed the discovery of the molecule forming fluorescent complexes with  $\text{Fe}^{3+}$  [54], but similarly did not demonstrate any conclusive evidence for the complex formation.

It was also observed in section 4.2.2.3 that the FD1 indicator became slightly fluorescent with time due to oxidation. Additionally, during the course of the experiments with FD1 as a potential corrosion sensor, it was shown that FD1 was sensitive to low pH (i.e. fluorescence appeared under acidic conditions as described in section 4.3.2.2). This sensitivity was also mentioned in the supplementary data of the publication by Zhang et al. [57], however the authors only showed the change in FD1 fluorescence (at 583 nm,  $\lambda_{\text{ex}}$



=510 nm) as a function of pH (Figure 53), without detailed mechanistic understanding of this phenomenon.

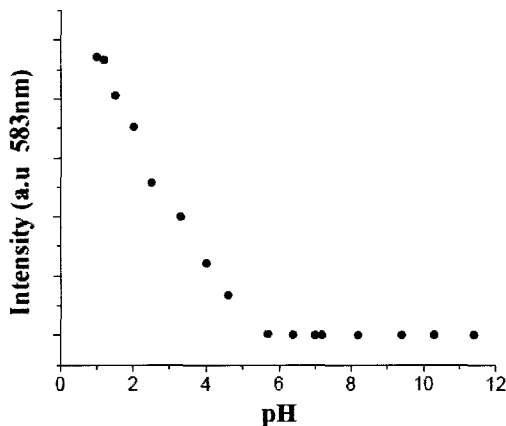


Figure 53. FD1 fluorescence (at 583 nm) as a function of pH;  $\lambda_{\text{ex}}=510$  nm [57].

FD1 sensitivity to acidic pH however is an additional advantage, when using the molecule as a corrosion sensor, since at the anodic sites of localized corrosion not only iron ions are produced but also a decrease in pH is observed (as described in sections 1.2.2). This could possibly expand the application of FD1 as a corrosion indicator in smart epoxy coatings to other important metals such as aluminum (since acidic pH is also observed at the anodic site of aluminum corrosion as described in section 1.1.3).

Thus three mechanisms can be considered as possible explanations for FD1's ability to sense steel corrosion via "turn-on" fluorescence:

1. FD1 binds  $\text{Fe}^{3+}$  produced at the anodic site of corrosion forming a fluorescent complex (as claimed by Zhang et al. [57])
2. FD1 is oxidized by  $\text{Fe}^{3+}$  ions to a fluorescent form ( $\text{Fe}^{3+}$  reduces itself to  $\text{Fe}^{2+}$ )

### 3. FD1 becomes fluorescent upon reaction with $H^+$ (under acidic pH)

Since an aqueous solution of  $FeCl_3$  is highly acidic ( $pH \approx 2$ ) and also acts as a strong oxidizer, all the mechanisms mentioned above can explain the fluorescent response of FD1 (when embedded in an epoxy coating; experiments described in sections 3.3.4 and 3.3.5) to the  $FeCl_3$  aqueous solutions. Even in the experiment AA2-19, where FD1/ $CH_3CN$  solution was titrated with  $FeCl_3/CH_3CN$  solution, since a trace amount of water is present in the system ( $CH_3CN$  contains 0.01% of water and additionally anhydrous  $FeCl_3$  used for this experiment readily absorbs water from air), the reason for FD1 fluorescence can be explained by mechanism number 3.

In order to determine if the FD1-epoxy smart coating systems can be used to sense corrosion of metals, other than steel, the detailed understanding of the FD1 corrosion sensing mechanism was necessary. Thus the purpose of this chapter is to determine which of the mechanisms mentioned above are responsible for the appearance of FD1 fluorescence due to corrosion.

## **5.2 Experimental Section**

### **5.2.1 Reagents and Materials**

FD1 was synthesized in our lab as described in section 3.3.2.1. Acetonitrile ( $CH_3CN$ , HPLC grade), tetrahydrofuran (THF) (HPLC grade), water (HPLC grade), xylenes (ACS grade), ferric chloride, anhydrous ( $FeCl_3$ ), hydrochloric acid (ACS grade, 36.5–38.0%)

and molecular sieve (0.4 nm) were purchased from EMD chemicals. Sodium hydroxide (NaOH) (ACS reagent, pellets, 97+ %), cyclen (97 %), potassium phosphate, monobasic (KH<sub>2</sub>PO<sub>4</sub>) and sodium phosphate, dibasic (Na<sub>2</sub>HPO<sub>4</sub>) were purchased from Acros Organics. The pH 7 and pH 12 buffers were prepared by mixing appropriate amounts of KH<sub>2</sub>PO<sub>4</sub> and Na<sub>2</sub>HPO<sub>4</sub> respectively with NaOH in DI water. HEPES buffer (4-(2-hydroxyethyl)-1-piperazineethanesulfonic acid, SigmaUltra, >99.5% titration) was purchased from Sigma-Aldrich. Ferric ammonium citrate, purified brown pearls, was purchased from Mallinckrodt. Triethanolamine (TEA, 99 %) was purchased from Pfaltz&Bauer. Deuterated solvents (water (D<sub>2</sub>O), chloroform (CDCl<sub>3</sub>), tetrahydrofuran (THF-d<sub>8</sub>) and toluene-d<sub>8</sub>) were supplied by Cambridge Isotope Laboratories, Inc. Gallium nitrate hydrate (Ga(NO<sub>3</sub>)<sub>3</sub>•xH<sub>2</sub>O), 99.9 % was purchased from Alfa Aesar. Sulfuric acid (ACS reagent) was purchased from Fisher Scientific. Rhodamine b hydrazide (RBH, AA2-80) was synthesized in our lab as described in section 3.3.2.2. D.E.R.<sup>TM</sup> 332 Epoxy Resin (high purity bisphenol A diglycidylether, DGEBA) was purchased from The Dow Chemical Company. Tetraethylenepentamine (TEPA, technical grade) was purchased from Acros Organics

## 5.2.2 Sample Preparation

### 5.2.2.1 Experiments proving FD1-Fe<sup>3+</sup> Complexation & FD1 Hydrolysis in Acidic pH

**AA2-17;**  $2 \times 10^{-5}$  M solution of FD1 in CH<sub>3</sub>CN was diluted twice with NaOH/KH<sub>2</sub>PO<sub>4</sub> buffer solution (pH 7). 3 ml of this mixture was titrated with  $4 \times 10^{-3}$  M solution of FeCl<sub>3</sub> in CH<sub>3</sub>CN. Each drop of FeCl<sub>3</sub> solution (0.02 ml) was equal to one Fe<sup>3+</sup>/ FD1 equivalent. The solution was titrated up to 80 Fe<sup>3+</sup>/ FD1 equivalents. The fluorescence response of FD1 to FeCl<sub>3</sub> was recorded on the spectrofluorometer.

**AA2-19;** Experiment was described in section 3.3.3.

**AA2-76;** Experiment was performed as described by Zhang et al. [57]; HEPES buffer was prepared by adjusting the pH of a 20 mM aqueous solution of HEPES to pH 7 with NaOH.  $10^{-5}$  M solution of FD1 in CH<sub>3</sub>CN was diluted 20 times with HEPES buffer and titrated with aqueous solution of FeCl<sub>3</sub> (0.001 M). Each addition of FeCl<sub>3</sub> solution (0.01 ml) was equal to 0.66 Fe<sup>3+</sup>/ FD1 equivalents. The solution was titrated up to 7 Fe<sup>3+</sup>/ FD1 equivalents. Then 0.5 M aqueous FeCl<sub>3</sub> solution was added to the mixture. The pH of this solution was checked with a pH-indicator strip. The fluorescence response of FD1 to FeCl<sub>3</sub> was recorded on the spectrofluorometer.

**AA2-45;** The fluorescence of 2 ml of the solution of FD1 in THF ( $3 \times 10^{-3}$  M) was examined on the spectrofluorometer ( $\lambda_{\text{ex}} = 510$  nm) before and after addition of  $\text{Fe}^{3+}$  from  $\text{Fe}(\text{acac})_3$  in THF ( $3 \times 10^{-2}$  M, orange solution). Each addition of 0.05 ml of  $\text{Fe}(\text{acac})_3/\text{THF}$  solution was equal to 0.5  $\text{Fe}^{3+}/\text{FD1}$  equivalent.

**AA2-75;** FD1 solution in  $\text{CH}_3\text{CN}$  ( $1.9 \times 10^{-4}$  M) was titrated with yellow-brown solution of ferric ammonium citrate (FAC). The FAC used in this experiment was a mixture of FAC Brown (16.5-18.5 % iron) and FAC Green (14.5–16 % iron). The pH of FAC aqueous solution was measured using pH-indicator strips. 2 ml of 1.3 % solution of FAC in HPLC water added to 0.5 ml of  $\text{FD1}/\text{CH}_3\text{CN}$  was calculated to be 1  $\text{Fe}^{3+}/\text{FD1}$  equivalent. The fluorescence of the  $\text{FD1}/\text{CH}_3\text{CN}$  solution upon addition of FAC was monitored on the spectrofluorometer ( $\lambda_{\text{ex}} = 510$  nm).

**AA2-74;** A few drops of triethanolamine (TEA) were added to 0.5 ml of an aqueous solution of  $\text{FeCl}_3$  ( $7.2 \times 10^{-4}$  M). The pH of this solution was measured with the pH-indicator strips. Then the mixture was diluted 5 times with the  $\text{Na}_2\text{HPO}_4/\text{NaOH}$  buffer solution (pH 12). The solution of FD1 in  $\text{CH}_3\text{CN}$  ( $1.9 \times 10^{-4}$  M) was titrated with the  $\text{FeCl}_3/\text{TEA}/\text{buffer}$  mixture. The fluorescence of the FD1 solution (1 ml) upon dropwise addition of  $\text{FeCl}_3/\text{TEA}/\text{buffer}$  was monitored on the spectrofluorometer ( $\lambda_{\text{ex}} = 510$  nm).

**AA3-39;** 3 ml of the FD1 in THF solution ( $20 \mu\text{M}$ ) was titrated separately with  $\text{FeCl}_3$  in THF (0.01 M) and  $\text{FeCl}_3$  in  $\text{H}_2\text{O}$  (0.01 M). The change in FD1 fluorescence was monitored on the spectrophotometer ( $\lambda_{\text{ex}} = 510$  nm) after each addition of  $\text{Fe}^{3+}$  solution.

Each drop (1.2  $\mu$ l) was equal to 0.2 Fe<sup>3+</sup>/FD1 equivalents. After reaching one Fe<sup>3+</sup>/FD1 equivalent the amount of FeCl<sub>3</sub> solution added was increased to 2.4  $\mu$ l each time (0.4 Fe<sup>3+</sup>/FD1 equivalents). The solutions were allowed to equilibrate for one minute after each FeCl<sub>3</sub> addition. Both FeCl<sub>3</sub> solutions were titrated to the point where no more increase in fluorescent emission was observed (3 and 5.8 Fe<sup>3+</sup>/FD1 equivalents for FeCl<sub>3</sub> in H<sub>2</sub>O and for FeCl<sub>3</sub> in THF respectively).

**AA3-40**; Identical to experiment AA3-39, the FD1/THF solution was titrated with FeCl<sub>3</sub> in THF (0.01 M) and FeCl<sub>3</sub> in H<sub>2</sub>O (0.01 M) but in this case the UV-vis absorption of the solution was recorded. Each addition (2.4  $\mu$ l) was equal to 0.4 Fe<sup>3+</sup>/FD1 equivalents. The solutions were allowed to equilibrate for one minute after each FeCl<sub>3</sub> addition. Both FeCl<sub>3</sub> solutions were titrated to the point where no more increase in absorption was observed (3.2 and 6 Fe<sup>3+</sup>/FD1 equivalents for FeCl<sub>3</sub> in H<sub>2</sub>O and for FeCl<sub>3</sub> in THF respectively).

**AA3-42A**; 0.1 ml of FD1 solution in anhydrous THF (8 mM) was diluted with 0.9 ml THF. The solution was examined by ESI-MS.

**AA3-42B**; 0.1 ml of FD1 solution in anhydrous THF (8 mM) was mixed with 0.2 ml of FeCl<sub>3</sub> solution in anhydrous THF (4 mM) to obtain 1 Fe<sup>3+</sup>/FD1 equivalent. The whole mixture was then diluted with 0.7 ml THF. Once FD1 was mixed with FeCl<sub>3</sub>, the color of the mixed solution turned bright magenta. The solution was examined by ESI-MS.

**AA3-42C**; 0.1 ml of FD1 solution in anhydrous THF (8 mM) was mixed with 0.6 ml of FeCl<sub>3</sub> solution in anhydrous THF (4 mM) to obtain 3 Fe<sup>3+</sup>/FD1 equivalents. The whole mixture was then diluted with 0.3 ml THF. Once FD1 was mixed with FeCl<sub>3</sub>, the color of the mixed solution turned bright magenta. The solution was examined by ESI-MS.

**AA2-44**; FD1 was dissolved in THF-d<sub>8</sub> (dried overnight with 0.4 nm molecular sieve). The <sup>1</sup>H NMR spectra were collected. Then excess of FeCl<sub>3</sub> in THF-d<sub>8</sub> was added. The color of the solution turned from colorless to dark magenta. The <sup>1</sup>H NMR spectra were collected again. Then excess of cyclen (metal chelator) was added to the solution to remove Fe<sup>3+</sup>. The solution became clear but orange precipitate appeared. The next day the precipitate was filtrated on 0.45 μm filter. Deuterated chloroform (CDCl<sub>3</sub>) was added to the supernatant and the solution was investigated again by <sup>1</sup>H NMR.

**AA2-81B**; 0.1 ml of FD1 solution in THF (8 mM) was mixed with 0.1 ml of FeCl<sub>3</sub> aqueous solution (8 mM) to obtain 1 Fe<sup>3+</sup>/FD1 equivalent. The whole mixture was then diluted with 0.8 ml of water/THF mixture (1:1 by volume). Once FD1 was mixed with FeCl<sub>3</sub>, the color of the mixed solution turned bright pink. The solution was examined by ESI-MS.

**AA2-81E**; 0.1 ml of FD1 solution in THF (8 mM) was mixed with 0.6 ml of FeCl<sub>3</sub> aqueous solution (8 mM) to obtain 6 Fe<sup>3+</sup>/FD1 equivalent. The whole mixture was then diluted with 7 ml of water/THF mixture (1:1 by volume). Once FD1 was mixed with

FeCl<sub>3</sub>, the color of the mixed solution turned bright pink. This solution was left at ambient temperature for 48 h before ESI-MS measurement.

**AA2-39**; Excess of gallium nitrate (Ga(NO<sub>3</sub>)<sub>3</sub> xH<sub>2</sub>O) was dissolved in D<sub>2</sub>O and added to the FD1/THF-d<sub>8</sub> solution. The solution before and after Ga<sup>3+</sup> addition was investigated by <sup>1</sup>H NMR

**AA2-92A** and **AA2-92B**; Solutions of FD1 (AA2-92A) and RBH (AA2-92B) (20 μM in CH<sub>3</sub>CN) were examined on the spectrofluorometer before and after addition of HCl solution (0.01 M). Each HCl addition (1.2 μl) was equal to 0.2 H<sup>+</sup>/FD1 equivalents. For both solutions the acid was added up to the point where no more significant increase in the fluorescent emission was observed (around 2 H<sup>+</sup>/FD1 equivalents in both cases).

**AA2-47**; FD1 was dissolved in THF-d<sub>8</sub> and investigated by <sup>1</sup>H NMR. Then a large excess of H<sub>2</sub>SO<sub>4</sub> (dissolved in D<sub>2</sub>O) was added to the solution causing the appearance of a bright pink color and some pink precipitation. To dissolve this precipitate more D<sub>2</sub>O was added. <sup>1</sup>H NMR spectrum was collected again. Then the excess of NaOH (in D<sub>2</sub>O) was added dropwise until the pink color disappeared. The mixture was investigated by <sup>1</sup>H NMR.

**AA2-81D**; 0.1 ml of FD1 solution in THF (8 mM) was mixed with 0.3 ml of HCl aqueous solution (8 mM) to obtain 3 H<sup>+</sup>/FD1 equivalent. The whole mixture was then diluted with 0.6 ml of water/THF mixture (1:1 by volume). Once FD1 was mixed with



HCl, the color of the mixed solution turned bright pink. The solution was examined by ESI-MS.

**AA2-81F**; FD1 was dissolved in THF (8 mM) before the measurement. To examine the effect of low pH on FD1, 0.1 ml of the FD1 solution was mixed with 0.6 ml of HCl solution (8 mM), leading to a 1:6 FD1/HCl molar ratio, and then diluted with 0.3 ml of water /THF mixture. The color of the FD1 solution turned bright pink instantly after HCl addition. This solution was left at ambient temperature for 48 h before ESI-MS measurement.

**AA3-24**; To compare response of FD1 and RBH (Rhodamine B hydrazide) to low pH, solutions of FD1 and RBH were prepared by dissolving both chemicals in THF-d<sub>8</sub> (~ 8 mM) and then 6 molar excess of HCl solution in D<sub>2</sub>O was added to both solutions. The change in chemical structure upon addition of acid was examined on <sup>1</sup>H NMR.

#### 5.2.2.2 Experiments Exploring RBH as a Potential Early Corrosion Indicator

**AA2-94**; Solutions of DGEBA and RBH in toluene-d<sub>8</sub> were investigated by <sup>1</sup>H NMR separately. Peak for toluene was used as an internal reference (7.09 ppm) in all spectra. Then RBH was added to the solution of DGEBA in toluene-d<sub>8</sub> (~ 1 RBH/DGEBA equivalent which is also 1:1  $\nabla$ :NH ratio). This slightly red mixture (due to RBH) was placed in the oven at 70°C. <sup>1</sup>H NMR spectra were collected at time=0 and after 24 h and 3 days. Then more toluene-d<sub>8</sub> was added and the solution was placed in a 25 ml round

bottom flask and refluxed at 155°C for 2 h. After that another  $^1\text{H}$  NMR spectrum was collected. The solvent was evaporated and 0.125 M aqueous  $\text{FeCl}_3$  solution was added to see if RBH was able to sense low pH after reaction with DGEBA. After 1 h the  $\text{FeCl}_3$  solution changed color to purple and after longer time the precipitate also became dark magenta.

**AA3-25;** RBH and DGEBA (5 DGEBA/RBH equivalents) were dissolved in xylenes and placed in the oven at 123°C for 44 h. Color of the solution changed from slightly yellow to dark dirty yellow after this time. Then slight tetraethylenepentamine (TEPA) excess was added to the RBH/DGEBA solution to fully cure the epoxy resin and the whole mixture was poured onto an aluminum pan and placed in the oven at 80°C for 20 h to facilitate the curing reaction. After curing, a hard yellow film was formed. Then the aluminum pan with the film adhered to it was placed in a cellulose extraction thimble for Soxhlet extraction. THF was used as the solvent during Soxhlet extraction, refluxed at 70°C for 12 h. The purpose of this extraction was to remove any unreacted RBH from the cured film. To make sure that all unreacted RBH was removed from the epoxy film, the aluminum pan with the epoxy coating was cut into small pieces, placed in a glass jar with THF and stirred with the magnetic stirrer for another 3 days. After that time the THF solution was examined on a UV-vis spectrophotometer. The resulting spectrum was compared with the spectra for RBH and DGEBA in THF. The piece of the epoxy coating (after extraction and washing with THF) was then placed in 0.1 M HCl solution. Pink color at the edges of the epoxy film appeared after a few seconds and after 1 h a deep

pink color was observed in the whole film. Also under UV light (365 nm) from a handheld UV lamp the epoxy film appeared bright orange.

### **5.2.3 Characterization Methods**

Fluorescence emission spectra in experiments AA2-17, AA2-19, AA2-74, AA2-75, AA2-76 were obtained with a Cary Eclipse fluorescence spectrofluorometer with an excitation wavelength of 510 nm. The examined solutions were placed in a 3 ml quartz cuvette. Fluorescence emission spectra in experiments AA2-45, AA2-75, AA2-74, AA3-39, AA2-92A and AA2-92B were obtained with an AMINCO-Bowman Series 2 (AB2) spectrofluorometer with an excitation wavelength of 510 nm. The examined solutions were placed in a 3 ml quartz cuvette. The fluorescent response of the samples to UV light was recorded using a handheld UV lamp with excitation 365 nm (model UVGL-25, MINERALIGHT<sup>®</sup>). UV-vis absorption spectra in experiment AA3-40 and AA3-25 were obtained on ISS-UV-VIS spectrophotometer from Ocean Optics Inc. The examined solutions were placed in a 3 ml quartz cuvette. All <sup>1</sup>H NMR spectra were collected on a Varian Mercury 400 MHz NMR with autosampler capabilities. In cases when THF-d<sub>8</sub> was used as a solvent, peaks for THF-d<sub>8</sub> were used as an internal reference (1.73 and 3.58 ppm) since this solvent does not include tetramethylsilane (TMS) as internal standard. Electrospray ionization mass spectrometry (ESI-MS) (experiments: AA2-81B, AA2-81C, AA2-81D, AA2-81E and AA2-81F) spectra were recorded on an LCQ Fleet instrument (Thermo Finnigan, San Jose, CA) equipped with an ion trap in the positive ion mode. Sample solutions were infused at a flow rate of 10 μl/min. ESI-MS spectra in experiment

AA3-42 were recorded on an LCQ Deca instrument (Thermo Finnigan, San Jose, CA) equipped with an ion trap in the positive ion mode. Sample solutions were infused at a flow rate of 10  $\mu\text{l}/\text{min}$ . Simulations of the isotopic distribution were obtained using the Isopro 3 program.

### **5.3 Results and Discussion**

#### **5.3.1 FD1 Corrosion Sensing Mechanism Based on Complexation with $\text{Fe}^{3+}$**

Zhang et al. [57] reported that a solution of FD1 in  $\text{CH}_3\text{CN}$  was able to sense  $\text{Fe}^{3+}$  ions (from an aqueous solution of  $\text{FeCl}_3$ ) when diluted with HEPES buffer at pH 7. However this result seemed to be surprising since it is known that soluble  $\text{Fe}^{3+}$  ions exist only in very acid solutions (pH = 0-2). An increase in pH to 2-4 causes ion hydrolysis and precipitation of the insoluble ferric hydroxide  $\text{Fe}(\text{OH})_3$  [65], and thus  $\text{Fe}^{3+}$  is no longer available for complexation in that pH range. A similar experiment to that of Zhang et al. [57] was performed to ensure that FD1 was able to detect  $\text{Fe}^{3+}$  at pH 7 (experiment AA2-17); FD1 was dissolved in  $\text{CH}_3\text{CN}$  ( $2 \times 10^{-5}$  M) and then diluted two times with NaOH/ $\text{KH}_2\text{PO}_4$  buffer solution (pH 7). The fluorescent response of this solution to  $\text{Fe}^{3+}$  was recorded on the spectrofluorometer ( $\lambda_{\text{ex}} = 510$  nm) after addition of  $\text{FeCl}_3$  solution ( $4 \times 10^{-3}$  M in  $\text{CH}_3\text{CN}$ ). No fluorescence was observed even after addition of excess of  $\text{Fe}^{3+}$  (80  $\text{Fe}^{3+}$ /FD1 equivalents). At 20  $\text{Fe}^{3+}$ /FD1 equivalents a slightly yellow precipitation appeared (probably  $\text{Fe}(\text{OH})_3$ ). However when the experiment was

performed without the buffer solution (experiment AA2-19 described in section 3.3.3 of chapter 3) the results were similar to the ones reported by Zhang et al. [57]. It was then concluded that HEPES buffer could have some influence on the results of the experiments. HEPES is a common buffer used in biochemical and psychological studies due to its biocompatibility and pKa value that is close to the physiological pH of 7.4 [66]. Even though it was considered a non-coordinating buffer (i.e. it does not form complexes with metal ions) for a long time, it was recently reported to weakly chelate copper [66] and uranium [67] ions in some systems. Thus there was a possibility for HEPES to coordinate with  $\text{Fe}^{3+}$  and keep the ion in solution, available for FD1 to complex with. The experiment described by Zhang et al. [57] was repeated using HEPES as a buffer (experiment AA2-76); 10  $\mu\text{M}$  solution of FD1 in  $\text{CH}_3\text{CN}$  was diluted 20 times with HEPES buffer (20 mM, pH 7) and titrated with aqueous solution of  $\text{FeCl}_3$ . The fluorescent response of FD1 was recorded on the spectrofluorometer ( $\lambda_{\text{ex}} = 510 \text{ nm}$ ). The addition of  $\text{Fe}^{3+}$  (0.3 to 5  $\text{Fe}^{3+}/\text{FD1}$  equivalents) again did not cause any fluorescence increase. Also with increasing amount of  $\text{FeCl}_3$ , a yellowish precipitate was observed. Only when a drop of concentrated  $\text{FeCl}_3$  solution (0.5 M) was added the fluorescence with maximum emission at 583 nm was recorded. However, at this point, the pH of the mixture was around 3 (as checked by pH-indicator strips) which indicated that the buffer capacity was overcome. This result suggested that the fluorescent response of FD1 in this system could only be due to acidic pH of the solution (as shown before in Figure 53, FD1 fluorescence increases with decreasing pH). Since no other experimental evidence (besides the fluorescent and absorbance spectra) was shown by Zhang et al. [57], to confirm that FD1 can form a fluorescent complex with  $\text{Fe}^{3+}$ , we had reasons to doubt the

actual complex formation. Even though, in experiment AA2-19 (FD1 in CH<sub>3</sub>CN titrated with FeCl<sub>3</sub> in CH<sub>3</sub>CN) the fluorescence was recorded upon titration with FeCl<sub>3</sub> solution, some traces of water were still present in the system indicating that the low pH could be the reason for the increase in fluorescence. Therefore the FD1/Fe<sup>3+</sup> complexation was not unquestionably proved as the sensing mechanism.

Thus it was necessary to demonstrate that FD1 fluorescence could be caused by the complexation with Fe<sup>3+</sup> and not only by the low pH. The following experiments were designed to examine whether FD1 was able to form a fluorescent complex with Fe<sup>3+</sup>.

Since most of the aqueous solutions of ferric salts are acidic (e.g. FeCl<sub>3</sub> aqueous solution has pH around 2) it was challenging to determine if the FD1 fluorescence is caused by the acidity of the added solution or by complexation with Fe<sup>3+</sup>. In experiment AA2-45, iron (III) acetylacetonate (Fe(acac)<sub>3</sub>, Figure 54) was used as a source of Fe<sup>3+</sup> ions. Since this ferric coordination complex is not soluble in water, no low pH issue exists in the system even when trace amounts of water are present.

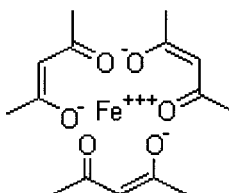


Figure 54. Chemical structure of iron (III) acetylacetonate

The fluorescence of the solution of FD1 in THF ( $3 \times 10^{-3}$  M) was examined on spectrofluorometer ( $\lambda_{\text{ex}} = 510$  nm) before and after addition of Fe<sup>3+</sup> from Fe(acac)<sub>3</sub> in THF

( $3 \times 10^{-2}$  M, orange solution). FD1/THF solution showed only weak fluorescence with maximum fluorescent emission ( $\lambda_{em,max}$ ) around 570 nm. After addition of 0.5  $Fe^{3+}$ /FD1 equivalents the color of the mixture was yellow-orange (due to the color of  $Fe(acac)_3$  solution) but no pink-red color was observed (as in case of titration with  $FeCl_3$ ). Also no increase in fluorescence was recorded on spectrofluorometer. Even addition of 4  $Fe^{3+}$ /FD1 equivalents (large  $Fe^{3+}$  excess) did not enhance the fluorescence intensity of FD1. This experiment proved that  $Fe^{3+}$  from  $Fe(acac)_3$  does not complex with FD1 causing the increase in its fluorescence. However the lack of fluorescence emission from FD1 could be the result of strong acetylacetonate coordination with  $Fe^{3+}$  (i.e.  $Fe^{3+}$ /acetylacetonate binding constant is much higher than the binding constant for potential  $Fe^{3+}$ /FD1 complex). Thus the FD1 ability to form a fluorescent complex with ferric ion could not yet be excluded at this point.

A similar experiment to AA2-45 was performed with ferric ammonium citrate (FAC) as a  $Fe^{3+}$  source (Figure 55). The pH of the solution of this ferric salt in water is between 6 and 8 depending on the concentration [68]. Since the 1.3 wt% solution of FAC in water was pH 6 (as measured with the pH-indicator strips) there was no acidic pH issue when this solution was added to the solution of FD1 in  $CH_3CN$  ( $1.9 \times 10^{-4}$  M). The color and fluorescence (as measured on the spectrofluorometer) of the FD1/ $CH_3CN$  was not changed even after addition of excess of  $Fe^{3+}$  from FAC solution.

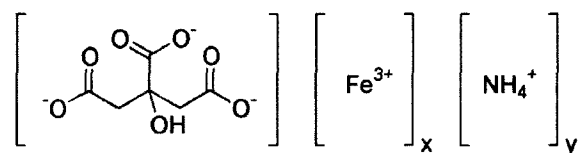


Figure 55. Chemical structure of ferric ammonium citrate

This experiment proved that FD1 could not sense  $\text{Fe}^{3+}$  from FAC aqueous solution. However, similarly to the experiment with  $\text{Fe}(\text{acac})_3$ ,  $\text{Fe}^{3+}$  in FAC salt can be chelated by citrate [69] which could make ferric ions unavailable for complexation with FD1. FD1 would have to be a much stronger chelating agent than citrate (i.e.  $\text{FD1}/\text{Fe}^{3+}$  binding constant many orders of magnitude larger than  $\text{citrate}/\text{Fe}^{3+}$  binding constant) to be able to remove the  $\text{Fe}^{3+}$  ions from the citrate chelation. Thus again,  $\text{FD1}/\text{Fe}^{3+}$  complexation could not be excluded at this point.

To ensure that FD1 can form a fluorescent complex due to its binding with  $\text{Fe}^{3+}$  (after addition of  $\text{FeCl}_3$  to the FD1 solution) and not due to the low pH caused by addition of acidic aqueous solution of  $\text{FeCl}_3$ , auxiliary complexing agents (ACA) can be utilized. These agents are often used to prevent the precipitation of heavy metals as hydroxides or basic salts in higher pH [69]. Their metal complexes are soluble in water so the metal stays in solution and can continue to react. The most common ACAs are ammonia, citrate and triethanolamine. In the experiment AA2-74, triethanolamine (TEA) was used as an ACA. Several drops of TEA were added to the aqueous  $\text{FeCl}_3$  solution ( $7.2 \times 10^{-4}$  M). The pH of this mixture was around 9 but no  $\text{Fe}(\text{OH})_3$  precipitate was observed proving that TEA formed a soluble complex with  $\text{Fe}^{3+}$ . Even after dilution with  $\text{Na}_2\text{HPO}_4/\text{NaOH}$  buffer solution (pH 12) no precipitation was present. One drop of the  $\text{FeCl}_3/\text{TEA}/\text{buffer}$



mixture was added to the solution of FD1 in CH<sub>3</sub>CN (1.9×10<sup>-4</sup> M) however no pink color or fluorescence appeared (unlike the case when FeCl<sub>3</sub> was added to this solution) even after addition of excess of Fe<sup>3+</sup>. This suggested that FD1 did not form a fluorescent complex after addition of Fe<sup>3+</sup> at high pH. Again the formation of the FD1/Fe<sup>3+</sup> complex could not be excluded at this point since FD1 could simply be a weaker complexing agent than TEA, not able to remove Fe<sup>3+</sup> from the Fe<sup>3+</sup>/TEA complex.

Another way to prove that FD1 becomes fluorescent due to complexation with Fe<sup>3+</sup>, and not due to low pH, was to perform the experiments in a non-aqueous environment where no water is present and thus no acidic pH issue exists. To observe FD1 fluorescent response to Fe<sup>3+</sup> in non-aqueous solution and also to observe the difference in the FD1 fluorescent response upon addition of Fe<sup>3+</sup> (from FeCl<sub>3</sub>) in non-aqueous and aqueous solution, experiment AA3-39 was performed. The fluorescence of FD1 in THF (20 M) upon addition of FeCl<sub>3</sub> in THF (0.01 M) and FeCl<sub>3</sub> in aqueous solution (0.01 M) was compared on the spectrofluorometer when excited with 510 nm (Figure 56). If FD1 was able to bind Fe<sup>3+</sup> in both aqueous and non-aqueous solutions its fluorescence response should be identical for both solutions since the Fe<sup>3+</sup> concentration was the same (0.01 M). However, as seen in Figure 56, the fluorescent intensity of FD1 solution, upon addition of Fe<sup>3+</sup>/H<sub>2</sub>O, was increasing only up to 1.8 Fe<sup>3+</sup>/FD1 equivalents (left plot in Figure 56), where upon addition of Fe<sup>3+</sup>/THF it was increasing up to 5.8 Fe<sup>3+</sup>/FD1 equivalents (right plot in Figure 56). Further addition of the Fe<sup>3+</sup> solutions did not cause increase in the fluorescent emission intensity for both solutions.

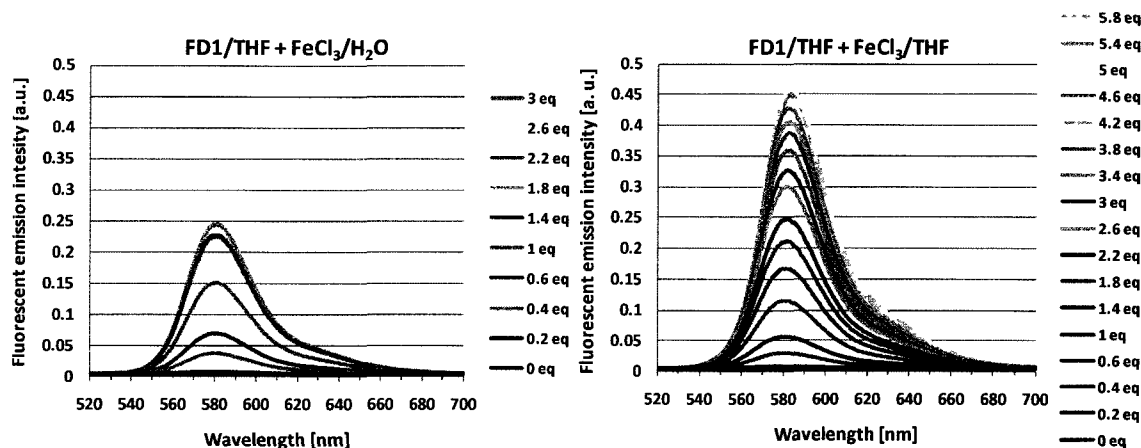


Figure 56. Fluorescent emission spectra of FD1/THF solution (20  $\mu$ M) titrated with FeCl<sub>3</sub>/H<sub>2</sub>O solution (left) and with FeCl<sub>3</sub>/THF solution (right).  $\lambda_{ex}$  = 510 nm.

This result proved that FD1 fluorescent response differs when titrated with the aqueous versus non-aqueous Fe<sup>3+</sup> solution. It is also worth mentioning that the fluorescent intensity and  $\lambda_{em,max}$  were the same for both solutions at 2.2 Fe<sup>3+</sup>/FD1 equivalents (2.5 a. u. and 583 nm respectively), however the color of the solutions differed significantly as seen in Figure 57. The FD1 solution titrated with FeCl<sub>3</sub>/H<sub>2</sub>O showed only light pink color (left image in FeCl<sub>3</sub> in Figure 57), where the solution titrated with FeCl<sub>3</sub>/THF solution had much more intense magenta color (right image in FeCl<sub>3</sub> in Figure 57).



Figure 57. Difference in color of the FD1/THF solutions upon addition of 2.2 Fe<sup>3+</sup>/FD1 equivalents from FeCl<sub>3</sub> in water (left image) and in THF (right image).

To investigate this difference in the color response, experiment AA3-40 was performed. Again FD1/THF solution (20 M) was titrated separately with FeCl<sub>3</sub>/THF (0.01 M) and FeCl<sub>3</sub>/H<sub>2</sub>O (0.01 M). The change in UV-vis absorption was recorded each time after addition of 0.4 Fe<sup>3+</sup>/FD1 equivalents. The collected absorption spectra (Figure 58) proved that the fluorescent emission at 583 nm corresponds to the absorption at 560 nm (as also shown by Zhang et al. [57] when FD1 solution in CH<sub>3</sub>CN was titrated with FeCl<sub>3</sub> solution). As seen on the left plot in Figure 58, the absorption at 560 nm, for FD1/THF solution titrated with FeCl<sub>3</sub>/H<sub>2</sub>O, reached maximum at around 2 Fe<sup>3+</sup>/FD1 equivalents similar to the value at which the highest fluorescent emission was obtained in experiment AA3-39 (left plot in Figure 56). Also for the FD1/THF solution titrated with FeCl<sub>3</sub>/THF (right plot in Figure 58) the absorption at 560 nm reached the maximum at the Fe<sup>3+</sup>/FD1 equivalent value close to the one at which the highest fluorescent emission was recorded in experiment AA3-39 (left plot in Figure 56). Also, similarly to the experiment AA3-39, the absorption at 560 nm was the same for both solutions at around 2.4 Fe<sup>3+</sup>/FD1 equivalents confirming that the fluorescence emission at 583 nm corresponds to absorption at 560 nm. Thus the difference in color of the solutions shown in Figure 57 could not be related to the absorption at 560 nm. It must be then caused by the slight differences in the absorption spectra in the UV and near visible range (240-440 nm) as shown in Figure 58. This change in absorption could be related to the presence of iron in the fluorescent FD1/Fe<sup>3+</sup> complex for FeCl<sub>3</sub>/THF solution (as will be verified by ESI-MS below), compared to the mixture in a water solution.

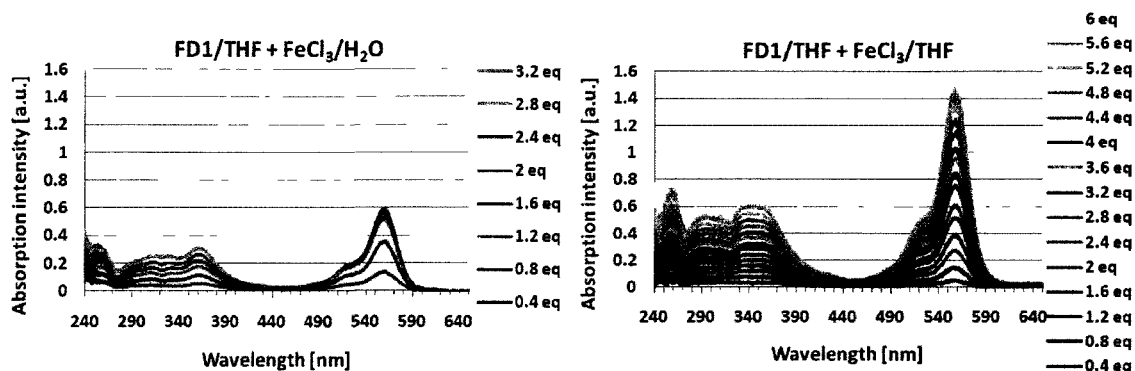


Figure 58. UV-vis absorption spectra of FD1/THF solution (20 M) titrated with FeCl<sub>3</sub>/H<sub>2</sub>O solution (left) and with FeCl<sub>3</sub>/THF solution (right).

This experiment has demonstrated that in a non-aqueous solution (where the pH issue is excluded) a fluorescent Fe<sup>3+</sup>/FD1 complex may be formed. Also the fluorescent response of the FD1/THF solution to Fe<sup>3+</sup> from the non-aqueous solution reached a much higher maximum fluorescence than Fe<sup>3+</sup> from an aqueous solution. The highest fluorescent intensity and absorbance was reached after addition of around 6 Fe<sup>3+</sup>/FD1 equivalents suggesting that the large Fe<sup>3+</sup> excess is required to push the equilibrium into the complex formation since FD1 seemed to be a weak complexing agent. This finding is consistent with the results from experiments AA2-45, AA2-75 and AA2-74, described at the beginning of this section, in which FD1 was not able to capture ferric ions from stronger complexing agents (acetylacetonate, citrate and ethanolamine respectively).

FD1/THF solution, upon addition of Fe<sup>3+</sup> from aqueous solution, reached its maximum fluorescence (and absorption at 560 nm) much faster (only after about 2 Fe<sup>3+</sup>/FD1 equivalents). However the intensity was much lower when compared to the maximum fluorescence (and absorption at 560 nm) after addition of Fe<sup>3+</sup> from non-aqueous solution (Figure 56 and Figure 58). This could suggest that in this case the pH (and not binding

with ferric ions) is responsible for the appearance of fluorescence. The FD1 fluorescence due to the acidic pH is described in the following section of this chapter (section 5.3.2).

To observe if FD1/Fe<sup>3+</sup> complex is indeed formed in non-aqueous solution, the mass spectra of the solution of FD1 in THF before (experiment AA3-42A) and after addition of FeCl<sub>3</sub> (also in THF, 1 Fe<sup>3+</sup>/FD1 equivalent, experiment AA3-42B) were collected with the electrospray ionization technique (ESI-MS) as shown in Figure 59 and Figure 60 respectively. This method was used previously to show the structures of Fe<sup>3+</sup> complexes [70, 71].

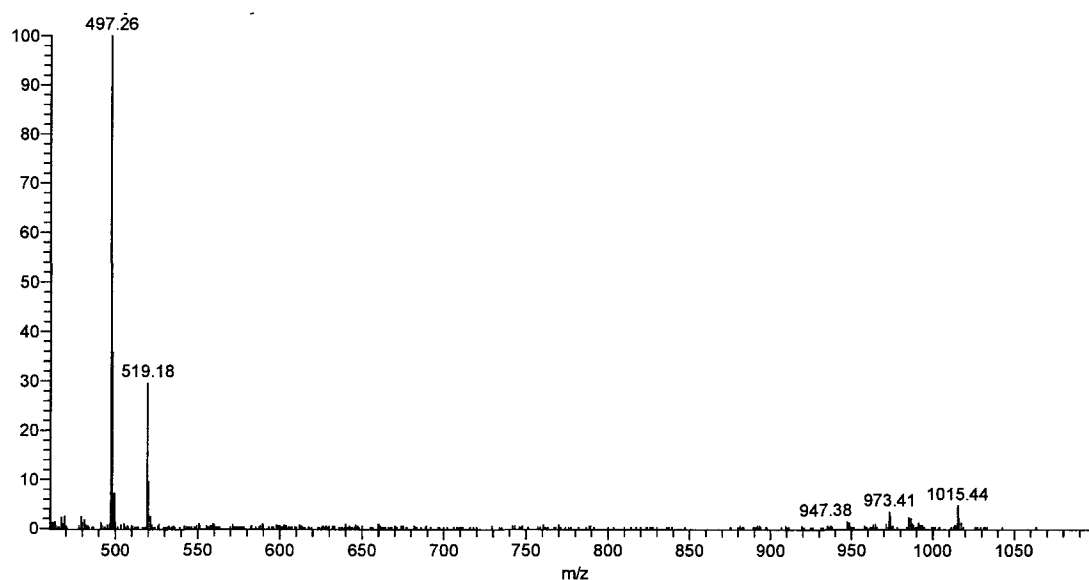


Figure 59. ESI-MS spectrum of FD1 in THF.

Two major peaks were observed for FD1 (Figure 59): the peak at  $m/z = 497.26$  can be assigned as  $[\text{FD1}+\text{H}]^+$  (since  $M_{\text{FD1}} = 496.61$  g/mol) and the peak at  $m/z = 519.18$  is due to  $[\text{FD1}+\text{Na}]^+$ . Also, a smaller peak at  $m/z = 1015.44$  was present corresponding to the cluster  $[2\text{FD1}+\text{Na}]^+$ , as confirmed by the MS<sup>2</sup> technique.

When FeCl<sub>3</sub>/THF was added to FD1/THF, the magenta color appeared instantly in the previously colorless solution. Several new peaks appeared at  $m/z = 622.05$ ,  $730.92$ , and  $1280.77$ , along with the two peaks characteristic for FD1 ( $m/z = 497.25$  and  $m/z = 519.19$ ) (Figure 60).

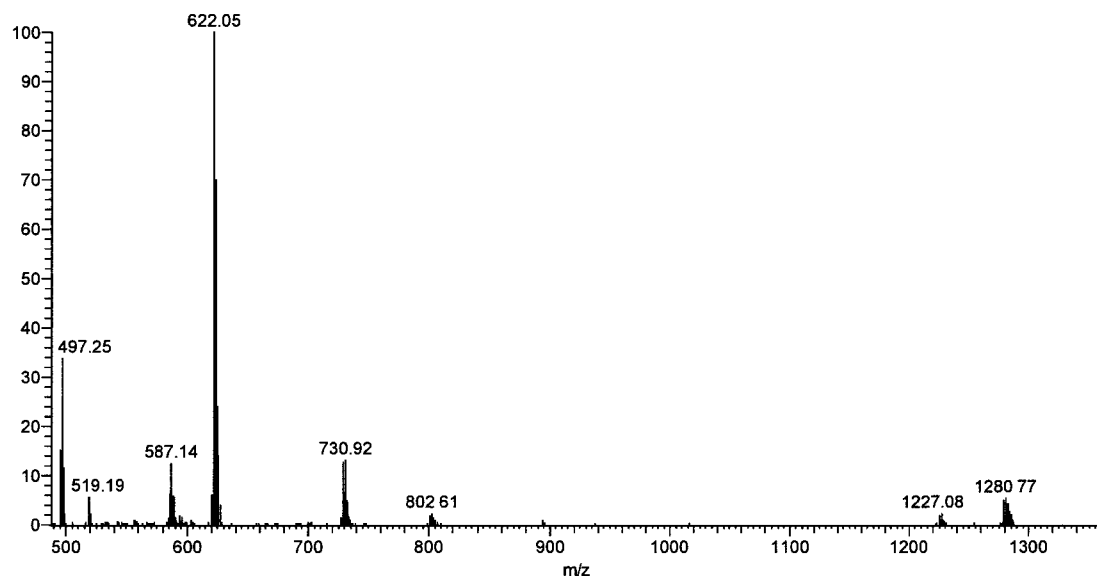


Figure 60. ESI-MS spectrum of FD1/FeCl<sub>3</sub> solution in THF (1 Fe<sup>3+</sup>/FD1 equivalent).

The large peak at  $m/z = 622.05$  appeared to be due to the complex [FD1+Fe(III)+2Cl]<sup>+</sup>. The determination of this complex structure was unambiguously confirmed by the perfect agreement between the experimental and simulated isotopic distribution shown in Figure 61, characteristic of a species containing both Fe and Cl.

The presence of the Fe(III)-FD1 complex was further corroborated by the peak at  $m/z = 1280.77$ , which was attributed to the cluster  $[2*(FD1+Fe(III)+2Cl)+Cl]^+$ , as again confirmed by the isotopic distribution (Figure 62).

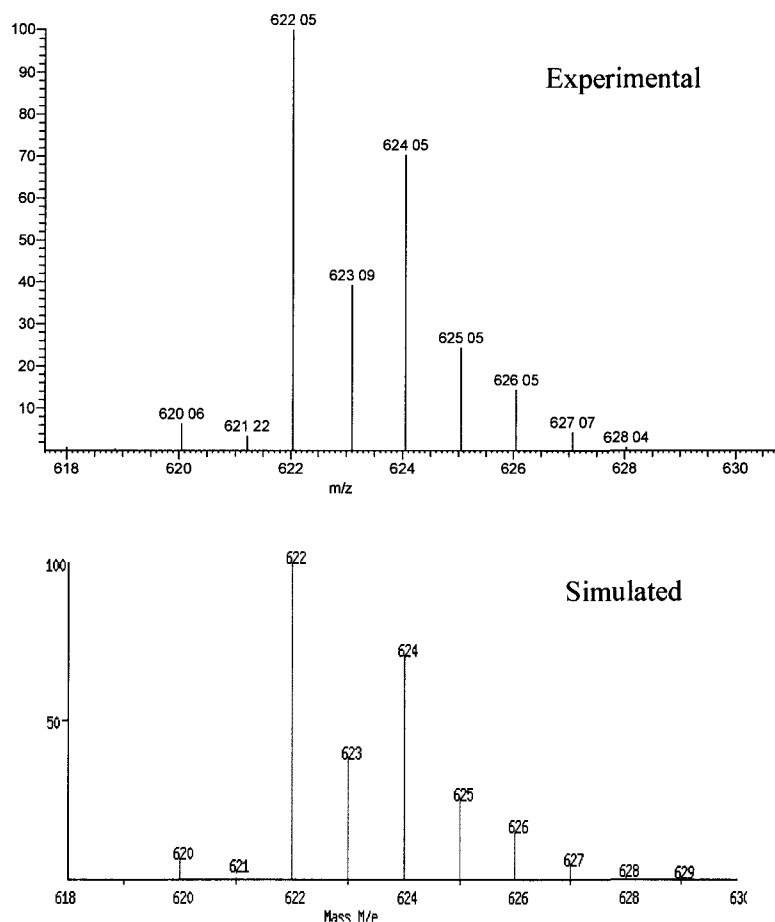


Figure 61. Enlarged area around the  $m/z = 622.05$  peak from the Figure 60 (top spectrum). Bottom spectrum shows the simulated isotopic distribution of  $[FD1+Fe(III)+2Cl]^+$

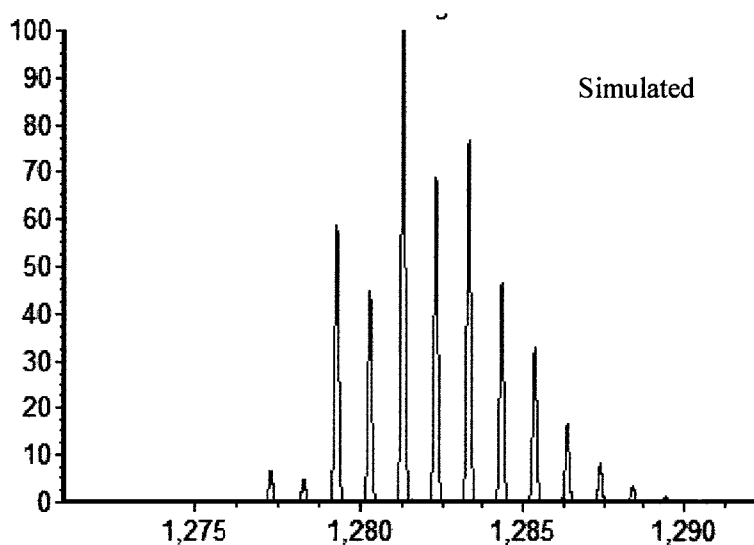
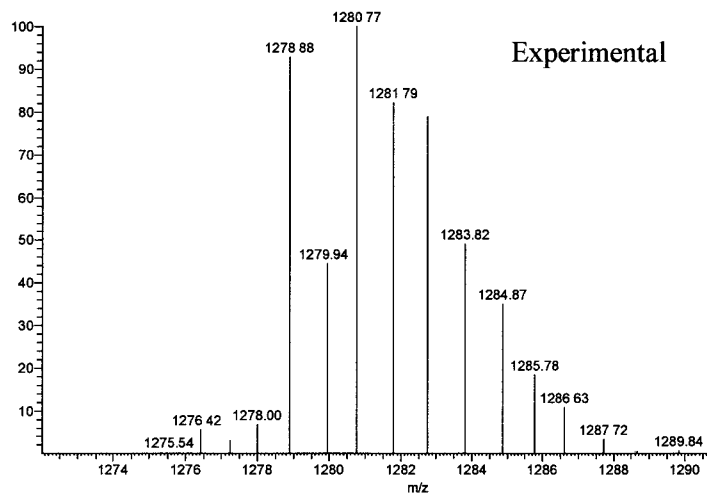


Figure 62. Enlarged area around the  $m/z = 1280.77$  peak from Figure 59 (top spectrum). Bottom spectrum shows simulated isotopic distribution of  $[2*(FD1+Fe(III)+2Cl)+Cl]^+$  cluster.

The peak at  $m/z = 730.92$  appeared to be due to a compound containing both Fe and Cl (isotopic distribution shown in Figure 63). The  $m/z$  value suggested the complex had a possible formula  $[(FD1+Fe(III)+2Cl) + (Fe+Cl+O)]^+$ ; the precise structure of this complex was not determined.



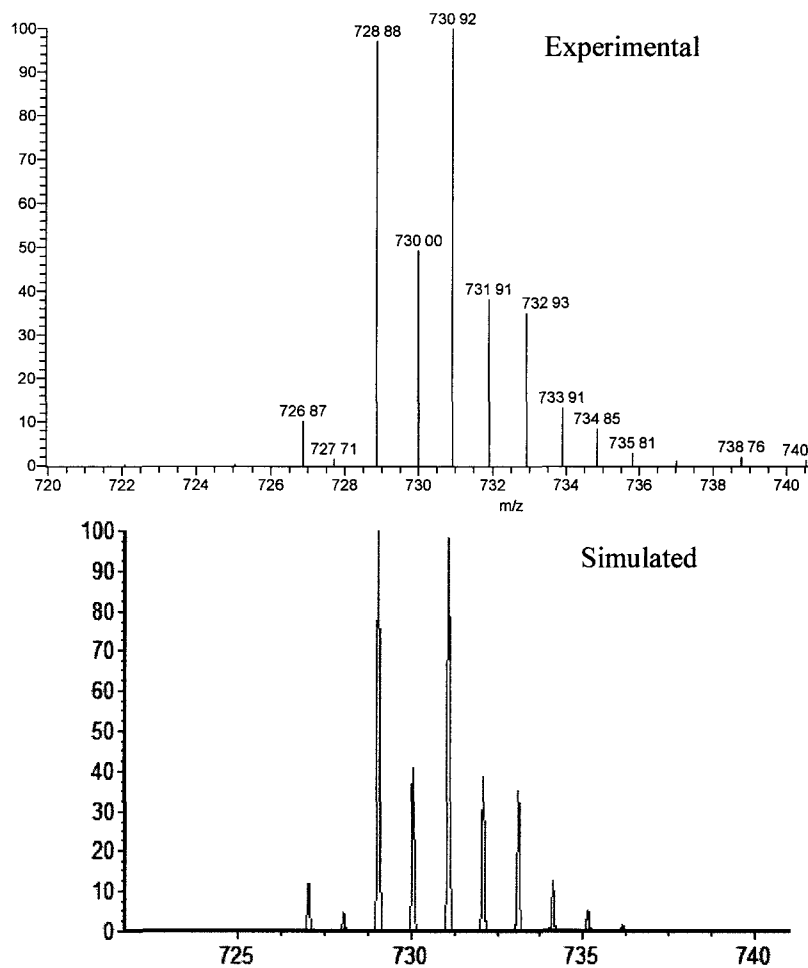


Figure 63. Enlarged area around the  $m/z = 730.92$  peak from the Figure 59 (top spectrum). Bottom spectrum shows the simulated isotopic distribution of  $[(FD1+Fe(III)+2Cl) + (Fe+Cl+O)]^+$ .

Other peaks at  $m/z = 587.14$ ,  $802.61$ , and  $1227.08$  were difficult to identify at this point but did not show isotopic distribution characteristic of Fe.

Similar spectra were also obtained in experiment AA3-42C where 3  $Fe^{3+}/FD1$  equivalents were used.

The presented results from ESI-MS clearly confirmed that the FD1/Fe<sup>3+</sup> complex was formed in a non-aqueous solution.

The reversibility of the FD1/Fe<sup>3+</sup> complex was examined in experiment AA2-44. FD1 was first dissolved in THF-d<sub>8</sub> (dried over night with 0.4 nm molecular sieve to remove traces of water). The <sup>1</sup>H NMR spectrum of this solution is shown in spectrum A of Figure 64. Addition of an excess of anhydrous FeCl<sub>3</sub> (in THF-d<sub>8</sub>) to that solution caused color change from colorless to dark magenta proving the FD1/Fe<sup>3+</sup> complexation. As can be seen in the spectra B in Figure 64 the addition of paramagnetic Fe<sup>3+</sup> caused broadening of the peaks. Then, cyclen (a metal chelator) was added to the solution to remove Fe<sup>3+</sup>. The solution became clear but orange precipitate appeared. This precipitate was probably due to formation of the THF-insoluble cyclen/Fe<sup>3+</sup> complex. After the precipitate was filtrated off, deuterated chloroform (CDCl<sub>3</sub>) was added to the supernatant (to increase the volume to the desired level for NMR measurement after THF evaporation). As can be seen in spectrum C of Figure 64 the original structure of FD1 was restored after cyclen addition. The only differences, when comparing with spectrum A, are the appearance of new peaks for cyclen (at 2.9 ppm), CDCl<sub>3</sub> (at 7.7 ppm) and a small peak for acetone (at 2.1 ppm). Traces of acetone could be present in the solution since it was used to clean the NMR tubes. Also peak C (in spectrum A) split into two peaks (in spectrum C). This is however not surprising since 6 protons, labeled C, appear as two singlets with integration 3H each [57] (as in case of spectrum C in Figure 64) when FD1 is dissolved in CDCl<sub>3</sub>, and they collapse into one doublet with integration of 6H (spectrum A in Figure 64) when FD1 is dissolved in THF-d<sub>8</sub>.

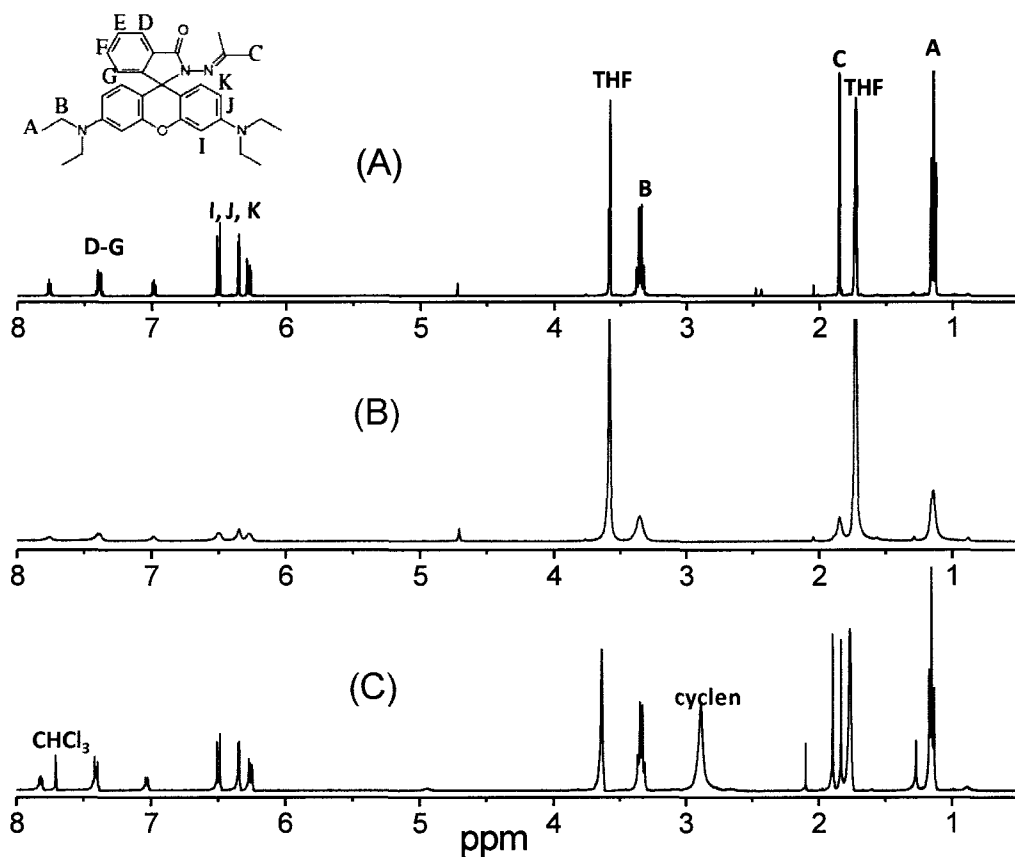


Figure 64.  $^1\text{H}$  NMR spectra of (A) FD1 in  $\text{THF-d}_8$ , (B) solution from spectrum A upon addition of  $\text{FeCl}_3$  in THF and (C) solution from spectrum B upon addition of cyclen (in mixed solvent system  $\text{THF-d}_8/\text{CDCl}_3$ ).

To determine if the  $\text{FD1}/\text{Fe}^{3+}$  complex is also formed in an aqueous system, the mass spectra of a solution of FD1 in THF upon addition of aqueous  $\text{FeCl}_3$  (1  $\text{Fe}^{3+}/\text{FD1}$  equivalent) were collected with ESI-MS (experiment AA2-81). The addition of  $\text{FeCl}_3$  caused the appearance of bright pink color and orange fluorescence (under UV light). As shown in Figure 65, besides the two peaks characteristic for FD1 ( $m/z = 497.4$  and  $m/z = 249.3$  assigned to  $[\text{FD1}+2\text{H}]^{2+}$ ), new peaks emerged at  $m/z = 229.3$ ,  $m/z = 457.5$ ,  $m/z = 935.4$  and  $m/z = 975.3$ . It turned out that, after careful calculation, these peaks were all related to Rhodamine B hydrazide (RBH,  $M_{\text{RBH}} = 456.8$  g/mol): the peak at 457.5 can be assigned to  $[\text{RBH}+\text{H}]^+$ , while the peaks at 229.3 and 935.4 can be assigned to

$[\text{RBH}+2\text{H}]^{2+}$  and  $[2\text{RBH}+\text{Na}]^+$ , respectively. The peak at 975.3 is due to the  $[\text{RBH}+\text{FD1}+\text{Na}]^+$  cluster. These ESI-MS results suggested that FD1, upon addition of acidic aqueous  $\text{FeCl}_3$ , is hydrolyzed to RBH. This process is described in detail in the following section of this chapter. It is important to note that no isotopic distribution characteristic of iron was found in the spectra (unlike in experiment AA3-42 where  $\text{Fe}^{3+}$  in non-aqueous solution was used) suggesting that the  $\text{FD1}/\text{Fe}^{3+}$  complex is not formed when  $\text{Fe}^{3+}$  from aqueous solution is added to the FD1 solution.

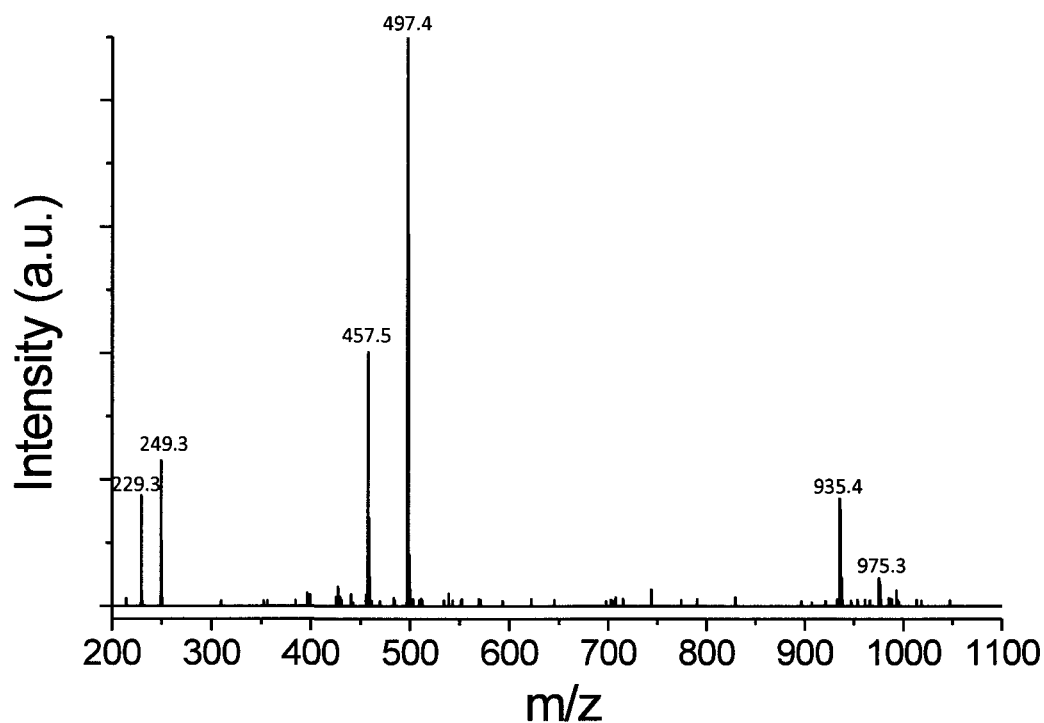


Figure 65. ESI-MS spectrum of FD1/THF upon addition of aqueous  $\text{FeCl}_3$  solution (1  $\text{Fe}^{3+}$ /FD1 equivalent).

This finding was also confirmed when a large  $\text{Fe}^{3+}$  excess (6  $\text{Fe}^{3+}$ /FD1 equivalents) was added to the FD1/THF solution and the mixture was allowed to react for 48 hr (Figure 66).

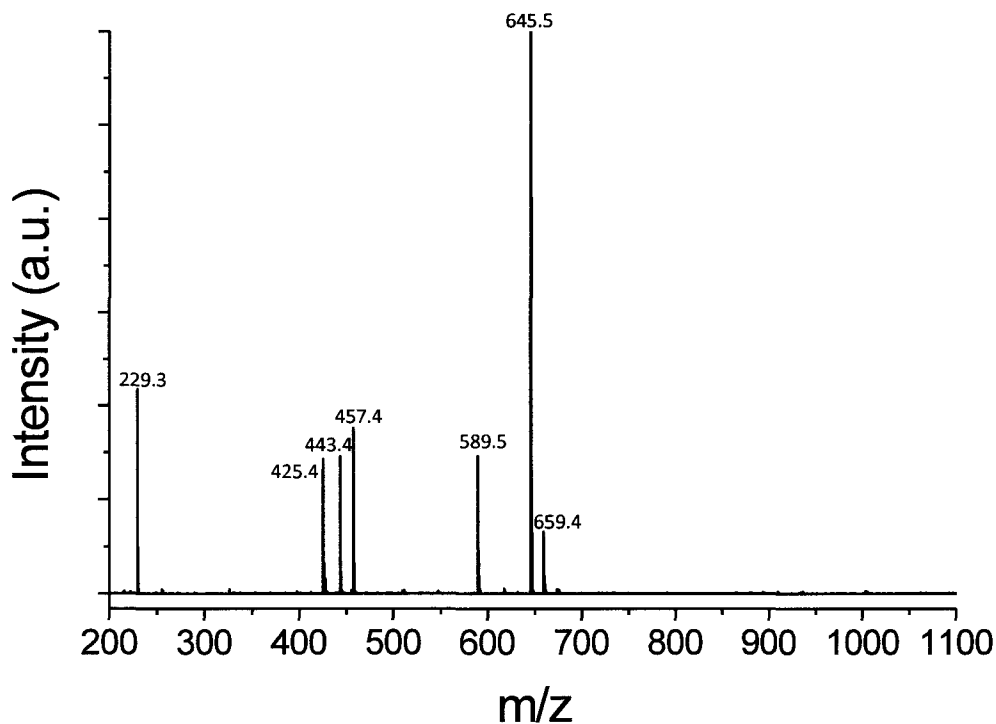


Figure 66. ESI-MS spectrum of FD1/THF upon addition of aqueous  $\text{FeCl}_3$  solution (6  $\text{Fe}^{3+}$ /FD1 equivalents).

In this case all the peaks characteristic for FD1 were completely vanished. The presence of the peaks characteristic for RBH ( $m/z = 229.3$  and  $m/z = 457.4$ ) indicated that hydrolysis took place. New peaks at  $m/z = 425.4$ ,  $443.4$ ,  $589.5$ ,  $645.5$ ,  $659.4$  also appeared. These peaks could not be identified at this time. However none of them showed the isotope distribution characteristic of iron, confirming again that in an aqueous

environment the complexation between FD1 and  $\text{Fe}^{3+}$  does not take place and that the acid catalyzed hydrolysis is the prevalent mechanism for the appearance of fluorescence.

This finding was also confirmed in the experiment AA2-39. In this experiment however, the changes in the FD1 structures were monitored with  $^1\text{H}$  NMR after addition of  $\text{Ga}^{3+}$  (in the form of an aqueous solution of gallium nitrate hydrate), and not  $\text{Fe}^{3+}$  (from aqueous solution of  $\text{FeCl}_3$ ).  $\text{Ga}^{3+}$  is a redox inactive analogue of  $\text{Fe}^{3+}$  and is often used as the ferric ion substitute [72]. It is a diamagnetic metal ion (unlike paramagnetic  $\text{Fe}^{3+}$ ) thus it does not cause peak broadening in NMR spectra. This property of  $\text{Ga}^{3+}$  allowed the accurate examination of the changes in the FD1 chemical structure upon addition of this metal ion without the necessity of removing it from the system (as would be the case for  $\text{Fe}^{3+}$ ) in order to obtain good quality spectra. Similarly to  $\text{FeCl}_3$ , the aqueous solution of this metal salt is acidic (pH around 4). The addition of an excess of aqueous  $\text{Ga}(\text{NO}_3)_3$  solution to the solution of FD1/THF- $d_8$  caused the instant appearance of pink color. The changes in the FD1 structure upon addition of  $\text{Ga}(\text{NO}_3)_3$  were monitored after a few days of reaction. The peak C (present in spectrum A in Figure 67) disappeared completely after addition of excess of  $\text{Ga}^{3+}$  as can be seen in spectrum B in Figure 67. Also the peak B shifted from 3.3 to 3.55 ppm and the peaks corresponding to aromatic protons (I, J, and K) shifted to lower fields. The down-field shifts of peaks B, I-K were probably due to the formation of the highly conjugated structure of the protonated, fluorescent RBH, as a result of acid catalyzed FD1 hydrolysis.

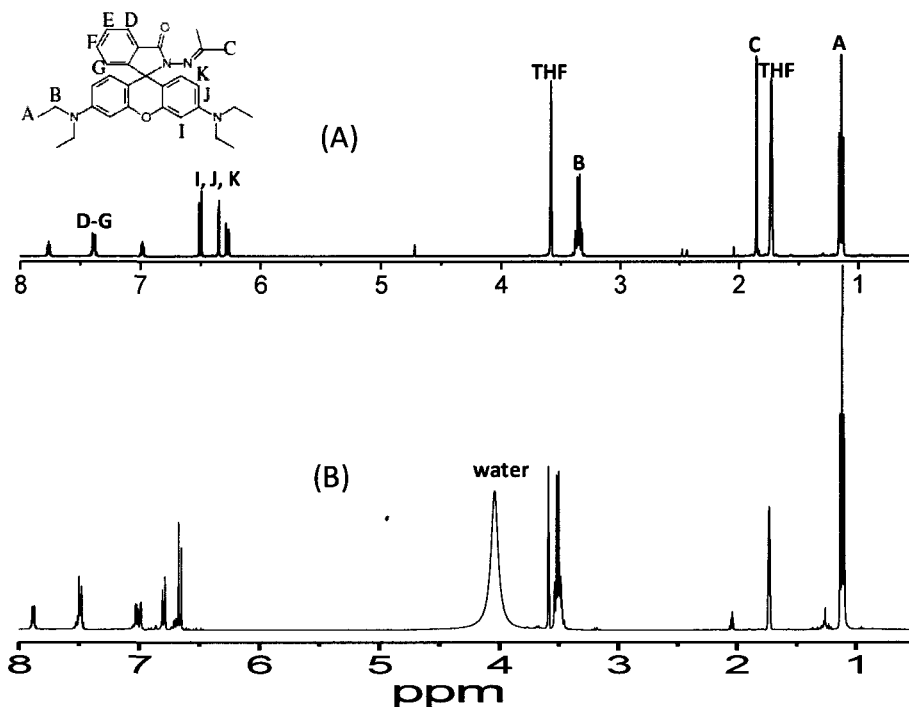


Figure 67. <sup>1</sup>H NMR spectra of (A) FD1 in THF-d<sub>8</sub>, and (B) the mixture of FD1/Ga(NO<sub>3</sub>)<sub>3</sub> xH<sub>2</sub>O.

Overall it was concluded, from the experiments described in this section, that 1) ferric ion (from FeCl<sub>3</sub>) forms a fluorescent complex with FD1 only in a non-aqueous solution (i.e. in our case THF) and 2) in the aqueous solutions the prevalent reason for the fluorescence to appear upon addition of FeCl<sub>3</sub> (or any other acid salt such as gallium nitrate) is acid catalyzed hydrolysis of FD1 to protonated RBH due to the acidity of the ferric salt. A detailed description of this process is described in the following section of this chapter. From a practical point of view, however, this distinction does not matter when FD1 is used as a corrosion sensor since in a corrosion cell water will always be present.

### 5.3.2 FD1 Corrosion Sensing Mechanism Based on Acid Catalyzed Hydrolysis

FD1 sensitivity to low pH reported by Zhang et al. [57] (Figure 53) and also observed in the previous experiments (Section 4.3.2.2) was investigated and is described in this section. FD1 fluorescent response to acidic solution was monitored in experiment AA2-92A. As shown in the plot in Figure 68, the fluorescence intensity of FD1 (in CH<sub>3</sub>CN) upon addition of HCl kept increasing (up to 1.8 H<sup>+</sup>/FD1 equivalents), with maximum fluorescence emission ( $\lambda_{em,max}$ ) shifting slightly from 582 to 585 nm. A color change from colorless to pink under visible light and to orange under UV was also clearly observed (inset in Figure 68).

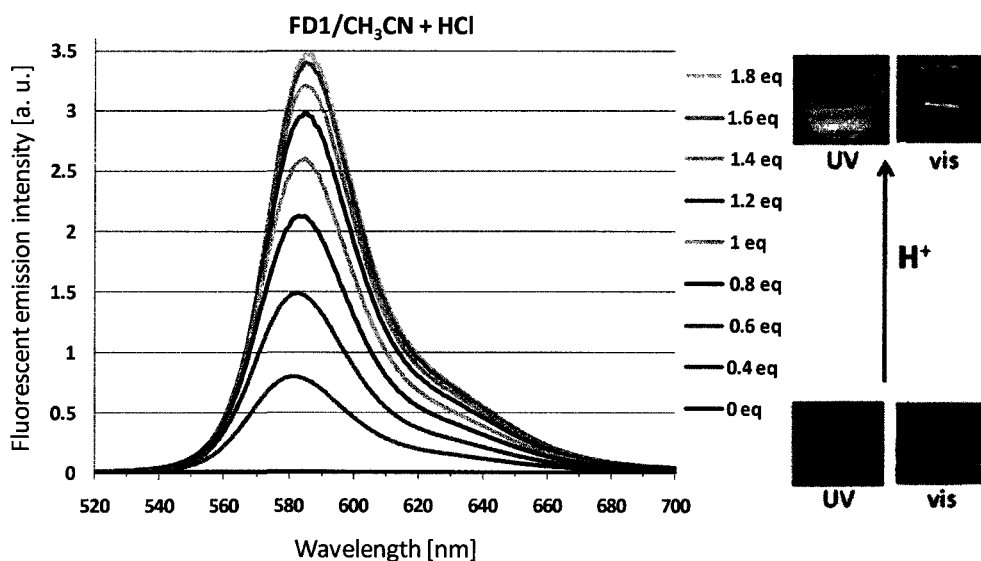


Figure 68. Fluorescent emission of FD1 solution in CH<sub>3</sub>CN (20  $\mu$ M) upon addition of HCl solution (up to 1.8 H<sup>+</sup>/FD1 equivalents) when excited at 510 nm. Right: color change of FD1 in CH<sub>3</sub>CN upon addition of HCl under UV and visible light.

The initial conclusion from this experiment was that the FD1 became fluorescent simply due to the protonation of the molecule and ring-opening as illustrated in Figure 69.



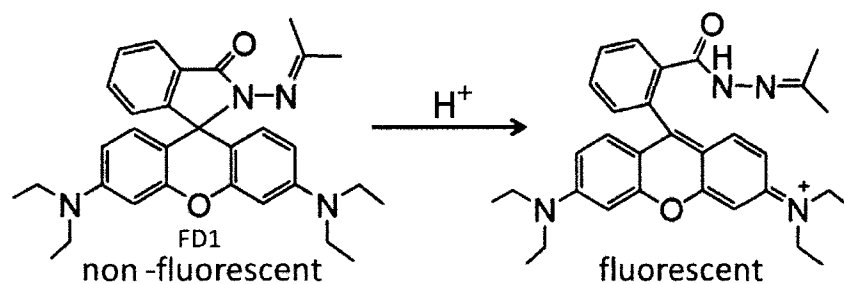


Figure 69. Proposed FD1 structure upon addition of acid (protonation).

However the results from the following experiment (AA2-47) proved that this conclusion was incorrect. FD1 dissolved in THF- $d_8$  was examined by  $^1\text{H}$  NMR before (spectrum A in Figure 70) and after addition of molar excess of sulfuric acid ( $\text{H}_2\text{SO}_4$ ) (spectrum B in Figure 70). The acid addition caused the pink color to appear instantly. As it can be seen in spectrum B of Figure 70, peak C, characteristic for FD1, disappeared almost completely. Instead, a peak at 2.08 appeared (labeled X) probably due to the acetone (that could be a byproduct of the acid-catalyzed FD1 hydrolysis as described later in this section). Also the peak B shifted from 3.3 to 3.55 ppm and the peaks corresponding to aromatic protons (I, J, and K) shifted to lower fields. The down-field shifts of peaks B, I-K were probably due to the formation of the highly conjugated structure. These changes were very similar to the changes observed in the FD1 structure upon addition of the acidic  $\text{Ga}^{3+}$  salt (spectrum B in Figure 67).

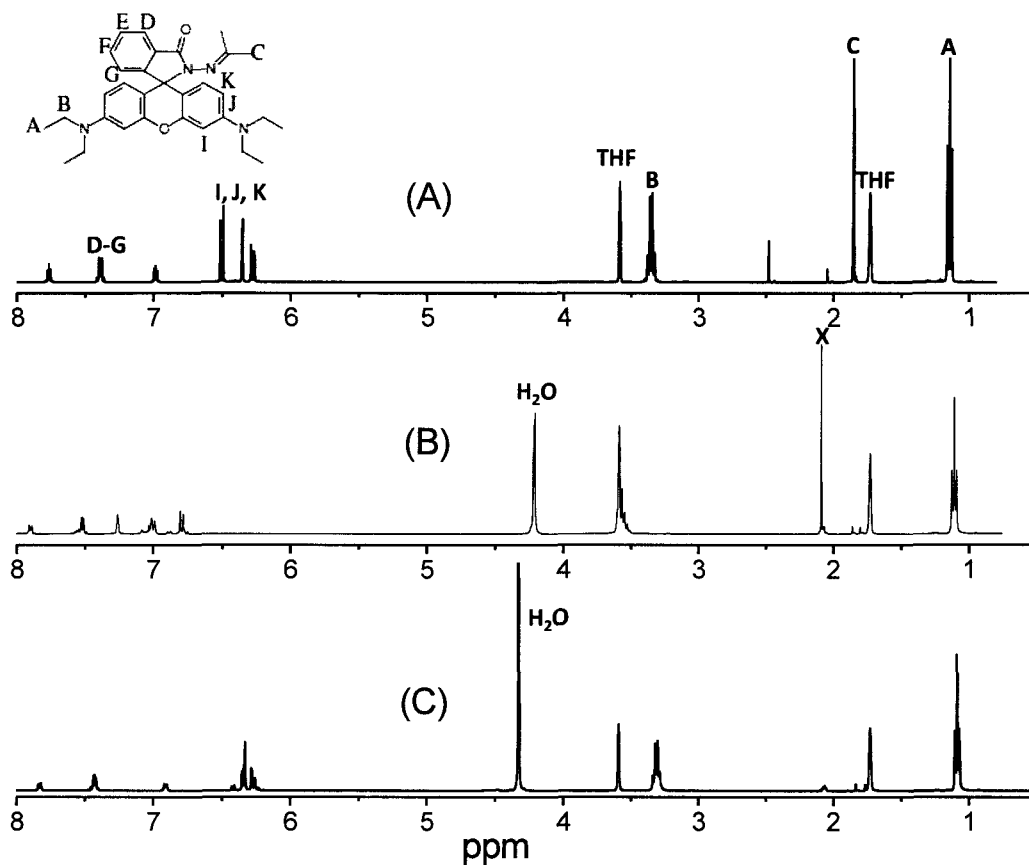


Figure 70.  $^1\text{H}$  NMR spectra of (A) FD1 in  $\text{THF-d}_8$ , as well as the mixtures of (B) FD1/ $\text{H}_2\text{SO}_4$  and (C) FD1/ $\text{H}_2\text{SO}_4$ / $\text{NaOH}$  in  $\text{THF-d}_8/\text{D}_2\text{O}$  mixed solvents.

To investigate if the pH increase will deprotonate the molecule back to its original structure (under the hypothesis that the protonation was the reason for the appearance of fluorescence as shown in Figure 69) excess of sodium hydroxide was added to the FD1/ $\text{H}_2\text{SO}_4$  mixture causing the pink color to disappear. As seen in spectrum C of Figure 70, peaks B and I-K shifted back to the higher fields. Peak X disappeared almost completely probably because acetone had evaporated. However peak C was not restored. This proved that the closed ring form of the molecule was brought back (since the pink color disappeared) but the chemical structure of FD1 was changed irreversibly.

To examine the possible species formed upon addition of acidic solution to FD1, the experiment AA2-81D was performed. ESI-MS spectra were collected for FD1/THF solution upon addition of hydrochloric acid (HCl) (3 H<sup>+</sup>/FD1 equivalents). The color of the solution turned bright pink after acid addition indicating the formation of a fluorescent molecule. Besides the peaks characteristic for FD1 (at  $m/z = 249.3$  and  $497.4$ ), peaks indicating the formation of RBH (at  $m/z = 229.3, 457.5, 935.4$  and  $975$ ) also appeared. This spectrum was almost identical to the spectrum in Figure 65 where an aqueous solution of FeCl<sub>3</sub> was added to FD1/THF, proving that the mechanism for fluorescence was identical in both cases. When an excess of acid (6 H<sup>+</sup>/FD1 equivalents) was used in experiment AA2-81F, and the FD1/THF/HCl mixture was allowed to react for 48 hr, the peak corresponding to FD1 disappeared completely (Figure 71). Only the peaks characteristic for RBH (at  $m/z = 229.3, 457.4, \text{ and } 935.4$ ) were still present. This ESI-MS finding suggested that the fluorescence of FD1 under acidic pH is due to the formation of a fluorescent species related to RBH via an acid induced hydrolysis process (Figure 72).

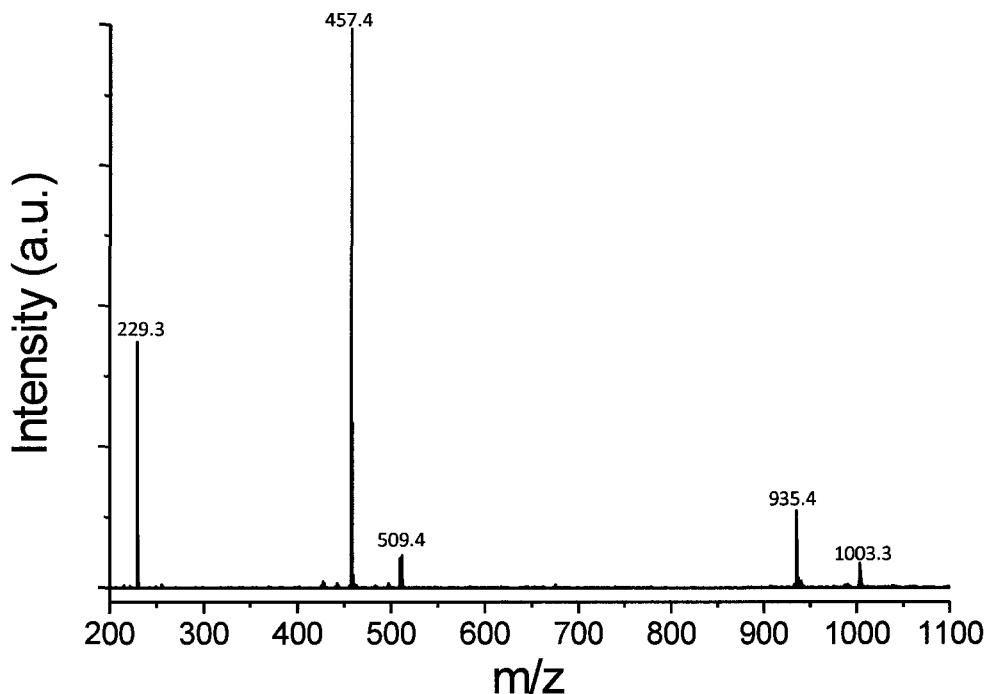


Figure 71. ESI-MS spectrum of FD1/THF upon addition of aqueous HCl solution (6 H<sup>+</sup>/FD1 equivalents).

RBH itself is a non-fluorescent molecule, however its protonated, ring-opened form is fluorescent (Figure 72) [73]. Thus it was concluded that the fluorescence observed when FD1 was mixed with HCl (or with aqueous solution of FeCl<sub>3</sub>, as shown in the previous section of this chapter) was due to the formation of fluorescent, protonated RBH.

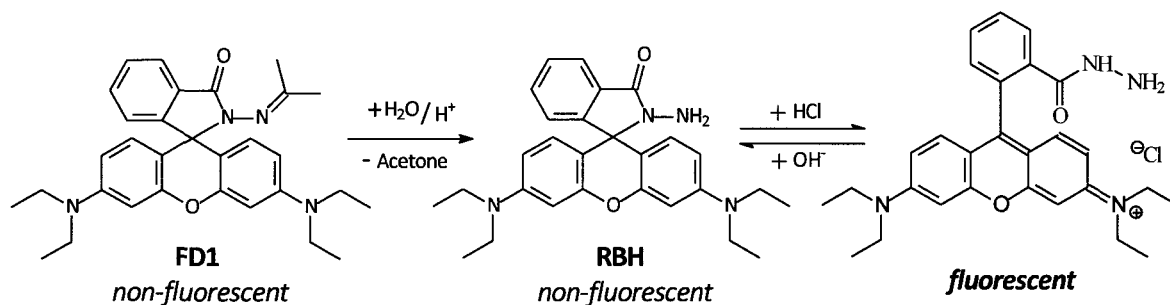


Figure 72. Proposed mechanism of FD1 fluorescence at low pH.

Since it was proposed that FD1 is hydrolyzed (via acid-catalyzed hydrolysis) into RBH, the final FD1+HCl structure should be identical to RBH+HCl structure. This finding was confirmed in experiment AA3-24. The changes in FD1 and RBH chemical structures upon addition of excess of HCl (6 H<sup>+</sup>/FD1 equivalents) were investigated by <sup>1</sup>H-NMR. The spectra of FD1 and RBH are shown in Figure 73a and Figure 73b, respectively, with their characteristic peaks indicated; a major difference between FD1 and RBH lies in the peak C at 1.8 ppm. Upon addition of HCl, there were a few major changes for the spectrum of FD1 (Figure 73c): (1) the peak C in Figure 73a disappeared completely, and a new peak X at 2.08 ppm emerged; (2) the peak B shifted from 3.3 to 3.55 ppm; and (3) the peaks corresponding to aromatic protons (I, J, and K) also shifted to lower fields. These changes were very similar to the changes observed in experiment AA2-39 and AA2-47 where acidic Ga<sup>3+</sup> salt and H<sub>2</sub>SO<sub>4</sub> were added to the FD1/THF-d<sub>8</sub> solutions respectively. It was then very interesting to notice that the mixture of RBH and HCl demonstrated an essentially identical spectrum (Figure 73d) to the FD1/HCl mixture except for peak X. It turned out that the peak X was due to acetone, which was the byproduct from the acid-induced hydrolysis of FD1 to RBH (Figure 72). The down-field shifts of peaks B, I-K were apparently due to the formation of the highly conjugated protonated RBH. This experiment confirmed that the fluorescence of FD1 at low pH is due to its acid-catalyzed hydrolysis to RBH that is subsequently protonated and becomes highly fluorescent.

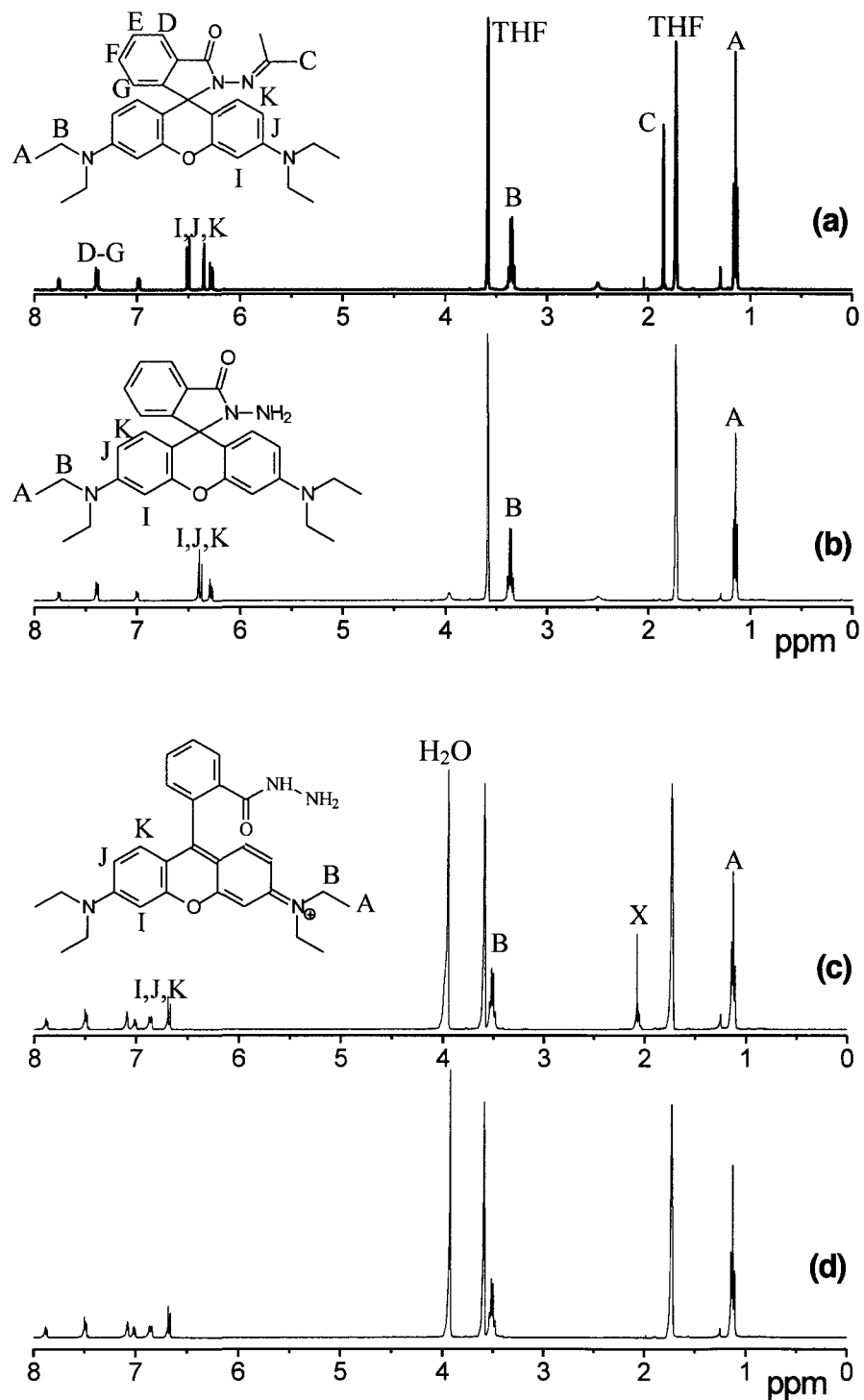


Figure 73.  $^1\text{H}$  NMR spectra of (a) FD1 and (b) RBH in THF- $d_8$ , as well as the mixtures of (c) FD1/HCl and (d) RBH/HCl in THF- $d_8$ /D<sub>2</sub>O mixed solvents. The huge water peak in (c, d) was due to HCl.

Since FD1 fluorescence, upon addition of acidic solution, was proved to occur due to its hydrolysis to RBH (and then RBH protonation), it was expected that RBH fluorescent response to HCl would be identical to the FD1 response. Interestingly however, in experiment AA2-81B, where RBH was titrated with HCl in the same way as in experiment AA2-81A (Figure 74), it was noticed that RBH fluorescent emission intensity was about 5 times lower than in the case for FD1 (when the fluorescent intensity in Figure 74 was compared to the one in Figure 68). After some time however both solutions faded to colorless and almost non-fluorescent probably due to the equilibration of the solutions towards the ring-closed RBH structure. Only the addition of large HCl excess caused a pink color and fluorescence (almost identical for both FD1/HCl and RBH/HCl solutions) to persist. The acid excess was probably necessary to push the reaction equilibrium to the protonated fluorescent RBH.

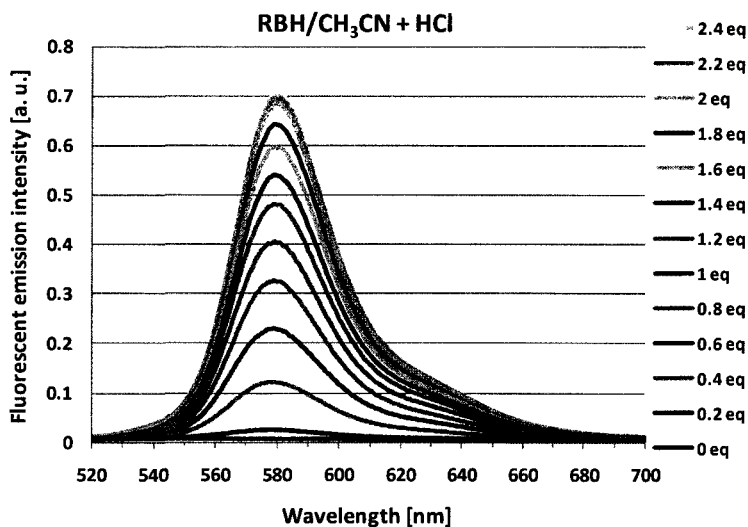


Figure 74. Fluorescent emission of RBH solution in  $\text{CH}_3\text{CN}$  ( $20 \mu\text{M}$ ) upon addition of HCl solution (up to  $2.4 \text{ H}^+$ / FD1 equivalents) when excited at  $510 \text{ nm}$ .

It was then postulated that the higher FD1 sensitivity to acidic solution could be caused by the formation of a non-stable intermediate of protonated FD1 (Figure 69) that

eventually hydrolyzes to RBH. This intermediate structure could modify the fluorescence efficiency of the molecule resulting in a fluorescence emission more intense than in the case of protonated RBH.

### **5.3.3 RBH as a Potential Early Corrosion Indicator**

At first FD1 was proposed to be utilized as an early corrosion indicator for steel not only due to its claimed sensitivity and selectivity towards  $\text{Fe}^{3+}$  [57] but also due to the desired chemical structure that would guarantee no chemical reaction with the epoxy matrix (as described in section 3.1.4). This lack of interaction was important to ensure that the chemical structure of the molecule will remain unchanged when mixed with the epoxy coating and thus its fluorescent response to corrosion. However the potential disadvantage of the indicator not being chemically bound to the coating is the possibility of the molecule to slowly diffuse through the epoxy matrix with time and eventually leach out (as it was shown for FD1 in section 4.3.2.3 of chapter 4)

Given that protonated, ring-opened and fluorescent RBH is a product of acid-catalyzed FD1 hydrolysis, and it is responsible for FD1's ability to sense corrosion (as shown in the previous section of this chapter), it was then considered to use RBH itself as an early corrosion indicator to sense the decrease in pH at the anodic site of corrosion when embedded in the epoxy matrix. The disadvantage of using RBH as an indicator, when compared to FD1, is its sensitivity to oxidation with time that showed to be more prevalent than for FD1 (i.e. the color of RBH in a solid state turned pink when expose to



light). It was also noted by others [73], and during the course of this work, that RBH is very sensitive to UV light. The molecule changed its color to pink even after only a few seconds of exposure to UV light from the confocal microscope. However a big advantage of RBH is that it possesses a  $\text{-NH}_2$  group in its structure and could potentially act as a curing agent and react with the epoxy ring, as shown in Figure 75.

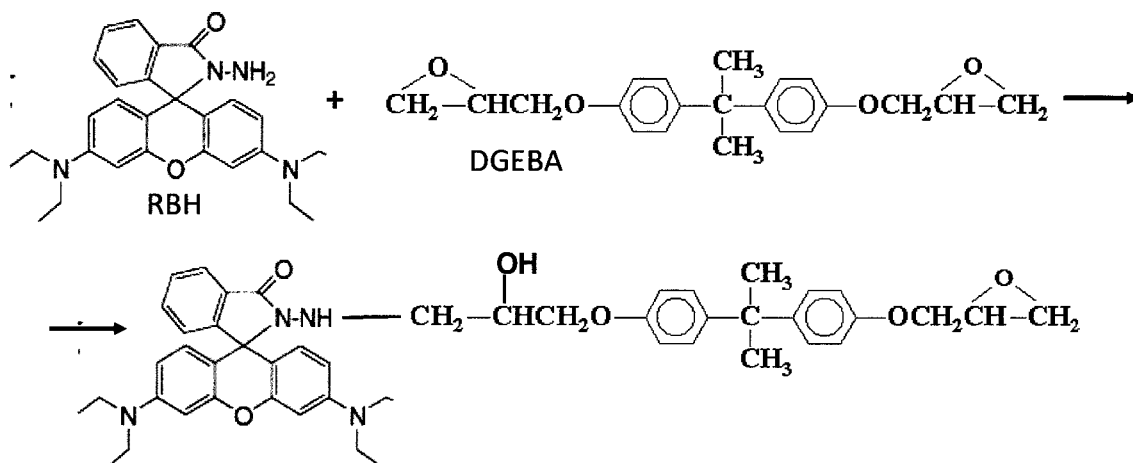


Figure 75. Potential reaction between RBH and epoxy ring from DGEBA.

This reaction should not cause the molecule to prematurely fluoresce since the RBH ring-closed structure is preserved. The covalent bonding to the epoxy resin would significantly reduce the molecule's diffusion through the epoxy matrix and as a result eliminate the possibility of the indicator leaching out of the coating with time. This chemical bonding however is only desired if the molecule's ability to respond to low pH is preserved and unaffected after the chemical reaction.

The following experiments were designed to investigate if RBH 1) is able to react and bind to the epoxy resin and 2) is able to respond to acidic pH after reaction with the epoxide ring.

In experiment AA2-94 the potential reaction between epoxy resin (DGEBA) and RBH was investigated by  $^1\text{H}$  NMR. RBH was mixed with DGEBA in toluene- $d_8$  (~ 1 RBH/DGEBA equivalent which is also 1:1  $\text{NH}_2/\text{NH}$  ratio) forming a slightly red solution (due to RBH) and heated to  $70^\circ\text{C}$  to allow the reaction between the  $-\text{NH}_2$  group from RBH and the epoxide ring from DGEBA. The spectrum C in Figure 76 represents the DGEBA/RBH mixture instantly after mixing (and before placing it at the elevated temperature). After heating of the mixture the reaction between RBH and DGEBA (resulting in the opening of the epoxide ring) was expected to be represented by the shifts in peaks marked E, F and G in spectrum B in Figure 76 and disappearance of peak C in spectrum A in Figure 76. Surprisingly however, the  $^1\text{H}$  NMR spectrum collected after 3 days at  $70^\circ\text{C}$  was no different (as shown the spectrum C in Figure 76).

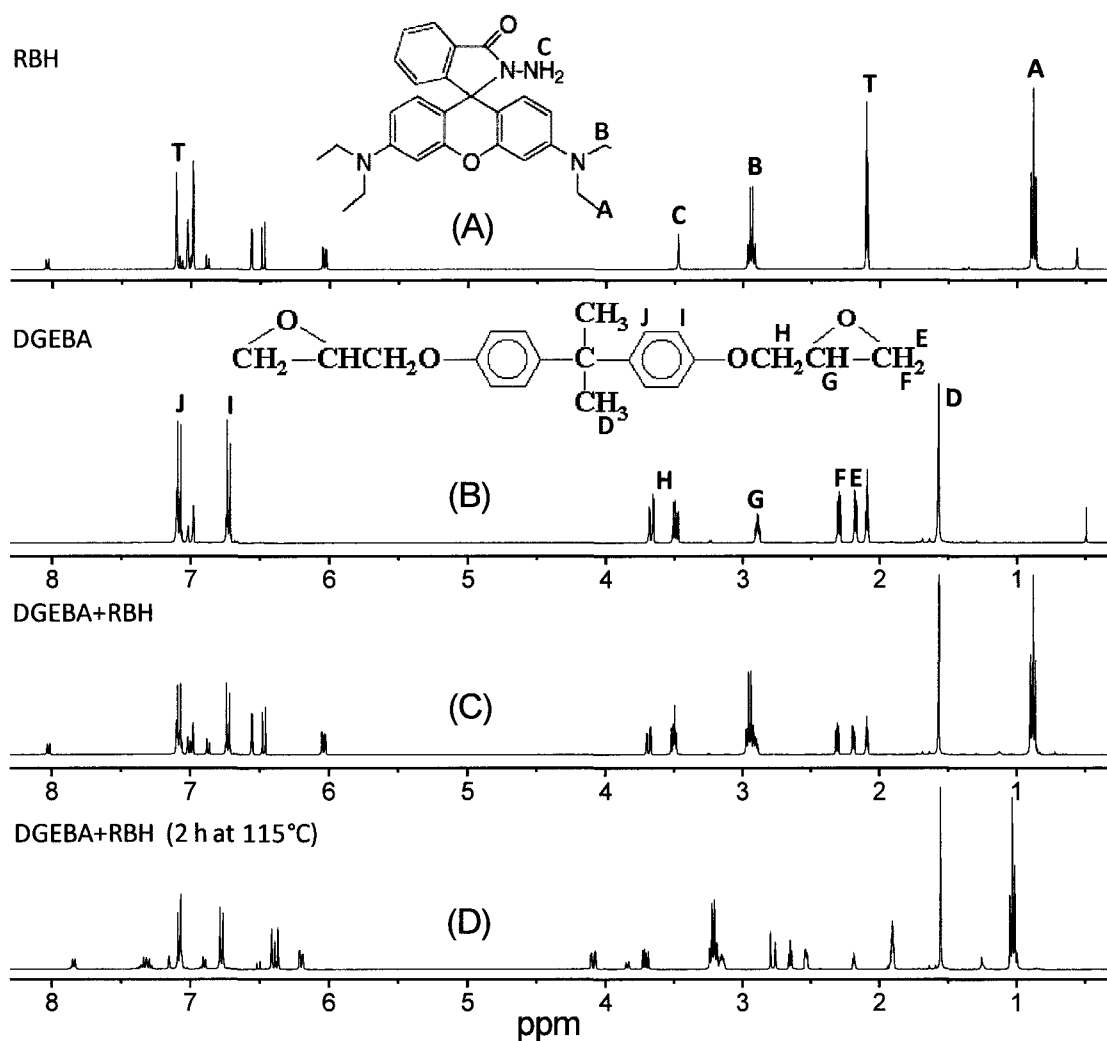


Figure 76.  $^1\text{H}$  NMR spectra of (A) RBH, (B) DGEBA, (C) mixture of RBH/DGEBA and (D) mixture of RBH/DGEBA after 2 h reflux at  $115^\circ\text{C}$ . Letter T represents peaks for toluene- $d_8$ .

Only when the DGEBA/RBH mixture was refluxed at  $115^\circ\text{C}$  for 2 h were the changes in the  $^1\text{H}$  NMR spectrum easily observed. Some rearrangements were observed for the aromatic peaks. All the peaks representing the epoxy ring (peaks E-H) shifted to lower field. Also peak C, representing protons of the  $-\text{NH}_2$  group in RBH, (previously at 3.47 ppm) disappeared. These changes could indicate that the epoxy ring was opened due to the reaction with RBH at this high temperature. This suggests that RBH could serve as a latent curing agent (i.e. cures only at highly elevated temperatures).

To make sure that the chemically bound RBH was still able to respond to low pH, the solvent was evaporated from the DGEBA/RBH mixture and an acidic aqueous solution of  $\text{FeCl}_3$  was added. After 1 h the  $\text{FeCl}_3$  solution changed color to purple and after longer time the precipitate also become dark magenta proving that RBH responded to the low pH. However there was no solid proof that the color response to  $\text{FeCl}_3$  was not due to the “free” RBH that did not covalently bind to DGEBA.

To ensure that RBH, when covalently bound to the epoxy, is able to sense low pH, experiment AA3-25 was performed. The solution of RBH and DGEBA (5 DGEBA/RBH equivalents) in xylenes was placed at  $123^\circ\text{C}$  for 44 h to facilitate the reaction between the reagents. Tetraethylenepentamine (TEPA) in slight excess was then added to the RBH/DGEBA solution to totally cure DGEBA and form a highly crosslinked epoxy coating. After 20 h at  $80^\circ\text{C}$ , a hard yellow epoxy film was formed. To remove all unreacted RBH (that did not build into the crosslinked structure after curing) the Soxhlet extraction method was used. After extraction for 12 h, the remaining epoxy film was again placed in a new THF wash solution and stirred for 3 days to make sure that all unreacted RBH was removed. That THF, which was collected after stirring, was characterized by UV-vis spectroscopy and showed that RBH was not present in the solvent (Figure 77) proving that all the unreacted RBH has been effectively removed.

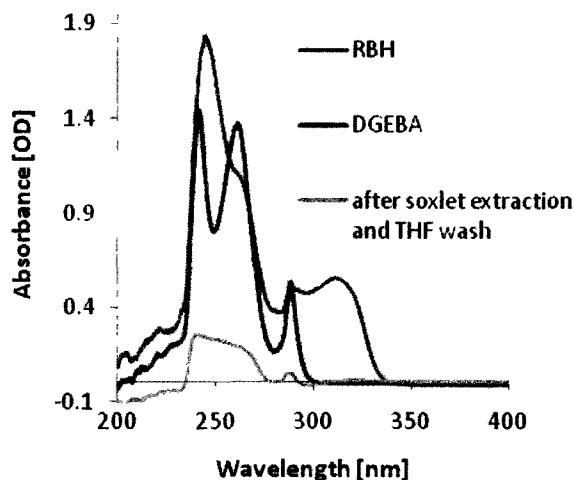


Figure 77. UV-vis absorption of the solutions of RBH and DGEBA in THF and the THF solution after extraction and wash of the cured RBH/DGEBA/TEPA sample.

When the remaining piece of the epoxy film (after extraction and wash in THF) was placed in 0.1 M HCl solution, pink color at the edges of the film appeared almost instantly. After 1 h, a deep pink color was observed in the whole film. Also under UV light (365 nm) the epoxy film appeared bright orange. This experiment proved that RBH built into the crosslinked epoxy matrix was still able to sense low pH. This result indicated that RBH is a very promising corrosion indicator and is not only highly sensitive to acid pH but also can be easily immobilized in the epoxy matrix. This chemical binding with the epoxy eliminates the possibility of the indicator leaching out of the matrix and as a result extends the lifetime of the smart epoxy-indicator system.

## 5.4 Conclusions

FD1 ability to sense corrosion of steel (as shown in chapter 3) at the anodic site (where the acidic pH is observed) was proved to be due to its acid-catalyzed hydrolysis to RBH.

The protonated, ring-opened RBH is a fluorescent molecule and it is believed to be responsible for the observed fluorescence when FD1 is used as a corrosion indicator for steel. FD1 was also shown to be a “turn-on” fluorescent sensor for  $\text{Fe}^{3+}$  ions in non-aqueous solution. In this environment, the fluorescent  $\text{FD1/Fe}^{3+}$  complex is formed. However FD1 “turn-on” fluorescence due to addition of an aqueous solution of ferric salt is caused by the acidity of the solution and not by the  $\text{FD1/Fe}^{3+}$  complex formation. This FD1 sensitivity to acidic pH advantageously extends its application as a corrosion indicator to other important metals such as aluminum. RBH was also proposed as a corrosion indicator due to its “turn-on” fluorescence at low pH and due to the fact that it can be covalently bonded to a polymeric network without losing its responsiveness to low pH. This eliminates the possibility of the molecule to leach out of the epoxy matrix with time and makes RBH a very promising early corrosion indicator.

## CHAPTER 6

### FD1 AS AN INDICATOR FOR EARLY DETECTION OF ALUMINUM CORROSION<sup>‡</sup>

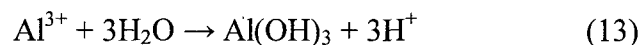
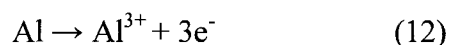
*Summary.* Since FD1 response to acidic pH results in “turn-on” fluorescence, this molecule was explored in this chapter as a corrosion sensor for aluminum when embedded in both model (clear) and commercial (filled) epoxy coatings. FD1 was proved to be an effective early corrosion indicator for both Al 1052 and Al 2024-T3 aluminum alloys even in the presence of pigments. Both clear and filled, FD1-containing smart epoxy coatings were capable of sensing acidic pH, produced at the anodic site of localized aluminum corrosion, at a low indicator concentration (0.5 wt %), as demonstrated by the fluorescent, bright-orange areas corresponding to localized pitting corrosion of the aluminum substrate under a handheld UV lamp. Therefore, early corrosion of aluminum can be easily and nondestructively detected via this “turn-on” fluorescence strategy.

---

<sup>‡</sup> Portions of this chapter have been published: Augustyniak, A.; Ming, W. Early detection of aluminum corrosion via “turn-on” fluorescence in smart coatings. *Prog. Org. Coat.* **2011**, 71, 406-412 (doi:10.1016/j.porgcoat.2011.04.013).

## **6.1 Introduction and the Objectives of this Chapter**

In the previous chapter (section 5.3.2) it was proved that FD1 shows “turn-on” fluorescence upon addition of acidic solutions. This responsiveness to low pH made the FD1 molecule an attractive candidate for sensing early corrosion of important metals, other than steel, such as aluminum. As described in section 1.1.3, at the anodic site of aluminum corrosion metal dissolution and subsequently metal ion hydrolysis takes place according to reactions (Equations 12 and 13):



As a result of the hydrolysis, a decrease in the local pH is observed. This change in pH could thus be detected by FD1 embedded in the epoxy coating.

Various fluorescent molecules were previously utilized to sense aluminum corrosion when embedded in an organic coating. As described in section 1.3.1.1 Zhang and Frankel [38] used acid-base fluorescent indicators, embedded in a clear acrylic coating, to sense increase in local pH at the cathodic site of aluminum corrosion (where reduction reactions take place). To sense the metal ions produced at the anodic site of corrosion a



variety of sensing molecules incorporated into the protective coating were used that show chelation enhanced fluorescence (CHEF) upon complexation with the  $Al^{3+}$  ion, as described in section 3.1.2. Additionally Liu and Wheat [41] exploited coumarin 120, incorporated in an epoxy primer coating, to sense the acidic pH associated with the anodic site of corrosion. The fluorescence of this indicator is quenched in acidic pH below 4. Therefore the sensing coating was initially fluorescent and its fluorescence decreased upon exposure to corrosive environment, making it very difficult to judge the onset of the corrosion due to lack of sharp contrast.

However no molecule has been utilized so far as an indicator for early corrosion detection of aluminum, which 1) can sense the decrease in pH at the anodic site when incorporated in the epoxy coating and 2) shows “turn-on” fluorescence. The purpose of this chapter was to investigate FD1 ability to sense corrosion of different aluminum alloys when embedded in both clear and filled epoxy coatings.

## **6.2 Experimental Section**

### **6.2.1 Reagents and Materials**

FD1 was synthesized in our lab as described in section 3.3.2.1 (sample AA2-27). Tetraethylenepentamine (TEPA, technical grade) was purchased from Acros Organics. D.E.R.<sup>TM</sup> 332 Epoxy Resin (high purity bisphenol A diglycidylether, DGEBA) was purchased from The Dow Chemical Company. Haze Gray Epoxy Polyamide coating, MIL-DTL-24441C, type III, Formula 151, was purchased from NCS Coatings, Inc.

Acetone (ACS grade) was purchased from PHMARCO-AAPER. Hexanes (HPLC grade) and sodium chloride (NaCl) were purchased from EMD chemicals. Toluene (ACS grade) was purchased from Fisher Scientific. All reagents were used as received. Al 2024-T3 panels with original dimensions: 2.54 cm × 10.16 cm × 0.16 cm were purchased from Q-Lab Corporation, and Al 1052 alloy was obtained from Hydro Aluminium Deutschland GmbH.

## **6.2.2 Sample preparation**

### **6.2.2.1 Preparation of Al 1052 Panel Coated with FD1-containing Clear Epoxy Coating (AA2-54)**

Corrosion sensing panels were prepared by applying the low-pH-sensing clear model epoxy coating onto an Al 1052 alloy panel cut to dimensions 5.0 cm × 2.5 cm × 0.03 cm. Before coating application, the panel was polished with 600-grit sandpaper and then washed with hexane and dried with argon. The low-pH-sensing coating was prepared by mixing TEPA (amine hardener) and DGEBA (epoxy resin) (at a NH/epoxy molar ratio of 1.0:0.8 to obtain full curing) with 0.5 wt% FD1. To aid in uniform mixing with the two other components, FD1 was first dissolved in toluene (0.1 wt% FD1). After mixing, the coating was applied onto Al 1052 panels using a drawdown bar. The coating was cured at 70 °C overnight and then at room temperature for another 2 days. Many defects in the form of air bubbles were present in the coating. The coating thickness was approximately 40 μm. To observe the response of FD1 in the clear epoxy coating to low pH at the

anodic site of aluminum corrosion, an open-ended glass cylinder was affixed and sealed to a part of the coated panel. The cylinder was then filled with a 3.5% NaCl solution so that only this circular portion of the sample was exposed to the corrosive environment. The surface of the area exposed to NaCl was monitored with a confocal microscope at different times of exposure to the NaCl solution for changes in the fluorescence intensity. Also, pictures of the sample surface under both UV and visible light were taken using a digital camera placed on the microscope eyepiece.

#### 6.2.2.2 Preparation of Al 2024-T3 Panel Coated with FD1-containing Filled Epoxy Coating (AA3-06F)

Another series of corrosion-sensing panels were prepared by applying FD1-containing, filled epoxy coating onto the Al 2024-T3 alloy panel cut to dimensions 2.5 cm × 2.5 cm × 0.16 cm. The aluminum panel edges were smoothed after cutting to avoid edge effects during coating application. Before coating application, the panels were polished with 600-grit sandpaper and then washed with acetone. The epoxy coating was prepared by mixing both components of commercially available filled Haze Gray Epoxy Polyamide coating (MIL-DTL-24441C) with 0.5 wt% FD1 (first dissolved in toluene at 0.1 wt%). After mixing, the coating was applied onto Al 2024-T3 alloy panels using a spin coater to obtain uniform thickness. The back of the sample was also coated with the Haze Gray Epoxy Polyamide coating since these panels were designed to be immersed into a corrosive solution. The coated sample was cured at 125°C for 24 h and then at room temperature for another 2 days. The coating thickness was approximately 23 μm. Coating

defects were present especially at the sample edges (due to poor coating coverage) and would be potential areas prone to corrosion. To observe the response of FD1 in the filled epoxy coating to low pH at the anodic site of aluminum corrosion, the sample was immersed in a 3.5% NaCl solution and placed in an oven at 70°C to increase the diffusion of corrosive solution through the coating and facilitate corrosion. The surface of the sample was monitored with the confocal microscope at different times of exposure to the NaCl solution for changes in the fluorescence intensity. Also, pictures of the sample surface under both UV and visible light were taken using a digital camera placed on the microscope eyepiece.

### **6.2.3 Characterization Methods**

Preliminary examination of fluorescence was performed using a handheld UV lamp (Model UVGL-25, MINERALIGHT®) with an excitation wavelength of 365 nm. Fluorescence imaging was conducted on a Zeiss LSM 510 Meta laser scanning confocal microscope with an Axio Imager M1 platform. In both experiments, a 514 nm ArMultiLine laser was used as the excitation source. An EC Plan- Neofluar 10×/0.30 M27 objective was used to observe the sample surface. The fluorescent emission wavelength was obtained from the mode function (using a Meta detector with a selected emitted fluorescence range of 520-700 nm with a 10.7 nm step). To compare the laser-excited images to those obtained by more practical end-use conditions, the confocal microscope's 100 W mercury lamp was used as a UV light source. Coating in experiment AA3-06F was applied using a P-6000 spin coater from Specialty Coating Systems, Inc.

The coating's thickness was measured with a CHECK-LINE coating thickness tester (model DAC-1KS).

## **6.3 Results and Discussion**

### **6.3.1 FD1 as a Corrosion Sensor in Clear Model Epoxy Coating on Al 1052 Alloy**

To examine if FD1, when embedded in a clear epoxy coating, is able to sense low pH at the anodic site of aluminum corrosion, an Al 1052 aluminum alloy coated with the model clear epoxy system (TEPA-DGEBA) was exposed to a corrosive environment of 3.5 % NaCl solution. Initially no fluorescence characteristic of FD1 was observed in the coating under UV light from a handheld lamp. However, after only 2 days of exposure, a small (1 mm in diameter) bright orange circular spot was easily observed under UV light by the naked eye (Figure 78a). This bright area most likely indicates the formation of a shallow pit. Figure 78a, top row, shows a close view of this area under UV light as observed under the confocal microscope. Also under visible light a slightly pink color was seen (Figure 78a, bottom row). The color and fluorescence was especially bright around air bubble defects, which is not surprising since corrosion occurred much faster in these defected areas due to faster diffusion of corrosive solution to these areas [19]. The fluorescent emission recorded from the confocal microscope's mode function showed that the maximum fluorescence emission ( $\lambda_{em,max}$ ) was at 583 nm, which was in accordance with the maximum fluorescent emission of FD1 in CH<sub>3</sub>CN solution upon

addition of  $H^+$  (Figure 68). Thus the fluorescent emission observed here was attributed to the low pH at the anodic site of aluminum corrosion, which may reach as low as 3.5 [10].

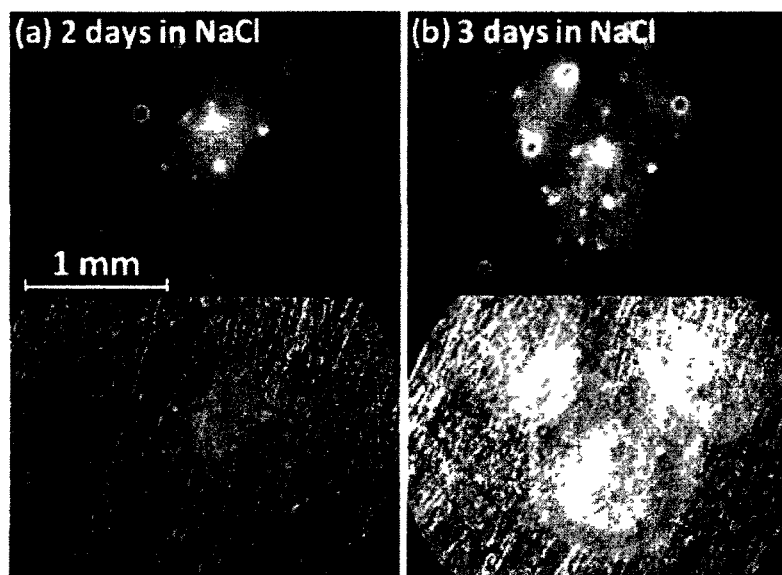


Figure 78. Images of Al 1052 coated with a FD1-containing, clear epoxy coating (AA2-54) after (a) 2 days and (b) 3 days of exposure to 3.5 % NaCl solution. Top row: digital camera images taken through the confocal microscope eyepiece under UV light. Bottom row: images of the same areas taken through the confocal microscope eyepiece under natural light.

After 3 days of exposure, two new bright orange circular spots (under UV) were seen next to the initial bright spot, which itself became less intense in fluorescence and color (Figure 78b, top row). Some white residue also built up in the form of a ring around the initial bright area (Figure 78b, bottom row), which were most likely aluminum corrosion products that formed after  $OH^-$  from the cathodic site of corrosion combined with  $Al^{3+}$  produced at the anodic site.  $OH^-$  ions can also be responsible for the decrease of the initial indicator fluorescence since RBH is not fluorescent when the highly conjugated structure (the right structure, Figure 72) is deprotonated by  $OH^-$  to the middle structure in Figure 72. A blister was also formed in this area; this is usually the early stage of coating

degradation and formed when water uptake increases due to osmosis when metal salts are present on the surface under the coating [19]. With longer time of exposure to the NaCl solution, two new blisters were also formed in the areas where fluorescence was observed previously. This experiment has demonstrated that FD1 embedded in a clear epoxy coating can successfully sense low pH generated at the anodic site during the early stages of aluminum corrosion before obvious corrosion and coating degradation (i.e. blisters) becomes evident.

### **6.3.2 FD1 as a Corrosion Sensor in Filled Epoxy Coating on Al 2024-T3 alloy**

The FD1 ability (when embedded in the filled epoxy coating in the presence of filler pigments) to detect corrosion of Al 2024-T3 aluminum alloy, a widely used material in aerospace and other industrial application [8] but at the same time highly susceptible to pitting corrosion [74], was demonstrated in experiment AA3-06F. The Al 2024-T3 alloy coated with the filled epoxy coating (MIL-DTL-24441C, type III, Formula 151), containing 0.5 wt% FD1, was exposed to a corrosive environment of 3.5 % NaCl solution at an elevated temperature (70 °C). Due to the excellent anticorrosion properties of the commercial epoxy coating used in this experiment, extended exposure to NaCl and higher temperature was required to initiate corrosion reactions in a short period of time. After 21 days of exposure to 3.5% NaCl, a few small areas at the edges of the sample, where corrosion was expected to happen due to defects in the coating, showed orange fluorescence when excited with a handheld UV lamp. When these areas were examined closely under the confocal microscope it became obvious that the bright areas were

mostly in the shape of a ring (Figure 79a in AREA 1 and 2, top row, circular areas marked with arrows). These rings are most likely related to the anodic sites of corrosion, where the local pH is expected to decrease, around the cathodic intermetallic particles [74].

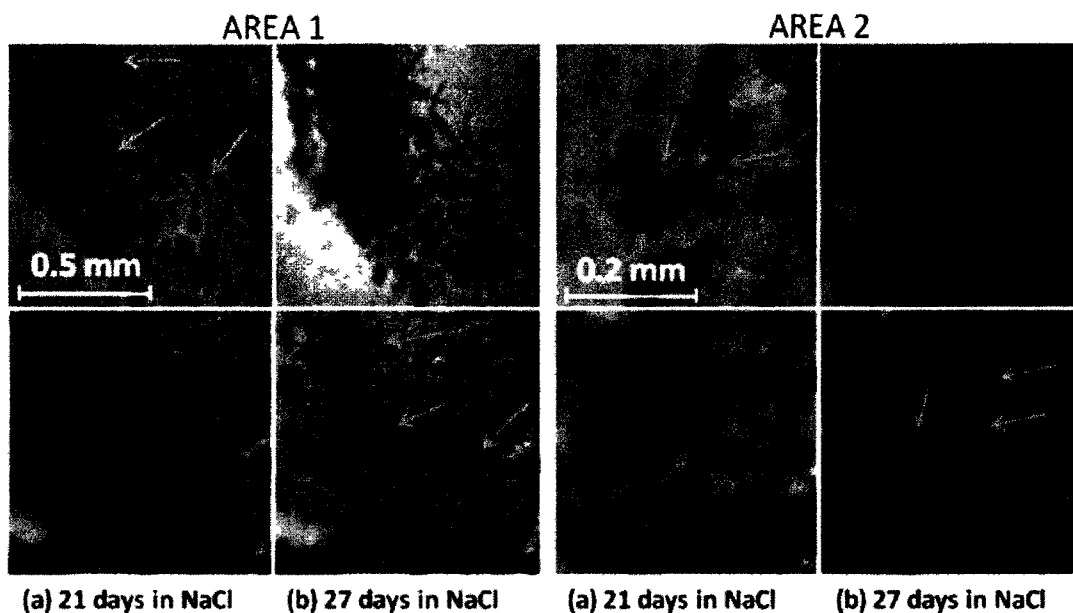


Figure 79. Images of Al 2024-T3 coated with FD1-containing filled epoxy coating (AA3-06F) after (a) 21 days and (b) 27 days of exposure to 3.5 % NaCl solution at 70 °C. Top row: digital camera images taken through the confocal microscope eyepiece under UV light. Bottom row: images of the same areas taken through the confocal microscope eyepiece under natural light.

Fluorescent emission recorded from the confocal microscope's mode function showed that the maximum fluorescence emission ( $\lambda_{em,max}$ ) was between 575 and 580 nm depending on the area examined, which clearly indicated that FD1 was capable of sensing the low pH in this filled coating system. The  $\lambda_{em,max}$  was slightly lower than the maximum emission wavelength at 583 nm in the FD1/HCl mixture in a CH<sub>3</sub>CN solution (Figure 68), which might be due to the low intensity of the spectra from the solid state. The effectiveness of the corrosion-sensing filled epoxy coating in detecting early stages of corrosion was confirmed after 6 more days of exposure to corrosive environment at 70



°C; the initially bright areas faded and rusty spots appeared in the same place where fluorescence was observed previously under UV light. These changes are marked with the arrows in the bottom row of Figure 79b, in both AREA 1 and 2 and are evidence that FD1 was an effective corrosion indicator for Al 2024-T3 aluminum alloy when embedded in the filled epoxy coating.

#### **6.4 Conclusions**

FD1 was proved to be an effective early corrosion indicator for both Al 1052 and Al 2024-T3 aluminum alloys in both model (clear) and commercial (filled) epoxy coatings. The results, when using FD1 to sense aluminum corrosion, are similar to the ones obtained for steel corrosion and described in the conclusions of chapter 3. The “turn-on” FD1 fluorescence was easily and non-destructively detected under UV light before any visible sign of corrosion appeared. In addition, only a low FD1 concentration (0.5 wt%) in the coating was needed for successful indication. FD1 does not prematurely interact with coating formulation components, and FD1 can “report” early aluminum corrosion even in the presence of pigments.

## CHAPTER 7

### CONCLUSIONS AND OUTLOOK

The successful development of a smart epoxy/indicator system to sense early stages of metal corrosion has been described in this thesis.

Since the experiments described in this thesis showed that using acid-base indicators, to sense increase in local pH at the cathodic site of corrosion, in the epoxy coating can be challenging due to the possibility of the indicator to interact with the coating components (both amine hardener and the epoxy resin) and to be prematurely activated, a new corrosion indicator, FD1, was proposed to be utilized in an epoxy matrix. This molecule, initially proposed as a  $\text{Fe}^{3+}$  chemosensor for biological applications [57], was proven to report early stages of steel corrosion, via “turn-on” fluorescence, when embedded in both model (clear) and commercial (filled) epoxy coating (in the presence of pigments). FD1/epoxy smart system was very effective for indicating early corrosion of steel, both for areas damaged through to the substrate (scribed areas) and areas without exposure of the substrate (*undercoating* corrosion). The “turn-on” FD1 fluorescence was easily non-destructively detected under UV light before any visible sign of corrosion appeared. In

addition, only a low FD1 concentration (0.5 wt%) in the coating was needed for effective corrosion detection.

FD1 showed a slight sensitivity to photooxidation which resulted in a small increase in the molecule's fluorescence. Yet when embedded in the clear epoxy matrix (both model and commercial epoxy system) the indicator showed no change in its fluorescence over time proving its stability to photooxidation in the epoxy matrix and lack of interaction with the epoxy components. However, a slight increase in the FD1 fluorescence over time was observed when the indicator was embedded in the filled commercial epoxy coating, only when the coating was scratched. This change was most likely due to the presence of coating additives, for example  $\text{TiO}_2$ , which could facilitate FD1 photooxidation.

FD1 has proven to be a robust corrosion indicator, when embedded in the epoxy coatings, capable of sensing corrosion even after prolonged exposure (28 months) to the aqueous solution.

FD1 ability to sense corrosion of steel at the anodic site (where the acidic pH is observed and  $\text{Fe}^{3+}$  ions are produced) was proved to be due to its acid-catalyzed hydrolysis to fluorescent protonated RBH. FD1 was also shown to form a fluorescent complex with  $\text{Fe}^{3+}$  in a non-aqueous solution. However, FD1 "turn-on" fluorescence upon addition of an aqueous solution of ferric salt is caused by the acidity of the solution and not by the FD1/ $\text{Fe}^{3+}$  complex formation. RBH was also proven to be a very promising "turn-on"

early corrosion indicator due to its fluorescence at low pH and due to the fact that it can be covalently bonded to a polymeric network without losing its responsiveness to low pH. This eliminates the possibility of the molecule to leach out of the epoxy matrix with time.

Since FD1 showed “turn-on” fluorescence upon addition of acidic pH, it was also utilized to sense decrease in local pH at the anodic sites of aluminum corrosion. FD1 was proved to be an effective early corrosion indicator for aluminum alloys in both model (clear) and commercial (filled) epoxy coatings.

FD1 was explored as a corrosion sensor in an epoxy coating due to the reactivity of this type of polymeric matrix. However this molecule (and potentially also RBH) can be easily applied to other types of protective polymeric coatings, such as acrylic or polyurethane.

To fully explore the practical aspects of using FD1, and perhaps also RBH, in the protective coatings as early corrosion indicators, further experiments could be performed. The maximum thickness of the filled coating, at which the indicator fluorescent response is still observable, could be investigated. Also the influence of the corrosion sensing molecules on the coating protectiveness could be assessed. Quantitative experiments exploring the lower limit of FD1 concentration in the polymeric matrix, able to effectively sense corrosion, could be performed as well.

Also in this thesis it was proved that fluorescent  $\text{Fe}^{3+}/\text{FD1}$  complex is formed in non-aqueous environment. Fluorescent “turn-on” ferric ion sensors are highly desirable due to the importance of this heavy metal ion in biological and environmental processes. Thus to fully evaluate FD1 as a  $\text{Fe}^{3+}$  chemosensor, further experiments, such as assessment of the  $\text{FD1}/\text{Fe}^{3+}$  complex binding constant, fluorescent quantum yield and selectivity over other metal ions, would be important to consider for the future.

## LIST OF REFERENCES

- 
- <sup>1</sup> D. A. Jones, "Principles and Prevention of Corrosion", 2nd edition, Prentice Hall, Inc., **1996**
- <sup>2</sup> J. R. Davis, "Corrosion: Understanding the Basics", ASM International, **2000**
- <sup>3</sup> Corrosion Cost and Prevention Strategies in the United States, September **2001**, Report FHWA-RD-01-156
- <sup>4</sup> A. J. Perez, "Office of Naval Research Corrosion Control S&T Program", DoD Maintenance Symposium October, **2006**
- <sup>5</sup> P. Sarin, V. L. Snoeyink, D. A. Lytle, W. M. Kriven, "Iron Corrosion Scales: Model for Scale Growth, Iron Release, and Colored Water Formation", J. Environ. Eng.-ASCE, **2004**, 130, 364-373
- <sup>6</sup> <http://www.corrosion-doctors.org>
- <sup>7</sup> P. E. Zapp, "Pitting Growth Rate in Carbon Steel Exposed to Simulated Radioactive Waste," presented at the NACE International Conference, Houston, TX, **1996**; paper 129
- <sup>8</sup> Z. Ahmad, "Principles of Corrosion Engineering and Corrosion Control", Elsevier/BH, **2006**
- <sup>9</sup> J. R. Davis, Ed., "Metals Handbook", vol. 13, pp 104-122 and 583-609. ninth edition, ASM International, Ohio, **1987**
- <sup>10</sup> J. R. Davis, Ed., Corrosion of Aluminum and Aluminum Alloys, ASM International, 1999, Chapter 3
- <sup>11</sup> M. Nunez, "Prevention of Metal Corrosion: New Research", Nova Publishers, **2007**
- <sup>12</sup> W. W. Kittleberger, A. C. Elm, "Diffusion of Sodium Chloride through Various Paint Systems", Ind. Eng. Chem., **1952**, 44, 326-329
- <sup>13</sup> D. Greenfield, D. Scantlebury, "The Protective Action of Organic Coatings on Steel: A Review" JCSE, **2000**, 3, Paper 5
- <sup>14</sup> S. Paul, Ed., "Surface Coatings. Science and Technology. Second Edition", John Wiley & Sons Ltd, Chichester, **1996**
- <sup>15</sup> C. A. May, Ed., "Epoxy Resins. Chemistry and Technology. Second Edition. Revised and Expanded", CRC Press, **1988**

- 
- <sup>16</sup> A. Forsgren, “Corrosion Control through Organic Coatings”, CRC Press, **2006**
- <sup>17</sup> G. Odian, “Principles of Polymerization. Fourth Edition”, Wiley-Interscience , Hoboken, NJ, **2004**
- <sup>18</sup> <http://www.pslc.ws/macrog/maindir.htm>
- <sup>19</sup> J. Sonke, W.M. Bos, “Scientific Methods for Qualification and Selection of Protective Coatings”, J. Protective Coat. Linings, June, **2008**
- <sup>20</sup> F. Mansfeld , “Corrosion Mechanisms”, CRC Press, **1987**
- <sup>21</sup> P. A. Schweitzer , “Corrosion of Linings and Coatings: Cathodic and Inhibitor Protection and Corrosion Monitoring”, CRC Press, **2006**
- <sup>22</sup> [http://www.corrosionclinic.com/types\\_of\\_corrosion/filiform\\_corrosion\\_underfilm\\_corrosion.htm](http://www.corrosionclinic.com/types_of_corrosion/filiform_corrosion_underfilm_corrosion.htm)
- <sup>23</sup> A. P. Kayes, M. J. Robinson, S. Impey, “The Influence of Cleaning and Surface Treatment on Filiform Corrosion of Aluminum Alloys”, JCSE, Vol. 2 Paper 1, **1999**
- <sup>24</sup> W. Feng, S. H. Patel, M. Y. Young, J. L. Zunion III, M. Xanthos, “Smart Polymeric Coatings-Recent Advances”, Adv. Polym. Technol., **2007**, 26, 1–13
- <sup>25</sup> A. Kumar, L. D. Stephenson, J. N. Murray, “Self-Healing Coatings for Steel”, Prog. Org. Coat., **2006**, 55, 244–253
- <sup>26</sup> S. H. Cho, S. R. White, P. V. Braun, “Self-Healing Polymer Coatings”, Adv. Mater. **2009**, 21, 645–649
- <sup>27</sup> L. M. Calle, W. Li, “Smart Coatings for Corrosion Sensing and Protection”, NASA Annual Report; NASA: Cape Canaveral, FL, **2005**
- <sup>28</sup> A. N. Khramov, N. N. Voevodin, V. N. Balbyshev, R. A. Mantz, “Sol–Gel-Derived Corrosion-Protective Coatings with Controllable Release of Incorporated Organic Corrosion Inhibitors”, Thin Solid Films, **2005**, 483, 191–196
- <sup>29</sup> M. Kendig, M. Hon, L. Warren, “‘Smart’ Corrosion Inhibiting Coatings”, Prog. Org. Coat., **2003**, 47, 183– 189
- <sup>30</sup> S. V. Lamaka, D. G. Shchukin, D. V. Andreeva, M. L. Zheludkevich, H. Möhwald, M. G. S. Ferreira, “Sol-Gel/Polyelectrolyte Active Corrosion Protection System”, Adv. Funct. Mater. **2008**, 18, 3137–3147



- 
- <sup>31</sup> D. Hughes, N. Wang, T. Case, K. Donnell, R. Zoughi, R. Austin, M. Novack, "Detection of Corrosion in Aluminum Panels Under Paint and Primer", AIP Conf. Proc., **2001**, 557, 460-466
- <sup>32</sup> S. Kharkovsky, R. Zoughi, "Millimeter Wave Nondestructive Evaluation of Corrosion Under Paint in Steel Structures", AIP Conf. Proc., **2006**, 820, 1277-1283
- <sup>33</sup> A. C. Ryley, M. T. Ghasr, S. Kharkovsky, R. Zoughi, G. Steffes, "Applied Microwave "Application of Millimeter Wave, Eddy Current and Thermographic Methods for Detection of Corrosion in Aluminum Substrate", AIP Conf. Proc., **2007**, Vol. 894, 1258-1265
- <sup>34</sup> J. S. Han, J. H. Park, "Detection of Corrosion Steel Under an Organic Coating by Infrared Photography", Corros. Sci., **2004**, 46, 787-793
- <sup>35</sup> C. H. Chang, J. H. Park, J. S. Kim, M. K. Joo, G.D. Lee, K.Y. Kim, A. Nishikata, T. Tsuru, "Nondestructive Evaluation of Corrosion Beneath Organic Coatings by Synchrotron X-rays", Corros. Sci., **2003**, 45, 2689-2695
- <sup>36</sup> N. Singh, S.C. Jain, A. K. Aggarwal, M. L. Singla, M. Singh, "A Simple Fiber Optic Technique for In-Situ Corrosion Sensing in Structures", SPIE proceedings series, Nondestructive Evaluation of Aging Materials and Composites. Conference N<sup>o</sup>4, Newport Beach CA, March **2000**, vol. 3993, pp. 201-205
- <sup>37</sup> L. Yu, V. Giurgiutiu, P. Pollock, "A Multi-Mode Sensing System for Corrosion Detection Using Piezoelectric Wafer Active Sensors", SPIE Proceedings Series, Sensors and Smart Structures Technologies for Civil, Mechanical, and Aerospace Systems 2008, San Diego, CA, March **2008**, vol. 6932, p. 69322H
- <sup>38</sup> J. Zhang, G. S. Frankel, "Corrosion-Sensing Behavior of an Acrylic-Based coating System", Corrosion, **1999**, 55, 957-967
- <sup>39</sup> R. E. Johnson, V. S. Agarwala, "Fluorescence Based Chemical Sensors for Corrosion Detection", Presented at the NACE International Conference, New Orleans, LA, **1997**, Paper 304
- <sup>40</sup> D. E. Bryant, D. Greenfield, "The Use of Fluorescent Probes for the Detection of Under-Film Corrosion", Prog. Org. Coat. **2006**, 57, 426-420
- <sup>41</sup> G. Liu, H. G. Wheat, "Use of a Fluorescent Indicator in Monitoring Underlying Corrosion on Coated Aluminum 2024-T4", J. Electrochem. Soc., **2009**, 156, C160-C166
- <sup>42</sup> M. P. Sibi, Z. Zong, "Determination of Corrosion on Aluminum Alloy Under Protective Coatings Using Fluorescent Probes", Prog. Org. Coat., **2003**, 47, 8-15
- <sup>43</sup> <http://corrosion-doctors.org/Corrosion-History/Action.htm>

- 
- <sup>44</sup> L. Nicholson, "Kinetics of the Fading of Phenolphthalein", *J. Chem. Educ.*, **1989**, 66, 725-726
- <sup>45</sup> A. S. Cushman, H. A. Gardner, "The Corrosion and Preservation of Iron and Steel", McGraw-Hill book company, **1910**
- <sup>46</sup> [http://www.sciencephoto.com/images/download\\_lo\\_res.html?id=847450073](http://www.sciencephoto.com/images/download_lo_res.html?id=847450073)
- <sup>47</sup> G. G. Guilbault, "Practical Fluorescence", Marcel Dekker, Inc., New York, NY, **1990**
- <sup>48</sup> J. R. Lakowicz, "Principles of Fluorescence Spectroscopy", Spring Science Business Media, LLC, Baltimore, MD, **2006**
- <sup>49</sup> V. A. Rebar, M. M. Santore, "A Total Internal Reflectance Fluorescence Nanoscale Probe of Interfacial Potential and Ion Screening in Polyethylene Oxide Layers Adsorbed onto Silica", *J. Colloid Interf. Sci.*, **1996**, 178, 29–41
- <sup>50</sup> L. K. White, R. B. Comizzoli, C. A. Deckert, G. L. Schnable, "The Detection of Corrosion Phenomena with *pH*-Sensitive Fluorescent Dyes on Aluminum- and Gold-Metallized IC Devices", *J. Electrochem. Soc.*, **1981**, 128, 953-956
- <sup>51</sup> M. A. Alodan, W. H. Smyrl "Detection of Localized Corrosion of Aluminum Alloys Using Fluorescence Microscopy", *J. Electrochem. Soc.*, **1998**, 145, 1571-1577
- <sup>52</sup> A.C. Gutierrez, M.H. Gehlen, "Time Resolved Fluorescence Spectroscopy of Quercetin and Morin Complexes with Al<sup>3+</sup>", *Spectrochim. Acta A*, **2002**, 58, 83–89
- <sup>53</sup> S. Bae, J. Tae, "Rhodamine-Hydroxamate-Based Fluorescent Chemosensor for Fe<sup>III</sup>", *Tetrahed. Lett.*, **2007**, 48, 5389-5392
- <sup>54</sup> (a) M. Zhang, Y. Gao, M. Li, M. Yu, F. Li, L. Li, M. Zhu, J. Zhang, T. Yi, C. Huang, "A Selective Turn On Fluorescent Sensor for Fe<sup>III</sup> and Application to Bioimaging", *Tetrahedron Lett.*, **2007**, 48, 3709–3712; (b) Y. Xiang, A. J. Tong, "A New Rhodamine-Based Chemosensor Exhibiting Selective Fe<sup>III</sup>-Amplified Fluorescence", *Org. Lett.* **2006**, 8, 1549–1552; (c) J. L. Bricks, A. Kovalchuk, C. Trieflinger, M. Nofz, M. Büschel, A. I. Tolmachev, J. Daub, K. J. Rurack, "On the Development of Sensor Molecules that Display Fe<sup>III</sup>-amplified Fluorescence", *J. Am. Chem. Soc.*, **2005**, 127, 13522– 13529; (d) J. Hua, Y.-G. Wang, "A Highly Selective and Sensitive Fluorescent Chemosensor for Fe<sup>3+</sup> in Physiological Aqueous Solution", *Chem. Lett.*, **2005**, 34, 98– 99
- <sup>55</sup> J. R. Lakowicz, "Principles of Fluorescence Spectroscopy", 3rd ed., Springer: New York, **2006**, pp 67–69

- 
- <sup>56</sup> H. N. Kim, M. H. Lee, H. J. Kim, J. S. Kim, J. Yoon, "A New Trend in Rhodamine-Based Chemosensors: Application of Spirolactam Ring-Opening to Sensing Ions", *Chem. Soc. Rev.*, **2008**, 37, 1465-1472
- <sup>57</sup> M. Zhang, Y. Gao, M. Li, M. Yu, F. Li, L. Li, M. Zhu, J. Zhang, T. Yi, C. Huang, "A Selective Turn On Fluorescent Sensor for Fe<sup>III</sup> and Application To Bioimaging", *Tetrahedron Lett.*, **2007**, 48, 3709–3712
- <sup>58</sup> Y. Xiang, A. J. Tong, "A New Rhodamine-Based Chemosensor Exhibiting Selective Fe<sup>III</sup>-Amplified Fluorescence", *Org. Lett.* **2006**, 8, 1549–1552
- <sup>59</sup> A. J. Weerasinghe, C. Schmiesing, S. Varaganti, G. Ramakrishna, E. Sinn, "Single-and Multiphoton Turn-On Fluorescent Fe<sup>3+</sup> Sensor Based on Bis(rhodamine)", *J. Phys. Chem. B*, **2010**, 114 (29), 9413-9419
- <sup>60</sup> X. Zhang, Y. Shiraishi, T. Hirai, "A New Rhodamine-Base Fluorescent Chemosensor for Transition Metal Cations Synthesized by One-Step Facile Condensation", *Tetrahedron Lett.*, **2007**, 48, 5455-5459
- <sup>61</sup> L.-J. Fan, W. E. Jones, Jr., "A Highly Selective and Sensitive Inorganic/Organic Hybrid Polymer Fluorescence "Turn-on" Chemosensory System for Iron Cations", *Am. Chem. Soc.*, **2006**, 128 (21), 6784-6785
- <sup>62</sup> J. H. Soh, K. M. K. Swamy, S. K. Kim, S. Kim, S.-H. Lee, J. Yoon, "Rhodamine Urea Derivatives as Fluorescent Chemosensor for Hg<sup>2+</sup>", *Tetrahedron Lett.*, **2007**, 48, 5966–5969
- <sup>63</sup> X.-F. Yang, X.-Q. Guo, Y.-B. Zhao, "Development of a Novel Rhodamine-Type Fluorescent Probe to Determine Peroxynitrite", *Talanta*, **2002**, 57, 883–890
- <sup>64</sup> K. Hashimoto, H. Irie, A. Fujishima, "TiO<sub>2</sub> Photocatalysis: A Historical Overview and Future Prospects", *Jpn. J. Appl. Phys.*, **2005**, 44, 8269-8285
- <sup>65</sup> A.F. Trendall, R.C Morris, Ed., "Iron Formation: Facts and Problems", Elsevier Science Publisher B.V., Amsterdam, **1983**, p. 241
- <sup>66</sup> M. Sokołowska, W. Bal, "Cu(II) Complexation by "Non-Coordinating" N-2-Hydroxyethylpiperazine N'-2-Ethanesulfonic Acid (HEPES Buffer)", *J. Inorg. Biochem.*, **2005**, 99, 1653–1660
- <sup>67</sup> N. Abo El-Maali, D. Abd El-Hady, "Square-Wave Stripping Voltametry of Uranium(VI) at the Glassy Carbon Electrode. Application to Some Industrial Samples", *Electroanal.*, **1999**, 11, 201-206
- <sup>68</sup> <http://www.avachemicals.net/citrates.html>

---

<sup>69</sup> P. Patnaik, "Dean's Analytical Chemistry Handbook", McGraw-Hill Professional, New York, **2004**

<sup>70</sup> Z. L. Chen, M. Megharaj, R. Naidu, "Confirmation of Iron Complex Formation Using Electrospray Ionization Mass Spectrometry (ESI-MS) and Sample Stacking for Analysis of Iron Polycarboxylate Speciation by Capillary Electrophoresis", *Microchem J.*, **2007**, 86, 94-101

<sup>71</sup> A. M. Zawazka, F. P. J. Vandecasteele, R. L. Crowford, A. J. Paszczynski, "Identification of *Pseudomonas Stutzeri*", *Can. J. Microbiol.*, **2006**, 52, 1164-1176

<sup>72</sup> M. Merckx, B. A. Averill "Ga<sup>3+</sup> as a Functional Substitute for Fe<sup>3+</sup>: Preparation and Characterization of the Ga<sup>3+</sup>Fe<sup>2+</sup> and Ga<sup>3+</sup>Zn<sup>2+</sup> Forms of Bovine Spleen Purple Acid Phosphatase", *Biochemistry-US*, **1998**, 37, 8490-8497

<sup>73</sup> T. Rieth, K. Sasamoto, "Detection of Nitric Oxide and Nitrite by Using a Rhodamine-Type Fluorescent Indicator", *Anal. Commun.*, **1998**, 35, 195-197

<sup>74</sup> M. Shao, Y. Fu, R. Hu, C. Lin, "A Study on Pitting Corrosion of Aluminum Alloy 2024-T3 by Scanning Microreference Electrode Technique", *Mater. Sci. Eng.*, **2003**, A344, 323-327